Open-path dual-frequency comb spectroscopy of methane from livestock production

by

Lindsay Morris

B.S., University of South Alabama, 2018

AN ABSTRACT OF A DISSERTATION

submitted in partial fulfillment of the requirements for the degree

DOCTOR OF PHILOSOPHY

Department of Physics
College of Arts and Sciences

KANSAS STATE UNIVERSITY
Manhattan, Kansas

2023

Abstract

This project focuses on providing outdoor open-path spectroscopic measurements for detection of methane and other agriculturally significant gases over long periods of time in an agricultural setting. The use of dual-comb spectroscopy for remote sensing on agricultural sites has led to an aptly named system, the Agrocombs. The decomposition and fermentation of food performed by microbes in the stomach of ruminants, known as enteric fermentation, is one of the largest sources of anthropogenic methane emissions in the US due in large part by the dense population of livestock such as cattle. Several long-range open-path remote sensing techniques, such as Fourier transform infrared spectroscopy or tunable laser absorption spectroscopy, could be considered to detect and identify methane in an agricultural setting, but limitations in these techniques prove to be deterrents in their applications. Dual-comb spectroscopy provides a unique advantage of simultaneously measuring several significant gases (such as CH_4, NH_3, CO_2, and H_2O) with no external reference system or large structural support. Applying this method to agricultural processes began the journey of the Agrocombs system, a dual-comb pulsed laser system designed to be mobile and noninvasive enough to be placed on a site without disruption of operations, while performing long-term measurements of significant agricultural gases to result in concentration data.

To prove the merit of this system, the Agrocombs research group performed a 2019 measurement at a KSU operated beef stocker site in parallel to a closed-path cavity ring-down system commonly used for trace gas measurements. The results of this experiment show an agreement between the two systems of 6% for methane, with the Agrocombs system providing a concentration precision of 1.25 ppm·m at 900 s. Additionally, the Agrocombs system was able to record concentrations for carbon dioxide, ammonia, and water vapor simultaneously without

additional equipment. After a successful measurement in a feedlot system, where the cattle are confined in pens and present in large numbers, the next step has been to move towards a pasture to capture measurements of cattle in another important lifestyle, grazing.

Grazing cattle in a pasture system provide a unique measurement potential for the Agrocombs system due to the low animal density and the presence of methane sinks that can detract from overall methane production and discharge, otherwise known as emissions. Traditional models for cattle emissions tend to lean towards the assumption that cattle contribute uniformly based on number of cattle in a system, but often neglect the complexity of a system's additional factors to the gas cycle. Pastures provide more area for less animals, allowing for free roaming and independent grazing, which differs greatly from our previous measurement. Additionally, microbial activity in the soil may prove to act as a methane sink in native grasslands, reducing the overall contributions of the grazing system. While feedlot emissions were found to be approximately 137±86 $\mu g/m^2/s$, we expect that the contributing factors of less cattle in a larger area of interest, combined with the methane sink of microbial activity in the soil, will garner us a net methane emission in a pasture of an order of magnitude less than the feedlot. In order to measure emissions from a pasture, the Agrocombs project must achieve a precision of approximately 0.2 parts per billion (ppb), significantly smaller than the approximate 3 ppb in our feedlot measurement, determined through simulation. To test our precision and work towards this goal, we will conduct a controlled release experiment to mimic cattle in a pasture. This also allows for testing a newly packaged system and its accompanying equipment, as well as techniques to handle the ever-moving cattle and their large area of mobility. This thesis details the beginnings and preliminary results of a controlled release in a pasture, as well as the steps taken to achieve such precision needed for this difficult sensing measurement.

Open-path dual-frequency comb spectroscopy of methane from livestock production

by

Lindsay Morris

B.S., University of South Alabama, 2018

A DISSERTATION

submitted in partial fulfillment of the requirements for the degree

DOCTOR OF PHILOSOPHY

Department of Physics
College of Arts and Sciences

KANSAS STATE UNIVERSITY
Manhattan, Kansas

2023

Approved by:

Co-Major Professor
Dr. Brian Washburn

Approved by:

Co-Major Professor
Dr. Brett DePaola

Copyright

Abstract

This project focuses on providing outdoor open-path spectroscopic measurements for detection of methane and other agriculturally significant gases over long periods of time in an agricultural setting. The use of dual-comb spectroscopy for remote sensing on agricultural sites has led to an aptly named system, the Agrocombs. The decomposition and fermentation of food performed by microbes in the stomach of ruminants, known as enteric fermentation, is one of the largest sources of anthropogenic methane emissions in the US due in large part by the dense population of livestock such as cattle. Several long-range open-path remote sensing techniques, such as Fourier transform infrared spectroscopy or tunable laser absorption spectroscopy, could be considered to detect and identify methane in an agricultural setting, but limitations in these techniques prove to be deterrents in their applications. Dual-comb spectroscopy provides a unique advantage of simultaneously measuring several significant gases (such as CH_4, NH_3, CO_2, and H_2O) with no external reference system or large structural support. Applying this method to agricultural processes began the journey of the Agrocombs system, a dual-comb pulsed laser system designed to be mobile and noninvasive enough to be placed on a site without disruption of operations, while performing long-term measurements of significant agricultural gases to result in concentration data.

To prove the merit of this system, the Agrocombs research group performed a 2019 measurement at a KSU operated beef stocker site in parallel to a closed-path cavity ring-down system commonly used for trace gas measurements. The results of this experiment show an agreement between the two systems of 6% for methane, with the Agrocombs system providing a concentration precision of 1.25 ppm·m at 900 s. Additionally, the Agrocombs system was able to record concentrations for carbon dioxide, ammonia, and water vapor simultaneously without

additional equipment. After a successful measurement in a feedlot system, where the cattle are confined in pens and present in large numbers, the next step has been to move towards a pasture to capture measurements of cattle in another important lifestyle, grazing.

Grazing cattle in a pasture system provide a unique measurement potential for the Agrocombs system due to the low animal density and the presence of methane sinks that can detract from overall methane production and discharge, otherwise known as emissions. Traditional models for cattle emissions tend to lean towards the assumption that cattle contribute uniformly based on number of cattle in a system, but often neglect the complexity of a system's additional factors to the gas cycle. Pastures provide more area for less animals, allowing for free roaming and independent grazing, which differs greatly from our previous measurement. Additionally, microbial activity in the soil may prove to act as a methane sink in native grasslands, reducing the overall contributions of the grazing system. While feedlot emissions were found to be approximately 137±86 $\mu g/m^2/s$, we expect that the contributing factors of less cattle in a larger area of interest, combined with the methane sink of microbial activity in the soil, will garner us a net methane emission in a pasture of an order of magnitude less than the feedlot. In order to measure emissions from a pasture, the Agrocombs project must achieve a precision of approximately 0.2 parts per billion (ppb), significantly smaller than the approximate 3 ppb in our feedlot measurement, determined through simulation. To test our precision and work towards this goal, we will conduct a controlled release experiment to mimic cattle in a pasture. This also allows for testing a newly packaged system and its accompanying equipment, as well as techniques to handle the ever-moving cattle and their large area of mobility. This thesis details the beginnings and preliminary results of a controlled release in a pasture, as well as the steps taken to achieve such precision needed for this difficult sensing measurement.

Table of Contents

List of Figures

Acknowledgements

There are not enough words to describe the amount of support I have had through this unique research project. To begin with, this project would have been impossible without a team of varied and brilliant minds coming together to take Agrocombs into the field (literally). I would like to first thank my advisors, Dr. Brett DePaola and Brian Washburn, both of whom have guided me through these years. Eduardo Santos of K-State's agronomy department has been endlessly helpful not only as an instructor in micrometeorology but also as a collaborator, consistently pushing me to learn more about agronomy. I also would like to thank my fellow K-State graduate student, Chinthaka Weerasekara, for constantly working side by side with me to mesh agronomy and physics together in a way to push forward. My thanks as well to Daniel Herman of CU Boulder, who worked tirelessly on the comb systems for our feedlot measurement and who stayed late nights with me in the field to perform repairs or better the transceivers. I would also like to thank Stephen Welch of K-State Agronomy for his modeling contributions and expertise.

Outside of my group, I would not have been able to move forward without my K-State classmates and colleagues. I would like to thank a few individuals in particular for their support. Pavan Muddukrishna, Kell Ruhnow and Sajed Hosseini-Zavareh, as friends and office mates, never stopped pushing me to continue my work. The entering class of 2018 in the department of physics have stuck strong together to keep us all moving towards our final goals, and I cannot imagine going through this process, through the classes and the transition to full-time research, without their support.

Finally, I would like to acknowledge my family. My husband, who has been my rock through the years in a new place as we both have worked hard to finish our degrees. My

grandmother and my grandfather have been a warm source of love and support from afar, even if my constantly rambling about cow rumination has been nothing short of confusing. My brothers, Carver and Andre, check on me and make sure to give me a laugh through their antics. And finally, my dad, who has been my greatest supporter through thick and thin, and always worked hard to give us any advantage he could.

This work would be impossible without funding by the NSF Division of Biological Infrastructure Award #1726304, the ARPA-E MONITOR program, the Habiger Heritage Fund, the William and Joan Porter Endowment, and NIST. Collaborative efforts between Kansas State University's Departments of Physics and Agronomy, combined with collaboration with NIST, have pushed forward this experiment into its newest iteration. Special thanks to K-State's Department of Animal Sciences for their granting of access to the Kansas State University Beef Stocker Unit.

Dedication

This thesis is dedicated to my husband (Bob), my grandmother (Teresa), and my father (Sonny). The three pillars of support in my life have never faltered and have always had more belief in me than I ever have in myself.

Chapter 1 - Introduction

In the modern age, booming populations and climate consciousness have created a tug-of-war of ideas when it comes to sustainable farming practices. When food production needs to stay at an all-time high, but the emission of greenhouse gases causes concern for our planet's future, there is a glaring hole in the equation that could provide some form of solution: a precise understanding of greenhouse gas emissions and their role in agricultural processes. Mitigation of these gases is important, but impossible without a strong understanding of how these emissions are related to the factors present in agricultural processes, such as feed types, fertilizer choice, pesticide usage, and livestock lifestyle, among others.

Today, we know that human activity has increased the production of greenhouse gases such as carbon dioxide (CO_2), nitrous oxide (N_2O), and methane (CH_4). The Environmental Protection Agency (EPA) found, from the pre-industrial age to about 2018, these gases increased in concentration by respectively 46, 23, and 165 percent [1]. Rising ammonia (NH_3) emissions are also a cause for concern as studies release linking direct effects of this gas with possible respiratory illnesses in humans, particularly those who work in livestock operations. This is due to the fact that approximately 81% of these emissions coming from agricultural sources across the globe [2]. These gases in particular each have strong links to the agricultural sector, where interest has risen in both stronger studies of these emissions and possible mitigation methods for these significant gases [1].

It is reported that methane has a significantly higher warming power in the first 20 years of its presence in the atmosphere, a power as high as 80 times the warming power of carbon dioxide [3]. The significant difference in warming power over 20 years means that mitigation of methane could lead to more immediate improvements in our warming climate. The sharp rise in

methane contribution has led to heavy interest in emission measurements and mitigation of this particular gas in agricultural operations. Figure 1.1 breaks down 2018 methane emissions by anthropogenic source, showing that the largest contributor to CH_4 is the process of enteric fermentation. Enteric fermentation tops the scale of CH_4 contributions, while manure management also contributes largely to these increasing emissions. Both processes are tied heavily to the agricultural sector, leading to a renewed interest in precision emission measurements in these systems. Enteric fermentation in particular is a biological process tied to the digestion in ruminants like cattle. In 2018, there was an estimated increase of methane emissions of 13.4 million metric tons (MMT) CO_2 Eq., or 8.2 percent, from 1990 [1]. Mitigation of methane is heavily debated, as the calls for shifts to plant-rich diets are weighed alongside studies of feed efficiency of ruminant livestock or efficiency in manure management [4,5]. This increase in methane emissions and growing list of mitigation ideas has led to a strong interest in precision measurements of emissions from livestock systems.

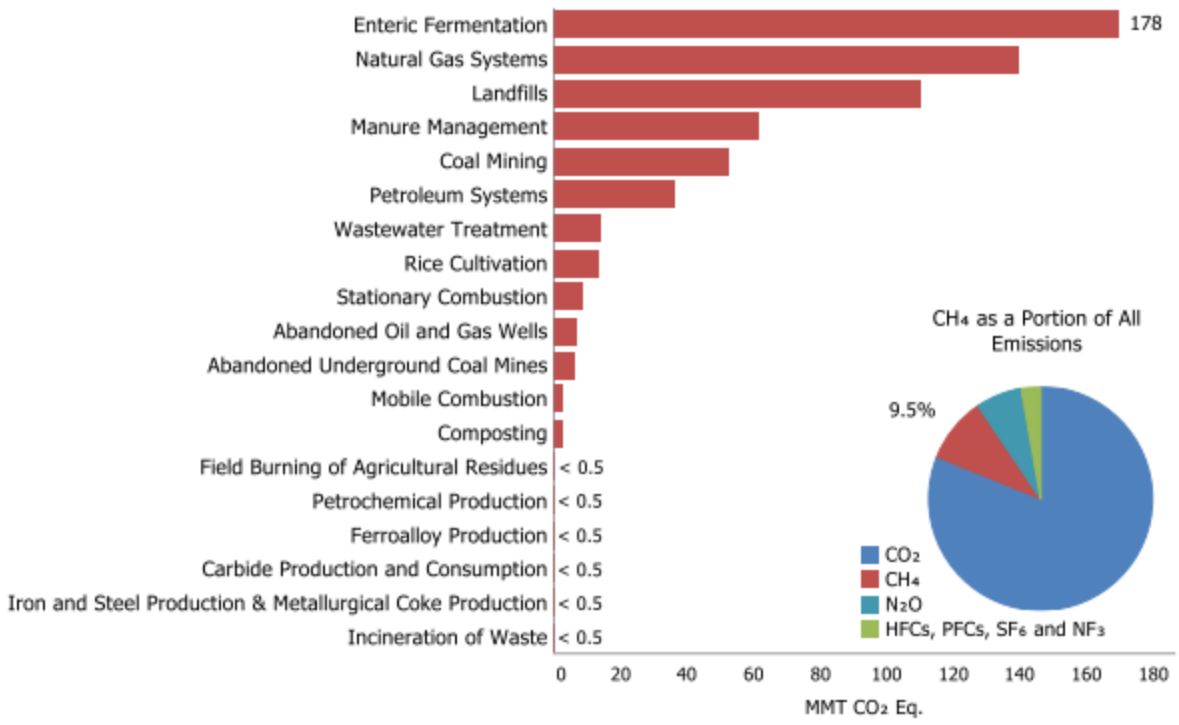

Figure 1.1 2018 methane emissions broken down by source (MMT CO_2). Image from Reference [1] considered under public domain.

Ammonia production has played a large part in livestock operations alongside methane. Livestock excreta include uric acid, urea, and feces, all of which can decompose or volatize to form ammonia emissions [2]. As these biological functions are necessary to livestock productions, the ideal situation is to mitigate NH_3 emissions from concentrated animal feeding operations and manure applications [6]. While ammonia is not a greenhouse gas, rising emissions still ring alarms, as its presence poses human health risks [2], as well as risks to biodiversity. The presence of ammonia creates nitrogen accumulation that tips the balance of biodiversity by allowing less nitrogen-sensitive plants to thrive or adapt while more sensitive species are less and less present [7]. Mitigation for livestock ammonia is a large topic of interest, with some conclusions drawn that fertilizer practices can be changed to reduce ammonia

emissions [8]. These mitigation techniques are still novel and may require precision detection systems to prove their efficacy in large field operations.

The current understanding of emissions from livestock can be overall summarized between the combined efforts of the United States EPA in their greenhouse gas inventory [1] and the IPCC reports [9,10] that provide guidance for some of these estimates. To simplify the process of estimating methane emissions from cattle specifically, the number of cattle (population) is multiplied by an enteric fermentation factor derived from the IPCC's guidelines on gross energy intake [10], which takes into account feed type, breed, and metabolic factors. Overall, the model that follows, known as the Cattle Enteric Fermentation Model (CEFM), considers the livestock in the system rather than the net emissions from the system. Methane is not created in a vacuum, just as it is not emitted without any external factors possibly consuming a portion of gas for other biological processes. It is more apt to look at an agricultural site in terms of the biosphere, the area in which animals, soil, and vegetation reside, and consider the continuum of gas as it moves through this system [11–13], with the final net methane emissions from the system being the contributing factor to atmospheric degradation. It is crucial to understand the relationship between individual emissions of cattle while also encompassing the net CH_4 emissions from a system, which allows us to better identify changes in emission rates as mitigation efforts are made to reduce methane production through changing factors such as lifestyle or feed type. With a proper support frame of detection for understanding the results of mitigation efforts, agricultural operations can work towards more sustainable practices.

1.1 Current Detection Methods and Challenges

Growing concerns for reduction of several greenhouse gases have sparked a wave of studies focused on mitigation through various approaches in agriculture. Nitrogen oxide reduction is heavily tied into changes in fertilizer and clean water practices [14]. Methane emissions are strongly sourced from enteric fermentation, leading mitigation studies to focus on the biological processes involved and possible changes in feed efficiency [4]. Ammonia's presence in animal urea production and fertilizer practices means that mitigation efforts are focused on efficient waste removal or changes in fertilizer development [8]. Due to its strong driving force in the current global warming picture, where at least 25% of today's warming is connected to methane emissions from human practices [3], we will focus our sights primarily on the mitigation of methane, with a focus on the agricultural sector.

Methane emissions are highly tied to the biological process in cattle known as enteric fermentation, leading to a heavy focus on the cattle specifically within a livestock operation. These ruminants naturally ferment food as a part of their digestive process [15], producing methane at rates predicted by the metabolic factors dependent upon the breed of cattle and the quality/metabolic efficiency of feed provided [10]. Studies to improve the CEFM previously discussed have focused on individual cattle emissions to narrow errors in these estimates, such as studies that measure methane emissions from bovines encased in calorimetric chambers [16]. These chambers can measure the methane production of a single animal, and an average of emissions from a sample of cattle each individually studied can be used to determine emission rates specific to breed or feed type. While these studies are precise, some view the practice as invasive to the normal operations of livestock handling.

The development of non-invasive measurements is important to capture a realistic view of emissions in daily operations on-site. From this principle, there have been groups focused now on portable or hand-held detector systems to avoid encasing cattle in chambers or disrupting their activity, as well as those activities of human operators in agricultural processes. One such system is a hand-held laser methane detector (LMD) [17]. This device is non-invasive, requires no actual contact with the animal, and uses a semiconductor laser to carry out infrared absorption spectroscopy. The primary challenge to this device is the lack of sample for analysis, as it relies on analysis of cattle breaths in real-time, causing fluctuations in readings. While this device is precise in its ability to detect methane emissions from a single bovine, and eliminates the invasive nature of calorimetric chambers, it does not follow a key principle discussed in the beginning of this chapter. While the methane emissions of cattle are a strong source of CH_4 in livestock operations, they are not the only contributing factor to net emissions for the entire operation. The LMD does not consider environmental factors on-site that can detract or add to net methane emissions.

If we wish to observe the net emissions of an agricultural process, we need to move away from “small-scale”, single-animal emissions and estimates based on cattle population. A new framework for methane emission detections is a shift to “big picture” emission detection, highlighted in the development of projects such as MethaneSAT [18]. This satellite-based project takes the detector away from the breaths of bovines and into orbit, showing large-scale methane emissions over massive sources that produce more than 500 kg/hour. This technology is most useful for the oil and gas industry, where methane emissions are also prevalent. As far as agricultural methane production, MethaneSAT’s resolution is currently touted as being able to detect in areas as small as approximately 1 km^2. While that area is much smaller than the large-

scale ability to detect an entire country's methane emissions, it does not reach the resolution of individual agricultural operations. The US agricultural sector still maintains a strong attendance of local and small-scale farming operations, meaning that the methane emissions of livestock operations that do not reach the satellite's minimum quantification resolution cannot be distinguished from other sources. This creates an issue opposite of the LMD, where instead of a lack of knowledge of the entire system's net emissions, we now cannot distinguish a single operation's net methane emissions from possible neighboring operations.

Precision sensing methods have become the forefront of detecting the emissions from agricultural systems, where these spectroscopic measurements detect the overall emissions from the system rather than estimating based on the number of cattle or determining an average emission rate from a sample size of cattle. Several examples can be made for what constitutes a precision measurement in the field, including the use of Fourier transform infrared (FTIR) spectroscopy [19,20], and tunable laser absorption spectroscopy (TLAS) [21,22]. These techniques often utilize the concept of molecular absorption, where light transferred through a sample can be directed to a detector, and the absorption particular to the sample identifies the presence of molecules. The transmission signal can also be used to determine the concentration of identifiable molecules with the support of databases that gather absorption information on many molecules of interest.

Outdoor measurements require robust equipment that can withstand possible extremes in weather, wind, and temperature, as well as staying flexible enough to work around an agricultural operation, rather than take away from some of the space or time needed to maintain regular operations in a livestock system. Ideally, an experiment would be able to simultaneously detect multiple gases of interest present in an agricultural operation (such as NH_4, CO_2, N_2O,

NH_3, and water vapor) while maintaining precision that allows for detection of minute concentrations of these gases, varying across different agricultural processes. For example, livestock operations are expected to yield high emission rates of methane from enteric fermentation, moderate yields in ammonia and carbon dioxide as by-products of urea application, and less yields of nitrogen dioxide than expected from a crop system in comparison [23]. The varying level of these gases call for precisions that allow us to broadly detect large yields in emissions while also still detecting the smaller underlying emissions from less prominent processes on-site.

A common methodology for outdoor measurements would be the use of a variety of tunable lasers for TLAS. There is a history of TLAS being able to detect emissions on the sub-parts-per-million level, giving it a reputation for its detection resolution [24]. The ability to detect smaller enhancements above background in field measurements is ideal for outdoor measurements, as well as the fact that tunable lasers are capable of both concentration measurements of particular gases and temperature measurements [25]. These tunable lasers are capable of concentration measurements for the agricultural gases of interest noted in this chapter but fail in their ability to simultaneously detect more than one gas at a time. Measuring multiple gases on-site would mean having independent TLAS systems for each gas studied, as well as a separate set of data for analysis. This complexity to a multi-gas detection setup ultimately leads to higher costs and more time spent in analysis.

FTIR, one of the most popular methods used in field measurements, is known for its high spectral resolution, ability to maintain long-distance measurements over open paths, and simultaneous detection of multiple gases [26]. These are desirable qualities to an outdoor measurement, as discussed prior, but come with possible detriments. FTIR requires a long

mechanical relay arm which adds bulk to the equipment, as well as some added sensitivity to external vibrations [27]. Outdoor measurements are unpredictable and the environment sometimes volatile in terms of weather and wind, meaning that a sensitivity to vibrations can be counterintuitive to an outdoor experiment. Furthermore, there is an inverse relationship between signal-to-noise ratio and measurement period in an FTIR spectrometer, meaning that minimum requirements in measurement period are set to ensure a proper signal-to-noise ratio [28]. This is due to the reliance on mechanically scanned mirrors in these systems to record resultant interferograms [29]. The reliance on a mechanical mechanism limits acquisition rates, therefore limiting the breadth of attainable data for measurements that are limited in timeframe (for example, seasonally dependent agricultural operations).

Agricultural measurements of greenhouse gas emissions are possible over open paths and are commonly carried out through the use of FTIR spectroscopy or TLAS. These methods are useful for detection of net methane emissions of a system, factoring in sinks and sources of CH_4, while also operating on a scale that benefits the net emission detection of a singular agricultural operation. While these methods provide concentration measurements for significant greenhouse gases, both methods have drawbacks that detract from the overall effectiveness of field experiments. With this in mind, it is best to propose a methodology that can provide high resolution, simultaneous detect of multiple agriculturally significant gases, and robustness against adverse elements in the field, all while still upholding a noninvasive nature to the agricultural processes on-site.

1.2 Dual-Comb Spectroscopy for Remote Sensing

In 2005, the North American Research Strategy for Tropospheric Ozone (NARSTO) partnership released a report that detailed the current state of inventories across the continent for emissions, as well as providing recommendations for future improvements to these inventories [30]. The EPA took these recommendations into consideration, and published their progress since the NARSTO report in 2019 [31]. This response to the recommendation details several progressions made to the models used in today's emission inventories, as well as outlines improvements made to sensing measurements in some anthropogenic sources. While progress has been made, progress as of 2019 still calls for better remote sensing of agricultural emissions, particularly from confined animal feeding operations, such as livestock operations. Reference [31] reports that conventional methods can be improved upon to capture difficult large-area emissions of these agricultural operations. As detailed in Section 1.1, an ideal agricultural measurement would be carried out despite adversities in the field, be it from weather conditions or daily operations on-site. Experimentation should be robust against the elements, while maintaining sensitivity in the measurement that allows for detection of minute enhancements above background levels of the significant gases in question. Simultaneous multi-gas detection is a sought-after quality, as this characteristic often alludes to experimental setups that negate multiple systems or additional costs.

Dual-comb spectroscopy (DCS) combines the simultaneous multi-gas detection of FTIR and the high sensitivity to small enhancements from TLAS. As a more novel method in the current state of emissions detection, DCS has shown its ability to maintain high signal-to-noise ratio while upholding absolute frequency accuracy for high resolution measurements across a broad band of spectral elements [32]. Much like FTIR, DCS can detect multiple gases

simultaneous due to its coverage of a broad spectral bandwidth in the near-IR [33]. In the near-infrared region, agriculturally significant gases such as CH_4, CO_2, NH_3, and water vapor have strong absorption lines, making it possible to detect these gases with dual-comb spectroscopy. N_2O has weaker absorption in this region, but stronger absorption in the mid-IR region, meaning that advances for DCS to operate in the mid-IR region can allow for further detection of N_2O, which is commonly produced in crop systems by way of fertilizer management. A dual-comb spectroscopy device is also free of the additional mechanical delay that FTIR relies upon, allowing for high rates of data acquisition over a set measurement period. Previous studies have pushed for open-path measurements utilizing DCS [34–36], and have shown promising results in its long-path field capabilities, which stands as a strong advantage in the potential for large agricultural operation site studies. Further discussion of DCS and its advantages are outlined in Chapter 2, section 2.1.

With DCS as a method of choice, we can strive for more precise and encompassing measurements of greenhouse gases in agricultural operations. As requested from the EPA in Reference [31], measurements performed with a field-ready DCS system could provide improvements upon current detection conventions, allowing for better inventories of emissions. The system focused on in this body of work is a collaborative effort between Kansas State University's Department of Physics and Department of Agronomy, encouraging interdisciplinary scientific research for the advancement of agricultural measurements in a state proud for its long-standing history of agriculture, particularly within the beef industry.

1.3 Thesis Outline

This thesis continues with the methodology of dual-comb spectroscopy applied to remote sensing in an agricultural setting, with an emphasis on determining methane flux in livestock systems. Chapter 2 of this thesis explains the basis of dual-comb spectroscopy and details of how this technique works. From there, the chapter will move into describing the robustness and characteristics of the Agrocombs system, the experimental setup at the heart of this research. Further discussion explains the basic idea behind our comparative method, a commercial cavity-ring down spectroscopy (CRDS) system.

Chapter 3 of this thesis delves into our proof-of-concept experiment, the feedlot measurement. Current livestock emission estimation will be explained to give an idea of how government agencies operate in today's understanding of cattle methane emissions. To properly understand the impact of this comparative measurement, this chapter will explain the measurement geometry and setup of both the Agrocombs and the CRDS system, as well as detail some of the challenges presented in the field. The methodology for feedlot data fitting and processing will be explained, as well as a brief overview of the conversion from concentration to flux. Finally, the chapter will discuss any conclusions of interest made from the measurement, as well as detail the results in comparison between the two systems, with a brief discussion showing the results from the Agrocombs against the expected emissions from the IPCC.

Chapter 4 describes the evolution from a feedlot measurement to a grazing system. The change in system comes with many challenges, and even more questions about the true net emissions of the system. Concerns over the accurate representation of grazing system emissions in comparison to feedlot emission estimates are explained. The complexity of a pasture measurement is discussed, leading to adaptation of the system for this new experiment. In order

to accurately measure emissions in a pasture, the Agrocombs system will need to detect smaller enhancements (on the order of 0.2 ppb) than its proven capabilities in a feedlot setting (on the order of 3 ppb), meaning that the system will need improved studies of its precision. The primary study to prove the efficacy of the Agrocombs system in a pasture is a controlled release, planned as a trial of emission detection through the use of a planned release of methane with a known flow rate. This chapter's focus will include the improvement of the system, the precautions taken in a pasture, and the care taken to ensure accuracy and precision for a significantly difficult measurement. Preliminary results will be discussed.

Chapter 5 will draw conclusions for the dissertation, comparing the details of experimentation between our feedlot study and the beginnings of a pasture measurement. While the controlled release is still underway, there are goals that can be discussed. There are a variety of viable paths for the system as experiments progress, and a few popular options will be explored for future possibilities.

Chapter 2 - The Agrocombs System

Chapter 1 discussed the environmental concerns surrounding rising emissions of gases such as CH_4 and NH_3, both of which have strong ties to the agricultural sector. Particularly in Kansas, the beef industry has a rich history within the state, adding to the importance of sustainable farming that does not detract from agricultural practices. Without proper detection mechanisms for net emissions of farming operations, mitigation studies will be unable to fully visualize the impact on methane and ammonia emission reductions. Section 1.2 gave examples of some current sensing methods and the challenges they face, while also highlighting the individual strengths of each methodology. In the end, if we wish to grasp the full net emissions of methane and ammonia from an entire agricultural site, while also distinguishing emissions from neighboring farming operations, it is proposed that dual comb spectroscopy would be an ideal method of sensing these significant gases from livestock emissions.

Before any discussion about experimentation, one must understand the basis of our measurement. Gas detection and spectroscopy are no strangers, though the challenge arises instead as the experiment moves from a controlled laboratory setting into the unpredictable outdoors. In order to fulfill our goals for a measurement of agricultural gases, we need a method that will provide a robust measurement of real-time concentrations of gases, while leaving behind massive structural support and intrusive equipment lines that could disrupt the observable agricultural processes. The equipment also would need to be resistant to the extreme weather conditions in Kansas on both sides of the thermal spectrum. Our experimental method of choice, dual-comb spectroscopy (DCS), meets these minimum requirements, as well as offering the advantage of detecting multiple gases of interest simultaneously.

2.1 Frequency Combs

Before one can discuss dual comb spectroscopy and its appropriate use in the field, we must build upon the principles of the method. DCS can be broken down beginning with just its name. If we look at a mode-locked laser with a known femtosecond scale pulse, the spectral content of the laser is our frequency comb. The repeated output from this system creates a train of pulses in the time domain, where the pulse train period can be described as $1/f_{rep}$ with a repetition frequency f_{rep}. This repetition rate is created by a pulsed laser signal trapped in a laser cavity, where a single pulse leaks from the cavity every roundtrip of the light, creating a train or uniformly spaced pulses. The time taken to travel roundtrip in the cavity is dependent on the length of the cavity, meaning that the length of a laser cavity ultimately decides the repetition rate f_{rep}, or the rate in which laser pulses are output from the cavity. In terms of the frequency domain, the laser's output is composed of a discrete set of narrow lines, each with an optical frequency f_n, that are evenly spaced out. The structure of this output gives rise to the name "frequency comb", in which these narrow lines resemble comb teeth [37].

This f_n can alternatively be described mathematically through two known radio frequencies (RF) characteristic to the comb. We see this in Eq. 2.1, where f_n is still the frequency of a particular narrow line, n is a large integer, and f_0 is an offset frequency determined by the carrier-envelope phase shift $\Delta\phi$ in Eq. 2.2 [38].

$$f_n = nf_{rep} + f_0 \qquad \textbf{2. 1}$$

$$f_0 = \frac{f_{rep}\Delta\phi}{2\pi} \qquad \textbf{2. 2}$$

Repetition rates are typically in the MHz range, meaning at least 10^6 laser pulses are released within one second of laser operation, granting us as many spectral components. The large number of spectral components, or "comb teeth", gives the advantage of a broadband spectrum for spectroscopic purposes, as each comb tooth can be resolved as we look at the overall spectrum of the frequency comb (see Figure 2.1A, the overall shape created by all comb teeth is the spectrum). In reference [39], it is stated that if the frequency spectrum is broad enough, one can directly measure both the offset frequency and the repetition rate. This fact allows frequency combs to be used in applications such as optical atomic clocks [40] and pulse synthesis [41].

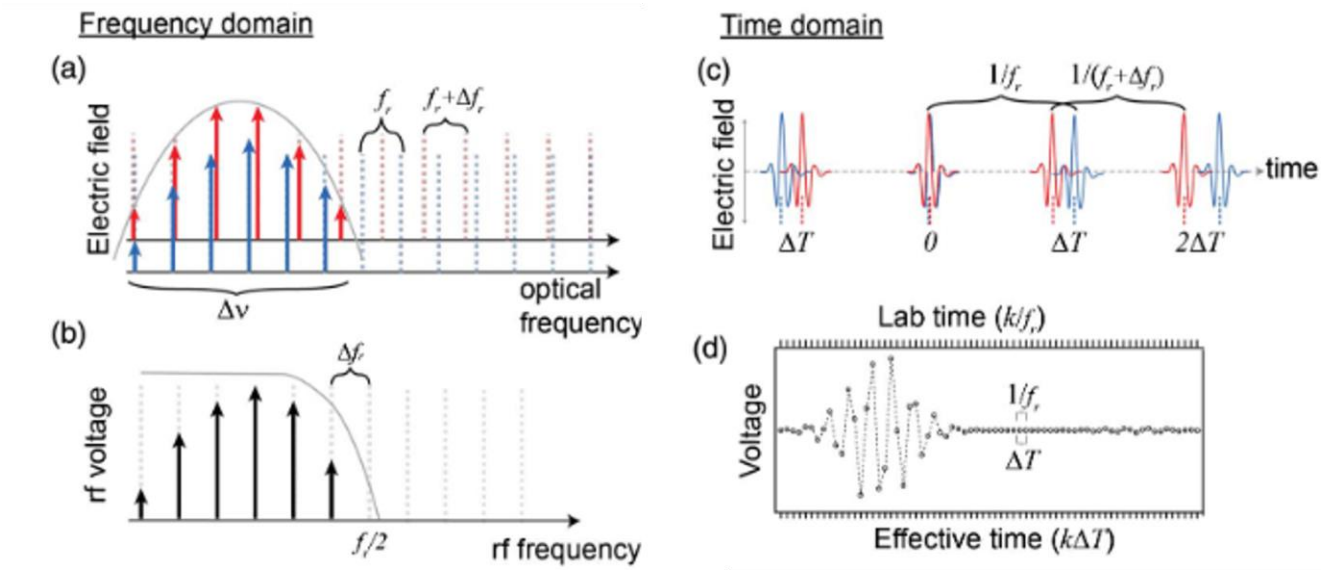

Figure 2.1 A) Depiction of two frequency combs (red and blue) in the optical frequency domain. Here, f_{rep} is labeled f_r, and Δf_{rep} is Δf_r. B) When mixed, the two frequency combs from A) result in a rf frequency comb with characteristic Δf_r. C) In the time domain, we see our two signals as pulse trains with walk-off between the pulses over time. D) The output of the pulse-to-pulse signals in C) come to a product shown in this voltage output, giving us interferograms at a time interval of $1/f_r$, much like FTIR interferograms. Adapted with permission from Reference [33].

From a frequency comb, one can predict our next step: “dual comb”, or two frequency combs used simultaneously. In order to utilize a dual comb experiment, the two frequency combs must have repetition frequencies slightly offset from one another with a difference in repetition frequency denoted as Δf_{rep}. From there, the two combs are interfered on a photodiode, in which distinguishable heterodyne beats are produced between pairs of optical comb teeth [33]. The resultant RF comb conveniently contains all of the necessary spectral content while being accessible via RF electronics.

2.2 An Overview of Dual Comb Spectroscopy

Spectroscopy with a dual frequency comb is performed by introducing a sample into one or both beam paths, dependent upon the desired measurement. For the purposes of open-path measurements over turbulent paths as intended for the Agrocombs system, the chosen technique is symmetric, or collinear, where the sample response that is encoded on the comb’s light is the sample’s absorption. Unlike a simple frequency comb experiment, where the comb light is sent through a sample and then into a spectrometer, the heterodyne beating involved in dual-comb spectroscopy negates the need for a spectrometer, whose presence adds to cost and further possibility for complexities in a field measurement that requires equipment to be capable of surviving in a mobile laboratory over long periods of time.

As stated above, a symmetric dual frequency comb measurement would result in absorption information encoded on the comb light after passing both comb beams through a sample. Measured spectrum covers a wide array of wavenumbers, while retaining resolution that allows for detection of small enhancements, as seen in Figure 2.2 b). This absorption can be

converted to concentrations with the use of curated databases such as HITRAN [42]. This database in particular acts as a spectroscopic compilation for heavily studied molecules, congregating results into line-by-line parameters to be used in conjunction with high resolution absorption measurements [42]. The process is not as simple as casting light over a path and receiving absorption information. Instead, the collection of data begins with the simplest geometry required of a dual-comb measurement.

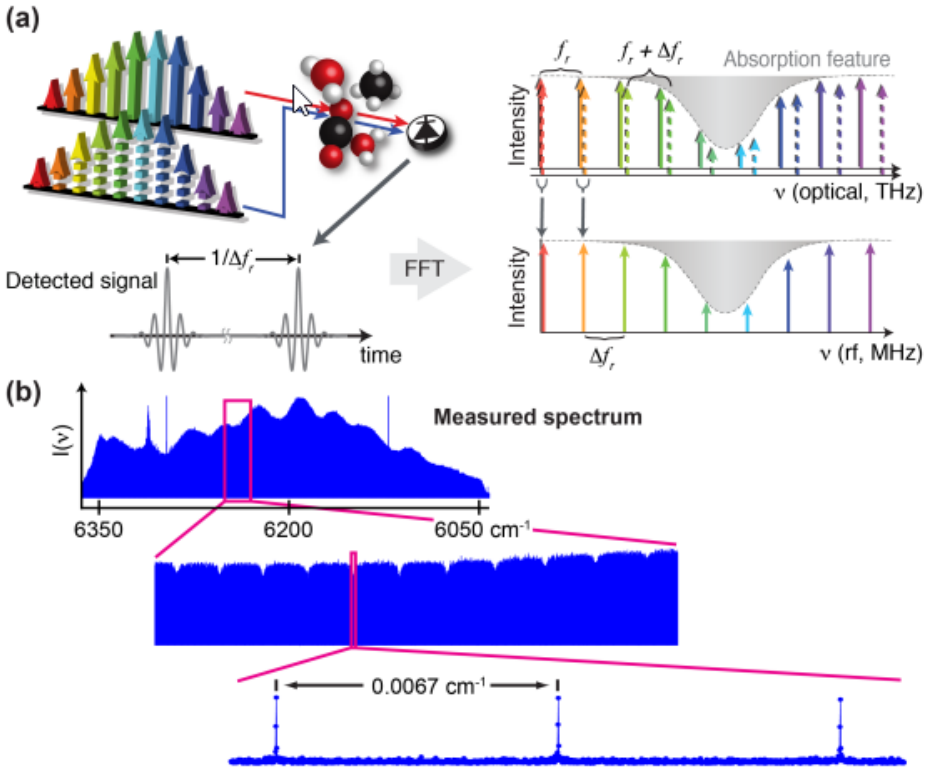

Figure 2.2 a) In a symmetric dual-comb measurement, the sample is introduced to both beams, which results in a detection signal (interferogram) in the time domain. The Fast Fourier Transform (FFT) of this interferogram gives an RF spectrum that maps to the optical spectrum as seen. b) Actual measured spectrum has a broad range of wavenumbers that can be interrogated, while retaining a resolution that allows analysis of small enhancements with fine spacing, as seen at the bottom of the image. Image from Ref [35] and licensed under CC BY 4.0.

In Figure 2.2 a), a frequency comb's light is introduced to a sample before being collected with a photodetector. A notable advantage of dual-comb spectroscopy is the absence of an additional spectrometer, as the comb light can instead be collected on a photodiode while preserving the encoded response, allowing for collection and analysis of retrieved light in the RF frequency domain as shown in the right side of Figure 2.2 a). The result of this collection is an interferogram signal in the voltage-time domain. If we look at the physical interaction of light and the sample, a light pulse introduced to a sample will excite molecules, giving way to resonant molecular transitions that behave as oscillating dipoles. The initial excitation is then followed by decaying oscillations of dipole elements that can be seen as forward-scattered radiation often referred to as free induction decay (FID), which represents the impulse response of gas molecules, or more simply, represents a reaction function of absorption of light that can be analyzed to reveal gas concentration [43]. A Fourier transform gives us a spectrum in the frequency domain in place of this interferogram, providing us with the transmission information necessary to process with a molecular database. The high signal-to-noise ratio (SNR) while covering a broad range of frequencies allows for detection of small enhancement features in the spectrum, indicative of different gas absorption features.

Data collection for real-time field measurement often comes with concerns regarding the acquisition speed, particularly the minimum time to collect a single spectrum in the case of DCS. It is important to establish a minimum data acquisition time that allows study of resultant emissions as agricultural processes are carried out throughout daily operations. This acquisition time is inversely proportional to Δf_{rep} [32]. In theory, the larger the difference in repetition rates, the quicker one could gather a spectrum. Reality poses a limitation to this relationship in regard to balancing the width of the spectrum. When the optical spectrum, characterized by its width

$\Delta\nu$, is mapped to an RF spectrum, the new width of that RF spectrum is described by the expression $\Delta\nu/m$, where m is a "compression factor", expanded upon in Eq. 2.3. This expression identifies the balancing act between spectral bandwidth and acquisition speed; higher speed of acquisition narrows the RF spectral window. That limitation is less daunting than it may appear, as compression factors are generally on the order of tens of thousands to approximately one million. Millions of spectral elements in a single spectrum can be retrieved within milliseconds with a frequency comb that has spacing of 100 MHz [33]. While there is a limitation to the acquisition speed in regards to the spectral window, DCS still holds an advantage in its high speed spectral measurements [44].

$$m = f_{rep}/\Delta f_{rep} \qquad \textbf{2. 3}$$

Another important aspect of signal collection is the signal-to-noise ratio. The concept of SNR simply relates the signal of the experiment to the noise of the equipment, giving a ratio that addresses the precision of the measurement [45]. In many methods, increasing the signal-to-noise comes from changing an array of factors particular to the experiment. For example, an FTIR ensemble's SNR may vary with the number of scans (the range of wavenumbers) made at a consistent resolution. In reference [33], the SNR for a dual-comb spectrometer is said to scale with the acquisition time τ and the number of spectral elements (or comb teeth), M, as shown in Eq. 2.4. This means that signal-to-noise also inevitably gives another tradeoff for the system, where the SNR and bandwidth are inverse related due to Eq. 2.5. With the previous conclusion that acquisition speed comes at the expense of the width of the spectral window, it is also important to correctly identify an averaging time that sets τ large enough to maintain a high

SNR. Detailed discussion of appropriate SNR and its implication for precision will resume in Chapters 3 and 4.

$$SNR \approx \sqrt{\tau}/M \quad \textbf{2. 4}$$

$$\Delta\nu = Mf_{rep} \quad \textbf{2. 5}$$

It is standard in experimentation to try and maintain a high SNR. For a DCS measurement, we can see that a balance of appropriate bandwidth and acquisition time are related to this ratio. A longer averaging time may set a higher SNR, but also comes with a disadvantage in terms of the resulting spectra. The repetition rates will set the rate of digitization of resulting interferograms, meaning that a repetition rate on the order of 100 Hz, we will receive 100 interferograms within a single second of acquisition. Quickly cumbersome data file size can hinder the accessibility of this measurement, leading to several filtering and averaging systems to make the resultant data more manageable. First, we hardware average the number of interferograms to a reasonable average over a small interval of the acquisition period. If we hardware average 25 interferograms, this cuts our rate of interferogram recording down by a factor of 25. Next, we phase average a small sample of successive interferograms in time, for example taking 3 interferograms and phase averaging them to one phase-corrected interferogram. This phase correction is performed in real-time through the use of a field-programmable gate array (FPGA) [46]. Finally, we can co-add point by point several sequential interferograms that represent up to a small sample period of time, such as 1 second [33]. Through the use of real-time co-adding of spectra and phase correction, massive data retention can be reduced to

meaningful phase-corrected interferograms for analysis. Implementing this practice can reduce the size of data files by a predicted factor of 10^4 [32]. This is only possible during phase coherence for both combs for the DCS system, leading to a continued reliance on appropriately chosen acquisition times to maintain high SNR.

In summary, DCS provides line source simultaneous multi-gas measurements with high signal-to-noise ratio, while still being relatively portable. This is important in an open-air measurement for multiple reasons. To begin with, a line source more accurately captures gas absorption over long open-air paths in turbulent conditions in comparison to point sensors, where spacing between sensors could lead to potential gaps in the measurement. Simultaneous detection of multiple gases allows for one spectroscopy system rather than one per sample of interest, leading to better cost effectiveness and simplicity in field application. In comparison to more commonly used systems, these changes result in a potential reduction of loss in signal-to-noise ratio [32]. Previously, two spectroscopic methods were primarily used in open-path measurements: TLAS and FTIR. Tunable lasers have a characteristically limited spectral region, allowing for detection of one gas at a time, leading to additional equipment per gas of interest (see Section 1.1). There is also concern with the loss of phase information, as TLAS does not record signal phase without additional configuration, which would be difficult to control in comparison to methods that already encode phase information. While FTIR can cover a broader spectral region than TLAS, it requires a mechanical delay line that increases the difficulty for field experimentation, as well as limited scan rates. In comparison, near-IR DCS has already shown promise with its broadband coverage of the optical spectrum with a need for only one photodetector [33]. The lack of additional spectrometer, broad spectral region, Measurements have already been conducted and shown that DCS can be applied to turbulent open-air systems

[47]. In reference [34], the users demonstrated an application of DCS over a 2 km path, where the resultant spectra allowed retrieval of dry-air mole fractions for a number of gases, including CH_4 and CO_2. This application serves as proof of the capabilities of this technique for potential agricultural measurements, where an open-path system is the ideal mode of data collection, encapsulating the net emissions of the agricultural operations on-site rather than individual bovines or a regional net emission rate.

2.3 Agrocombs

Thus far, it has been shown that the agricultural sector needs improved detection techniques for the overall understanding of emissions from agricultural processes. There are several gases that factor into these processes, and the presence of each can be studied at length for the improvement of inventories and future mitigation development. The production of urea and liming also contribute to small emissions of carbon dioxide [48], while livestock excreta can undergo chemical changes (decomposition or volatilization) that lead to ammonia production [2]. Methane is tied closely to enteric fermentation, but also emits from the management and storage of livestock manure. The ever-present water vapors can even be studied closely for identification of isotopologues to better understanding the water cycle, as well as modern agricultural processes' place in this atmospheric cycle [49,50]. The broad range of studies that can be conducted with adequate and appropriate sensing equipment is staggering, ever-growing as further questions are born from evolving understanding of the agricultural sector's impact on emissions and atmospheric cycles. Knowing this, and the requirements set forth to withstand long-term outdoor measurements, a dedicated agricultural detection system utilizing DCS was designed to address the gap in emission detection systems.

The purpose of this project has always been to achieve simultaneous multiple gas detection for rapid, field-based measurements using a dual frequency comb ensemble. With the ability to scan a long-range open-path beamline using only one mode-locked laser, we could not only detect real-time enhancements of gas concentrations while also identifying isotopologues of these greenhouse gases for furthering of other studies, such as studies of water vapor and carbon exchange through a variety of spatial scales [51]. Development of a dual-comb system for the purpose of interrogating agriculturally significant emissions has led to the project at the center of this thesis, known always as the Agrocombs system. This system would need to be able to withstand outdoor conditions for relatively long spans of time in order to capture emission cycles, while also standing independently without an ever-present operator. While DCS has shown its merit in field measurements as a light source and retrieval method [34], an agricultural experiment could often mean little to no structural support for delicate equipment against environmental factors. With portability and robustness in mind, the Agrocombs have been packaged with the use of pulsed fiber lasers and carefully constructed electronics for remote operation.

2.3.1 A fiber-based near-infrared spectrometer

If we look at the methods we've compared against in current agricultural sensing, particularly FTIR and TLAS, we can note the operation of near-infrared laser systems in each of these systems. For the Agrocombs system, we will continue this theme in order to detect strong absorption bands of significant agricultural gases in this near-IR region. Section 1.2 discusses the qualities present in current sensing methods, as well as their challenges, that set the bar for what properties are necessary for success in furthering the precision detection of methane emissions.

Keep in mind the important qualities we need to uphold for an optical system that can survive outdoor experimentation: robustness against the elements, strong stability over long periods of time, and precision capable of detecting small enhancements of gases like methane and ammonia above atmospheric background levels.

While the idea of a laser may invoke the mental image of light bouncing through a cavity in a more traditional sense, advances in the variety and application of fiber optics [52–55] have proven the efficacy of fiber-based cavities [56] to further fortify fiber optic systems. There have been several studies conducted combining the strengths of dual-comb spectroscopy as a method with the strengths of fiber optics [32,34,35,44,47,57–59]. For a proper agricultural measurement, a system would need to be able to collect data for long spans of time, ranging from weeks to months, if not longer. While fiber optics are robust enough to withstand harsh weather and environmental conditions, the operation of a laser for spectroscopy requires a step above in stability for long-term measurements. For the purpose of our desired measurements, the Agrocombs system will operate under the basis of a semiconductor-saturable absorber mirror, SESAM, based PM-fiber pulsed laser. There are three important characteristics of this laser to explore: its mode-locking ability, the semiconductor-saturable absorber mirror, and the polarization-maintaining (PM) fibers.

In simplest terms, mode locking can refer to several techniques that result in the generation of pulses in the ultrafast regime. An example of this might be a basic passively mode-locked laser, where light is introduced to a cavity with a saturated absorber on one end and an output coupling mirror at the other. A gain medium is aligned between these two pieces, and as the light hits the saturated absorber, it travels through the gain medium, to the output coupling mirror, in which a laser pulse is emitted from the cavity [60]. The light then travels back through

the gain medium to the saturated absorber to repeat the process. Pulse duration can be manipulated through choice of gain medium, saturable absorber, cavity length, or a variety of smaller variations to the cavity. If we translate this to fiber optics, we need to be able to transfer the concepts of these three major components: the saturable absorber, the gain medium, and an output coupling mirror.

Experimentation has shown that we have the capability to use an all-fiber cavity [61], with Erbium-doped fibers (EDF) behaving as a gain medium. These Erbium-doped fibers also operate at a convenient wavelength of 1.55 μm, which allows for mass-produced telecommunication fibers that also operate in this wavelength range to be used in conjunction with these EDFs. Development of erbium-doped comb systems have proven to be able to sustain mode-locked operation for spans reaching weeks at a time in a laboratory setting [62], gaining appeal in precision measurements. While mode-locking is important in any laser ensemble, an all-fiber cavity can also be configured to be bidirectionally mode-locked, allowing for common-noise cancellation and stabilization of repetition rate differences [63], which is important in the realm of dual-comb spectroscopy.

An all-fiber cavity is a beginning to a system that can withstand a field measurement, but so far, we have only converted our gain medium to a fiber component. If we are to maintain mode-lock for long periods of time, we need a saturable absorber analog that will allow pulses to periodically come back and reflect again. In the case of the Agrocombs system, the only free-space optics will be a small gap of the fiber leading to a lens that has a SESAM that has proven to assist in achieving high repetition rates [64]. These SESAMs are created typically from a single quantum well absorption layer near the surface of a semiconducting Bragg mirror. Reference [65] describes this Bragg mirror as allowing nearly no absorption due to its large band

gap energy. The low absorption is useful for upkeeping the intensity of outgoing light and is supported by the quick recovery time (typically on the order of picoseconds to hundreds of picoseconds) of the SESAM from saturation. The downside in this case is that our mode-locked laser will not be the quietest pulsed laser, in part because of this awkward free-space portion that we couple back into fiber. But any phase noise can be corrected in analysis after measurements.

In fiber, two polarization modes are allowed to propagate and interact with one another, and with the fiber's cross-section being elliptical and its material possessing some amount of birefringence, this can lead to the beam's polarization evolving over time. This evolution can lead to difficulties in keeping the combs mode-locked, as well as make the detection of the offset frequency more complex [64]. Many fiber comb systems are made more robust through use of PM fiber, a fiber specifically designed to reduce or eliminate polarization wander [58]. The use of both PM fiber and a SESAM allow for long-term mode-locking with reduced wander from polarization interactions in the fiber. With long-term locking of the combs and a high repetition rate (200 MHz region), the DC system maintains a large bandwidth in the optical spectrum (approximately 35 THz), per Eq. 2.5. In order to maintain cost effectiveness, we can construct our pulsed laser DCS system to be made with PM fibers until the two comb signals are combined, where we can continue on with readily available SMF fiber.

Aside from stability, an outdoor measurement would require the system to maintain its precision over time. In many methods, the spectrometer setup requires a reference gas, often through the use of a reference cell [66]. Inclusion of a reference gas can range from a relatively large (several feet tall) gas cylinder to further compacted reference cells, down to advances in hollow-core fibers that can be filled with reference gas and used as portable cells [67–70]. Dual-comb spectrometers have been shown to operate independently of frequency references [59] such

as reference cells, and can instead be referenced against a small, portable continuous wave (CW) laser [71]. Experiments in outdoor settings have been conducted already that prove the merit of referencing against a portable CW fiber laser [58], strengthening the argument in favor of DCS as a method for field measurements.

In summary, fiber systems are lightweight and flexible, making them portable and able to easily manipulate the transmittance of the beam around difficult geometries. Their cost-effective nature does not take away from the proven ability to stay mode-locked and stable for long periods of time, while doped fibers can also be used as laser cavities, further reducing traditional optics. One can compose an entire laser system of fiber components, while still performing highly precise measurements over long distances in less-than-ideal conditions, as proposed for future experiments with the Agrocombs system.

2.3.2 A Lab on Wheels

While fiber optics give our experimentation the advantage needed to no longer worry about transporting a beam over hundreds of meters (if not kilometers) of agricultural land, there are other considerations to be made for the robustness of an outdoor measurement. The Agrocombs system has several components to consider when performing a measurement: fiber for the transportation of beams, optical transceivers and their reflective partners, and the DCS system itself. In this section, we will discuss the major points of constructing a robust system, with further details of the implementation of the Agrocombs and the equipment specifications given in Chapter 3's discussion of the first experiment.

It has been established that any light from the DCS system will be transported by SM fibers, but it has yet to be discussed what we do with this light. To carry out a measurement, we

need a path for the beam to travel through and back, so that the collected light can be guided to a photodiode for analysis. The means by which Agrocombs intends to achieve this is through the use of optical transceivers, and retroreflectors. These transceivers are simple in design; a tripod at one end of the path balances a simple optical setup, while a retroreflector at the opposite end of the path awaits the beam to reflect back to the transceiver. The optical setup, in its simplest form, consists of the fiber output and an off-axis parabolic mirror. Light from the combs leaves the fiber output, hits the off-axis parabolic mirror, and then is propagated across the field to the retroreflector. Returning light will come from the reflection off the retroreflector, then hit the off-axis parabolic mirror, before returning to the fiber output. This is the simplest form of our optical transceiver, with a photodetector housed in the mobile lab for the transmitting light to couple into upon its return. The hollow retroreflector is a combination of three flat surface mirrors that are configured to make a corner cube [72], allowing light to hit the retro at any angle and reflect back along the same path. With this configuration, we are able to use the same fiber for the outgoing pulse train as we do for the incoming pulse trains.

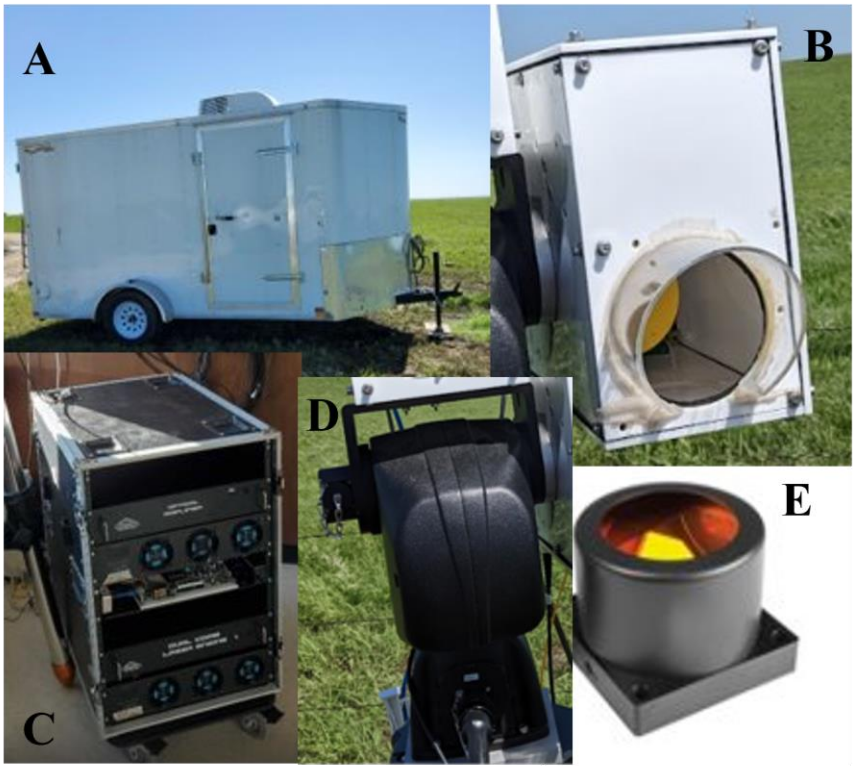

Figure 2.3 Images of main components of the Agrocombs system. A) Our mobile lab that houses the DCS system and additional tools. B) Optical transceiver, designed to transmit light across beam path and receive returning light to a photodiode. C) DCS rack, housed in our mobile lab. The rack is compacted to contain a fiber-based laser system and a rack-mounted computer. D) Gimbal for mounting transceivers, capable of movement for optical alignment. E) Retroreflector used to reflect light back into transceiver, mounted on the opposite side of the beam path from the transceiver.

The DCS system can be packaged with fiber components to be housed in an equipment rack. For our first iteration of the Agrocombs, this equipment rack was heavy enough to require the use of a forklift for transportation and was approximately five and a half feet tall. This rack encompassed not only fiber lasers, but also oscillators, temperature control units, current controllers, a CW laser, and the rack's own cooling fans to circulate air. Packaging the entirety of the system also allows for ease-of-use when connecting only the rack's power to electricity, rather than every separate component, allowing for the use of an uninterruptible power supply

(UPS) to protect from any possible short-term failures in the field. A computer for remote operation and control of mode-locking the combs must also be present for the measurement.

Figure 2.4 The DCS rack from our first experiment, discussed further in Chapter 3, is pictured on the left. The rack was compact enough to be moved but was far too heavy to escape the use of a forklift. On the right, the newly packaged system is far more compact, integrated as a full system, and light enough to be lifted by two people. Photo credits to Eduardo Santos and Brian Washburn.

Between the entirety of the DCS system and the computers needed to operate the DCS and other remotely accessed equipment, there has to be some form of structure. Further measurements in other agricultural systems call for the construction of some portable home for the Agrocombs, especially if we planned to stay noninvasive to the surrounding processes and daily operations. With this in mind, a trailer was purchased to house the system and any

accompanying electronics. The trailer can be hauled to a site, transceivers and retroreflectors can be set up to establish beam paths, and SM fiber can connect the trailer to the transceivers. This led to our mobile lab, pictured in Figure 2.5. The system can now be moved and set up without major construction, prepared for deployment in a field measurement.

Figure 2.5 A view of the Agrocombs trailer parked on-site for our first measurement, discussed further in Chapter 3. The trailer houses most electronics and computers related to the Agrocombs system and our comparative system, the CRDS. The trailer's temperature control is adequate to keep the combs stable, while access into the trailer is granted through portholes. Photo credit to Brian Washburn.

Chapter 3 - The Feedlot Measurement

Previous DCS measurements for gas detection have been implemented in the oil and gas industry [73], but the Agrocombs usher in a new line of experiments in the agricultural sector. An appropriate outdoor measurement must be conducted to observe whether or not the Agrocombs system could begin to address concerns in precision detection techniques discussed in Chapter 1. The unfamiliarity of measuring in a livestock system calls for proof of our ability to measure relatively low concentrations (parts per million) of methane, carbon dioxide, and ammonia, while also surviving conditions found in a Kansan farm site. A controlled beef stocker site provided ample opportunity for emissions detections, particularly of ammonia and methane from cattle, as the livestock would be homed in pens within a set area, with their consistent feed regularly provided by site operators. Furthermore, while DCS negates the need for a constant reference gas to be present for calibration, we must prove our accuracy and robustness against a system currently trusted by agronomists. This thought brought about the comparative measurement against a CRDS system, explained in section 3.1, a system well-known for its simultaneous detection of gases for outdoor measurements, and often used in methane detection experiments.

The 2006 IPCC report [10] gives guidelines for estimating cattle emissions per feedlot size, as will be cited in the results from this measurement. Similarly, the US EPA currently estimates cattle emissions through a calculation method known as the CEFM [74]. This model multiplies together two important factors: a gross energy intake and number of cattle present in a system. The CEFM's gross energy intake is derived from the guidelines in the IPCC reports. Gross energy intake is, in its essence, a calculable variable depending on the type of feed, digestibility of the feed, and metabolic function related to the type of cattle present. This means

that, in its entirety, the CEFM focuses on the idealized emissions of an animal and does not consider individual farm practices of the system that the animal exists within. Estimated methane produced from a feedlot can come down to a multiplier of one animal's expected emissions multiplied by the number of cattle. With the Agrocombs system, we can do two things simultaneously: We can test our system's results against a trusted and well-known system such as the CRDS, while also comparing results against the IPCC guidelines for a feedlot of the given size.

Our plan to test the Agrocombs system against the CRDS came to fruition in late 2019. The experiment would consist of measuring methane emissions in a feedlot setting, giving us ample gas from the high concentration of animals in a centralized location, and comparing results against the CRDS results and IPCC guidelines. Two paths would be utilized, allowing for comparison of concentrations, and eventually gas fluxes, between paths over time. Further discussion of gas flux computation will appear later in the chapter. The experiment also would require three-dimensional wind data taken in real-time for the site for two primary purposes: 1) comparison of concentration patterns against wind data and 2) use for calculating fluxes. The CRDS system would be used simultaneously, where the two systems would need to mimic similar paths for proper comparison. While the Agrocombs system can simultaneously measure methane, carbon dioxide, and ammonia with its wide spectral coverage, the closed-path CRDS system will not be providing ammonia measurements. Despite this difference, the large focus of the measurement should be the emissions of methane, due to its large presence in enteric fermentation processes, and its importance in overall greenhouse gas emissions. With these conditions set for the measurement, we set forth to prove the efficacy of the Agrocombs.

3.1 Closed-Path Cavity Ring Down Spectrometer: Picarro

Before any measurement can be performed, one must know the specifics of current methods in use. Current measurements of gas emissions from localized systems can be performed through various methods with commercial detectors, several of which utilize methods previously mentioned such as TLAS [75]. These detectors still face the limitations of their methodology (as discussed in Section 1.1), meaning that TLAS detectors need to be purchased to measure a specific gas of interest, leading to quickly mounting costs with any additional gas measurements. In the oil and gas industry, these systems tend to thrive for the purpose of leak detection, but in the face of agricultural measurements centered around several gases of significance, fall short in cost and operational efficiency. TLAS and FTIR have fallen short of the ideal measurement we wish to undertake, be it through a lack of capability in simultaneous multi-gas detection or additional reliance on mechanical components that affect acquisition time. In the stead of these methods, a forerunner in the commercial space of spectroscopic methods has pulled forward.

The Picarro is a commercial system that utilizes a patented cavity ring-down spectroscopy (CRDS) technique to perform precision gas concentration analysis. The system claims an impressive parts per billion precision, while maintaining simultaneous multi-gas detection over long-term field deployment with an insensitivity to ambient temperature fluctuations [76]. These closed-path systems are marketed to detect specified gases of interest, and have been proven as reliable sources of emission sensing in agricultural or atmospheric measurements [77–81], as well as reaching into the oil and gas industry [82–84] where TLAS and FTIR have traditionally been the standards. Previous studies have even been performed to detect emissions from cattle rumination [85], proving the efficacy of this system for the

Agrocombs measurement in question. While this system can maintain high sensitivity and multi-gas sensing, there is a fundamental difference in the method of gas detection between the CRDS system and the Agrocombs. The CRDS system utilizes a gas manifold scheme; several air inlets capture samples of the surrounding plume in their vicinity, where a constant flow rate transports the sample to and through the laser cavity for analysis, then vent the sample to open air in another area. This means that the CRDS system is a closed-path system, where the sample is introduced into the chamber and kept in a closed circuit of flow, whereas the DCS system is open-path, meaning that the beam interrogates the surrounding air rather than sampling and displacing it. As previously stated, the Agrocombs take advantage of a collimated and continuous beam path, sampling at all points of the beamline. Furthermore, the DCS system measures concentrations over the entirety of both beam lines at all times during a differential measurement (where two beam lines are used to look at the enhancement concentration over background concentration between the paths), while a single CRDS system must alternate analysis over two paths in a differential measurement. This leads to uptimes for each path of less than 50% with the CRDS, which can influence results based on stochastic gas plume variability [86]. These fundamental differences in sampling result in one system (DCS) sampling two continuous line paths continuously over a 5-minute averaging period, while the other system (CRDS) samples by alternating between two paths over a 5-minute averaging period as several point sensors in a line formation.

3.2 Measuring Feedlot Emissions

The Agrocombs system was deployed in an agricultural setting to validate its ability to detect enhancements of methane and ammonia emissions above atmospheric background levels,

as is necessary for improvement of global emission inventories. In order to prove its efficacy for cattle emission detection, we provide a comparative measurement against an industry standard, the CRDS system. The search for an appropriate setting landed our line of sight on a beef stocker site operated by Kansas State University's Department of Animal Sciences. The ideal situation for our first experimentation would involve a system with a succinct area to source methane and ammonia from, while also producing enough of the significant gases to lay in the range of our resolution. While simultaneous concentration data for methane, ammonia, water vapor, and carbon dioxide were collected, this dissertation focuses on the retrieval of methane emission data. This section will discuss the assembly and setup of the system, choice of measurement geometry, and detail the additional considerations we made in order to perform an outdoor measurement in an agriculturally industrial environment.

3.2.1 Setup and Measurement Geometry

Careful planning precedes any long-term measurement, with no exception for our feedlot experiment. The beef stocker unit houses approximately 300 cattle when the animals are present, the vast majority of which are penned in a centralized area with dirt paths surrounding them, making it easier to transport a trailer onto the site and park it in a corner of the unit. The basic idea for the measurement is to have two sampling paths in which wind can carry gas through over time. Weather data collected from previous years in the area shows the prevailing winds are northernly and southernly throughout the autumn and winter (correlating to the time of year in which we would begin the measurement), with an average temperature variation of -10°C to 20°C [86]. Past data were evaluated to identify that the most useful paths for gas flux through the area would be a north and south path. With the temperature range and precipitation data, we can

draw conclusions about possible weather patterns to expect and try to prepare our system to face such conditions. Figure 3.1 shows some of the data gathered during the feedlot experiment (from late as an example of some of the presentation of weather data and how to best interpret these results. The wind rose (as shown in Figure 3.1A) can be read as showing wind direction (labeled in cardinal directions on the outside of the circle), while the magnitude of the wind speed is shown through the binned colors labeled on the legend. The spokes within the wind rose help us understand the percentage of time within the data's gathering time frame. For our experiment, data were collected for a total of 59 continuous days [86].

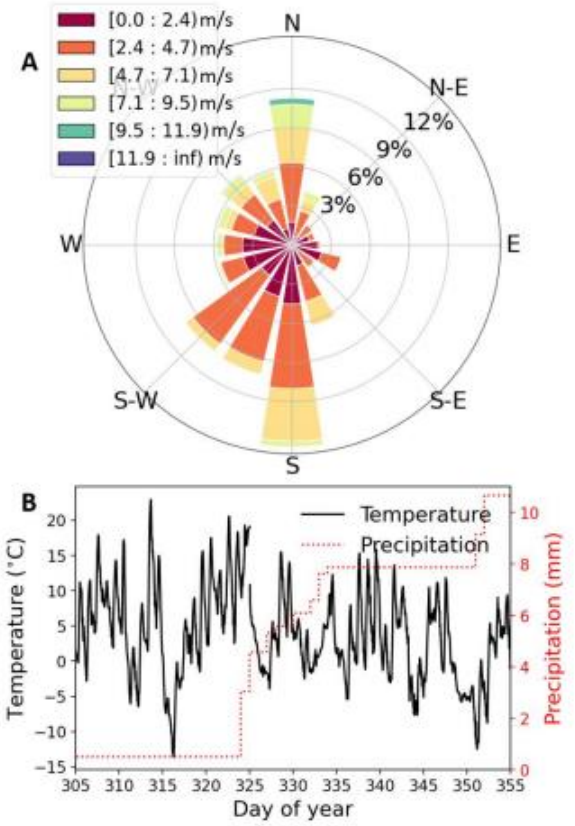

Figure 3.1 A) Windrose identifies that during days 303 to 362 of 2019 in Manhattan, KS. A large percentage of winds are north/south in direction, with winds reaching 2.4-4.7 m/s speeds regularly. B) Temperature and precipitation data for the corresponding time period in 2019. Image from Ref [86] and licensed under CC BY 4.0.

In October of 2019, we moved forward with the experiment assembly. Our mobile lab was moved to the beef stocker unit and parked in a far corner to avoid disrupting any routine traffic from site operators. We were eager to implement a comparative measurement between the Agrocombs and CRDS, leading us to mimicking the sampling paths after one another. This meant that we were able to lay the CRDS sampling inlets in a path similar to the continuous beamline produced by our optical transceivers. Figure 3.2 shows an aerial view of the feedlot and shows how we assembled our experiment to best perform without disrupting operations, while also using existing structure. Our retroreflectors were mounted to previously existing gate posts, while conduit housing the fiber, ethernet, and power connections to the far transceiver was aligned against troughs on the outside of pens to avoid being in the way of routine tractor travel.

Figure 3.2 Aerial view of beef stocker site. Approximately 300 cattle were present during the run in October of 2019 through January 2020. In the top right of the image, in the northeast of the site, we parked our mobile lab. Blue lines indicate our connections (fiber, ethernet, power) that were run and protected from the elements by conduit. Red arrows indicate the beamline, ending at the far west of the image by hitting retroreflectors. Each beamline is 50 meters in one direction, allowing for a 100-meter roundtrip beamline. White spools are indicative of CRDS sampling inlets. A weather tower with a 3D sonic anemometer was parked close to the trailer as well, for local real-time weather data collection. Base image courtesy of Riley County GIS.

Figure 2.3 was a simplified schematic of the Agrocombs system, but in actual field application, there are more pieces of the puzzle to consider. As stated before, this measurement will require two paths (a north and south path), meaning two optical transceivers and two retroreflectors. These paths, chosen due to the aforementioned principle winds, allow for measurement of significant gas in the upwind and downwind direction, which gives us a simultaneous log of background and enhancement concentrations, respectively [86]. Further, if

we wish to understand the net emission movements of methane and ammonia across the system, we cannot settle for concentrations of gases, and instead must shift our focus to the flux of gas in an area. By moving our sights onto flux, we need to collect real-time weather data to match our concentration measurements, leading to our usage of a small weather tower.

This tower was designed as a small flatbed with a vertical tower structure that allows for the attachment of our wind data instrument, a three-dimensional sonic anemometer [87], mounted at a known height of 3.5 m [86]. This device allows for collection of local temperature and wind data, the simplest of which would be the speed and direction of wind in the area. This is achieved by gathering orthogonal wind velocity components through the displacement of the pulses between the sensors on the anemometer, logged every 100 milliseconds [86]. Previous studies have proven the anemometer's nature is beneficial for a study like ours, while still being robust enough to survive the extreme weather conditions [88,89]. The weather tower also allows for pressure measurements. All weather information is sent to a datalogger [90] housed in the mobile lab. Precipitation was also logged by a nearby weather station in Manhattan, KS run by the Kansas State University Mesonet (MTNK1) [91].

A goal of the experiment was to achieve a large degree of remote operation, allowing us to develop the system as further noninvasive to operations on-site. Weather information was logged passively without operator interference, taking that responsibility away immediately from us. The interrogating beam must be aligned to the retroreflector in order to receive the resultant light, leading to an alignment procedure. Optical transceivers were already mounted onto motorized gimbals for alignment in setup, and so a remote connection through ethernet was established to the gimbals in order to operate the alignment remotely as needed. These transceivers are used to transmit light across the beam path, then receive returning light for

analysis after its reflection from the retroreflector. A more thorough discussion of optical transceivers can be found in section 2.3.2. To assist with this, we mounted small coaligned cameras to the breadboards on the gimbals and connected these cameras to a) the main operating computer for the north path or b) a small-frame computer hosted in a rugged box next to the gimbal of the south path. We were able to remote access these computers, run a program to send serial commands to the gimbals, and watch a set of carefully placed crosshairs on the camera image move in accordance with the commands. As we aligned, we also watched the returning spectrum from the transceivers, to ensure that we were maintaining an appropriate level of voltage return on our photodetector. Remote accessibility was also a requirement for the operation of the combs and will be explored further in section 3.2.2.

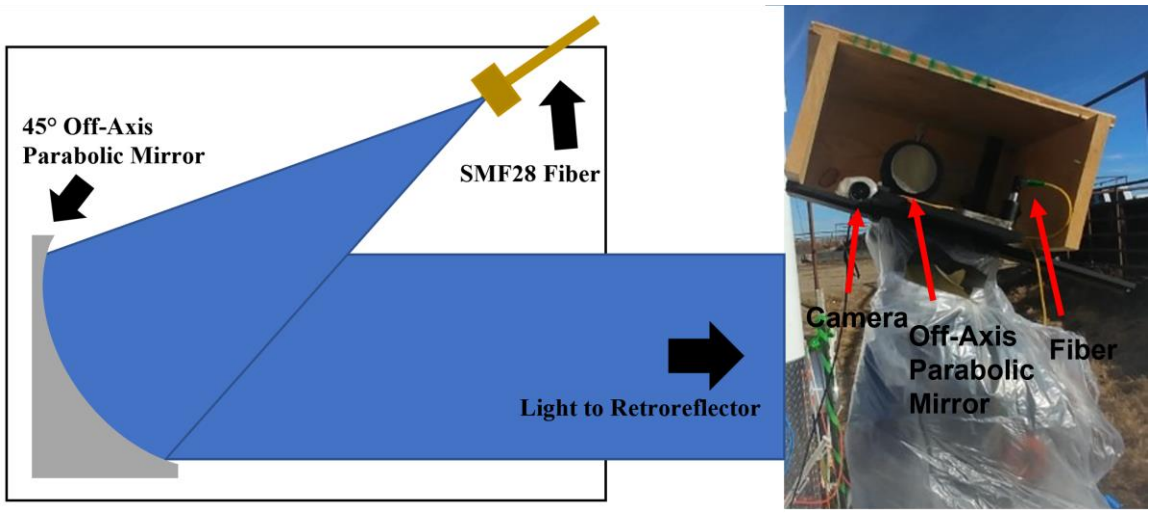

Figure 3.3 On the left, a schematic of our feedlot optical transceiver. The design is simple and utilizes fiber to carry back the returning light to the trailer where the photodetector is in the mobile lab rather than with the rest of the transceiver design (as described in section 2.3.2). North path transceiver on the right. We assessed the need for weather proofing around the gimbal and proceeded to wrap it in plastic to keep away moisture. The breadboard went through several iterations of protective shields before we settled on a wooden housing to keep out rain and minimize wind to the best of our ability.

Fiber connections to the transceivers differed in length depending on the path. The north path is the beamline closest to the trailer, which only required 10 meters of fiber to be run from the Agrocombs rack in the mobile lab to the tripod itself, achieved through the use of a single-mode fiber (SMF). The southern path proved the more complex for light supply, as the distance from the trailer and the geometry of the unpaved roads about the pens dictate a large degree of how we lay fiber. The final decision was to use 200 meters of SMF, protected largely by conduit alongside the ethernet and power cables, and lay it against the troughs outside of the pens, as seen in Figure 3.2. A partial trenching of the conduit allowed for crossing to a small grassy area to hold the transceiver, putting the beamline outside of the line of agricultural processes, keeping our measurement minimally invasive to the site. Furthermore, in order to guarantee a guard against a failure in one line of fiber while it is partially trenched, we employed a duplex SMF that allows us to have a second fiber line to change to if there is a failure in the first. With both transceivers supplied with light, and the experiment following the geometry of Figure 3.2, that leaves the Agrocombs system's initial measurement with two 50-meter paths in a single direction, resulting in 100-meter roundtrip paths for light. Approximately 10 mW of collimated, eye-safe light was sent out to reflect from the retroreflectors, which had diameters of 5 cm [86], return to the transceiver for analysis.

3.2.2 The Agrocombs System Performance

Our goal was to carry out a detection experiment for methane emissions from cattle in a controlled beef stocker situation, much like the measurements requested for improvement from the US EPA. We were successful in assembling a field-ready dual-comb spectroscopy ensemble, capable of simultaneously detecting several gases of interest: ammonia, methane, carbon dioxide,

and water vapor. This was achieved through our broadband spectral coverage, allowing for detection through several bands of well-known absorption in the specified gases, giving us total coverage of 35 THz. To minimize focus on frequencies without useful observable absorption, a band-stop filter was applied, catering to a 25-nm filtering width and centered at 1560 nm [86].

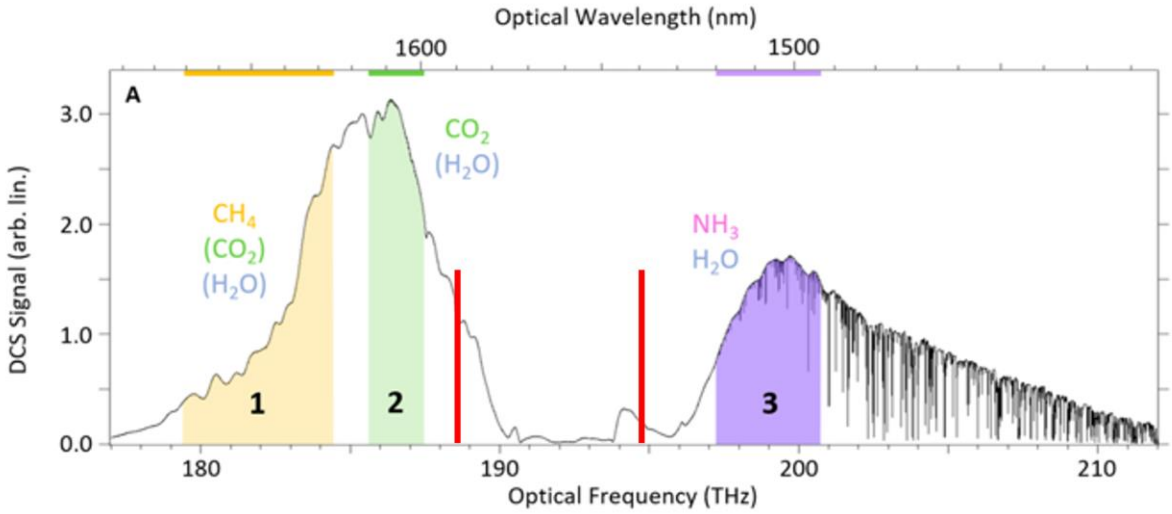

Figure 3.4 Full breadth of DCS spectrum, shown at 5-minute averaging time, exhibiting the use of our band-stop filter (red lines roughly outline the range of frequencies filtered out) and the bands that contain absorption for gases of interest. In parentheses are weaker absorbing gases within those bands. With the use of molecular absorption databases, we are able to analyze despite the constant and significant presence of water vapor in each band. Image from Ref [86] and licensed under CC BY 4.0.

The combs functioned with repetition rates maintained around 200 MHz, allowing for 175,000 individual comb teeth for encoding transmission [86], as a comb tooth is repeated every 200 MHz in our 35 THz spectral window. As discussed in Chapter 2, the most appropriate design of the system is a SESAM-modelocked, Erbium-doped fiber laser with polarization maintained through PM fibers. The use of an f-to-$2f$ interferometer allows us to phase lock f_0 for each comb, while an additional phase lock to an external-cavity 1560-nm diode laser establishes mutual coherence between the combs [59]. It is necessary to establish a difference in repetition

rate between the combs that can be maintained over long periods of time. Our operation under a Δf_{rep} of 208 Hz comes from a relationship built off of Equation 2.1. For a singular comb, we know the frequency of comb tooth n is determined by the relationship in Equation 3.1. If we have two combs whose repetition frequencies are offset by Δf_{rep}, then the frequency of comb tooth m in the second comb is determined by Equation 3.2.

$$\upsilon_n = nf_{rep} + f_{ceo} \quad \textbf{3. 1}$$

$$\upsilon_m = m(f_{rep} + \Delta f_{rep}) + f_{ceo} \quad \textbf{3. 2}$$

Both combs are locked optically locked to a frequency υ_0, meaning each comb has a tooth whose frequency is locked to the narrow linewidth (on the order of kHz) of a CW laser (υ_0). We therefore have comb tooth n_0 from comb 1 and comb tooth m_0 from comb 2 both relatively close to frequency υ_0, where the difference is our optical lock frequency f_{opt}. Therefore, the frequencies of these comb teeth can be described in the following expressions.

$$\upsilon_0 + f_{opt} = \upsilon_{n_0} \quad \textbf{3. 3}$$

$$\upsilon_0 + f_{opt} = \upsilon_{m_0} \quad \textbf{3. 4}$$

From there, we can use Equations 3.1 and 3.2 to solve for a ratio of f_{rep} to Δf_{rep}.

$$n_0 f_{rep} + f_{ceo} - f_{opt} = m_0(f_{rep} + \Delta f_{rep}) + f_{ceo} - f_{opt} \quad \textbf{3. 5}$$

$$n_0 f_{rep} = m_0(f_{rep} + \Delta f_{rep}) \quad \textbf{3. 6}$$

$$\frac{f_{rep}}{\Delta f_{rep}} = \frac{m_0}{n_0 - m_0} \quad \textbf{3. 7}$$

Assume that $n_0 \cong m_0$, or that $|m_0 - n_0| = k$, a small integer. If we set k to 1, we can solve for Δf_{rep} in terms of υ_0.

$$\Delta f_{rep,k=1} = \frac{\upsilon_0 + f_{opt} - f_{ceo}}{{n_0}^2} \quad \textbf{3. 8}$$

We then can generalize for our expression of Δf_{rep} for any k.

$$\Delta f_{rep,k} = k\Delta f_{rep,k=1} \quad \textbf{3. 9}$$

If we set $k = 1$, and know that the comb tooth number $n_0 \cong m_0$ is also equal to the number of desired points in our resultant interferograms (approximately 957462 points in a single interferogram), we can use this knowledge to solve for a $\Delta f_{rep,k=1}$ value to give us the ideal repetition rate difference between the combs for operations related to the number of points in the interferogram. We also know that υ_0 is determined by the CW laser and is approximately 191 THz (191495122962068.62 Hz), which will dominate the numerator in Equation 3.8. If we

then use our v_0 and n_0 values, we can find our desired Δf_{rep}, giving us the 208 Hz that we use for our operation's repetition rate difference between the combs.

$$\Delta f_{rep} = \frac{v_0}{{n_0}^2} = 208.8885488\ Hz \qquad \textbf{3.10}$$

Figure 3.5 shows a more tangible visual of the optics of the system. There is no additional need for a spectrometer outside of the DCS system, nor for field calibrations, but wavelength accuracy was ensured through the use of a quartz oscillator Global Positioning System (GPS). The schematic references the use of an Analog-to-Digital Converter (ADC), used to digitize RF frequency signal for computational analysis.

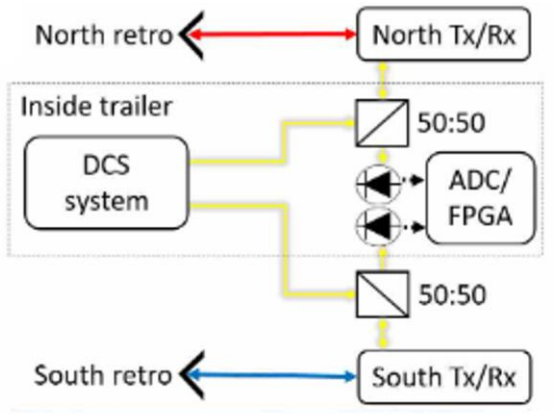

Figure 3.5 Simple schematic of the spectrometer used in the feedlot. Red and blue arrows indicate open-air path, while yellow indicates SMF lines. The labeled components were entirely fiber-based, and an FPGA was used to subtract phase noise on locks. Image from Ref [86] and licensed under CC BY 4.0.

Each comb had two locks to upkeep: an optical beat note (f_{opt}), or our "optical lock", and the carrier envelope frequency, known as f_{ceo}. By fixing the frequency of these two combs with the FPGA, we can ensure mutual coherence between the combs, resulting in the desired interferograms for analysis of emission concentrations on-site. Over time, the repetition rates of the combs may change, but the repetition rate difference is what is important to keep constant. First, we have f_{opt}, which is generated by mixing one of our comb teeth against the narrow signal of a CW laser. For the sake of outdoor measurement, a RIO Orion laser was chosen for this process, specifically for its more robust design and narrow linewidth. If we keep a comb tooth mixed against this CW laser, it is known that any change in the frequency of the CW laser would cause changes in our comb's repetition rate. To combat this, a servo is used to send feedback to adjust the temperature for the comb in order to adjust that particular comb's repetition rate to maintain a constant repetition rate difference between the two combs. Each comb has a tooth locked to this CW laser, giving us a f_{opt} lock for each comb. The second lock is f_{ceo}, which is generated from the interferometer and the use of supercontinuum generation, where the light goes through nonlinear processes to broaden its spectral contents from the original output of a pump beam, resulting in the broad, continuous spectrum seen in Figure 3.4.

Locking procedures for the comb are carried out through the use of graphical user interfaces (GUIs) developed to communicate to external equipment used in maintaining comb stability. For our system, two Red Pitaya boards are used to maintain and control the locks for the combs. The f_{opt} lock is upheld through adjusting the cavity length via a PZT, while also adjusting temperature for the cavity to keep within the correct voltage range for the lock. A PZT is a piezoelectric device, meaning that as an external electric field is applied, the device changes shape. The f_{ceo} lock is controlled by the modulation of the oscillator's pump diode current.

These functions are all performed by the Red Pitaya sending signals to adjust current or temperature. Before the Red Pitayas can perform these feedback functions, we must stabilize (or lock) specific conditions for the combs. Our system operates with a repetition rate difference of 208 Hz, with our f_{opt} and f_{ceo} both at approximately 28 MHz.

We begin locking after the oscillators are mode-locked and the system has had time to stabilize in its new environment (approximately 30 minutes). Then, we can set our oscillator temperatures to a previously recorded value to move closer to our designed repetition rate difference (Δf_{rep}). It is easiest to focus on one comb before moving to the next, meaning that we will first lock f_{ceo} for comb 1 in our GUI. It is imperative in the DCS system to designate the correct voltage-controlled oscillator (VCO) sign to avoid damage to the combs. The f_{opt} lock is known for having a negative VCO sign, while the f_{ceo} locks are known for having positive VCO values. The GUI makes possible our ability to modify gain, so once a beat note for f_{ceo} is locked, we can modify the gain to better the shape of the beat note. Once f_{ceo} for comb 1 is locked, we move to lock comb 1's f_{opt}. During this locking procedure, the quality of f_{opt} lock is determined by phase noise, which we aim to keep below 7 radms. Once comb 1 has both locks secured, we move to comb 2 with the same procedure. This is an iterative process, meaning that as we lock both f_{opt} and f_{ceo} for comb 2, we may need to go back and adjust the locking conditions for comb 1. There is an occasion where locking requires shifting from one comb tooth of focus to a new comb tooth for locking to maintain the desired repetition rate difference. This is possible by adjusting the temperature of the combs but must be done so to maintain the same VCO sign and f_{opt}. Increasing the temperature of the cavity will decrease repetition frequency for the comb. By doing so, we can keep the same f_{opt}, but shift to a new comb tooth, opening the possibility for a more stable locking condition for the comb in question.

In order to continue the theme of a primarily remotely operated system, the combs were required to be accessible from afar. As seen in Figure 3.5, the signal was passed to an FPGA for digitization and phase correction, detailed in the discussion of interferogram phase averaging in section 2.2, after its receival by a photodiode. This allows us to observe the received interferogram in real-time, as well as the corresponding spectrum, aiding us in our alignment of transceivers and maintenance of stabilized combs. The FPGA also aided us in the locking of the combs, where operators were able to use the two parameters necessary to maintaining all four locks for the two combs, with each comb dependent on two locks. Finally, the FPGA allows for stability for the repetition rates of each comb, as well as an external clock at 10-MHz [86].

In Chapter 2, discussion of SNR gave us relationships between this ratio and specifications of the system, such as the number of spectral elements or the averaging time. While this is a useful variable for discussing the system in itself, it gives us little leeway in the realm of discussing comparative precision against other methods. This has led to the arrival of a Quality Factory (QF), described in reference [44], and detailed in Equation 3.11.

$$\mathrm{QF} = \frac{\mathrm{SNR} \times M}{\sqrt{\tau}} \qquad \textbf{3.11}$$

This Quality Factor is particularly useful for measurements such as ours, where one of the main goals of the feedlot experiment was to test our precision against the CRDS system. The Agrocombs system functioned with a QF that exceeded 10^7 for our 5-minute averages, putting it in a comparable range against acceptable QF value for a comb system [44].

3.3 Feedlot Results

With approximately 300 cattle present at the feedlot, it was time to measure emissions. As this measurement began in late October 2019, and ran through January of 2020, the temperature conditions were sometimes widely varied, and often cold and humid enough to produce frost on equipment. Despite this, we were able to gather continuous long-term results over our operation period of approximately 50 days within our broad 35-THz spectral bandwidth to compare against the CRDS system. In total, our feedlot measurement was functional for approximately 59 days. In the time that we were present, from days 303 to 363 in the calendar year, there was an accumulated rainfall of 10.7 mm. This is minimal in comparison to the 61.0 mm rainfall in the month of October prior to our measurement, leaving the ground wet [86].

3.3.1 Methane Concentration and Measurement Stability

Weather data collected in the field included temperature and pressure, used to assist the beginning of a fit model for analyzing the spectra. This fit model implements the previously mentioned molecular database HITRAN, both the 2008 [92] and 2016 [42] databases. The fit model also made use of the cepstral-domain technique [93], which simplifies spectroscopy for non-ideal transmission giving way to reflections in results. This technique instead applies a technique for audio signal processing that allows the transmission to be converted to a molecular free induction decay in the time-domain for ease of use in analysis, separating this spectrum from the source intensity [93]. The feedlot measurement used a cepstral-domain filter to remove broad baseline structures that created unwanted reflections in the fit [86].

Methane concentration measured from both the DCS and CRDS systems can be found in Figure 3.6A. This time series represents an eight-hour span of measurement on the night of

November 17th, 2019, giving us a long-term stable measure of methane through the night. It was common to see our enhancement over the background to be in range of 600 parts per billion (ppb) to upwards of 1 part per million (ppm) in a particularly windy timeframe. Background measurements were, as expected at the time, approximately 2 ppm, while the DCS maintained precision of 1.25 ppm·m at 900 s. This is derived from precision of 25 ppb being averaged over the given path [86]. Previous precision for a DCS ensemble of similar specifications was stated to be between 1 and 3 ppm·m [35], landing our precision neatly into that range, as expected. From Figure 3.6A, we see that the two methods agree closely on both paths, following similar behavior and often overlapping.

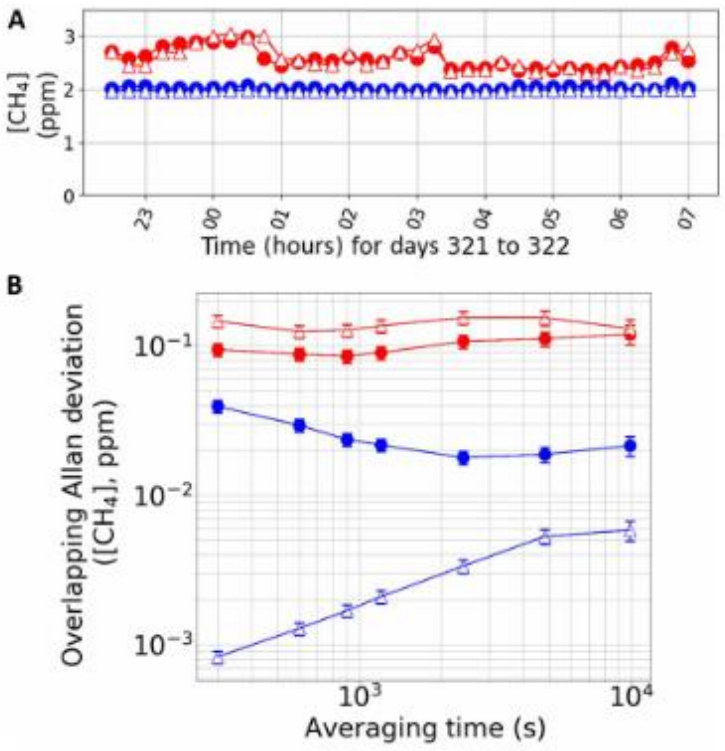

Figure 3.6 A) Concentration data between the Agrocombs and CRDS systems. Open triangles represent Piccaro, while closed circles are Agrocombs. Blue data is indicative of the south path, red for the north path. B) Allan Deviation for the two systems, red being the downwind path, blue being the upwind path. Circles are still DCS, triangles are still CRDS. Image from Ref [86] and licensed under CC BY 4.0.

Previous models and studies [94–97] have stressed the importance of a minimum averaging time of 15-minutes, leading to the averaging of data visible in the figure.

With the enhancements so minute above the background, a proper assurance of our measurement's stability could investigate the difference between systems more thoroughly. Figure 3.6B shows overlapping Allan-Werle Deviations (AWDEV) for both systems on both paths, giving us a closer look into instability over averaging time [98]. The A-W Dev is an adaptation of a longstanding Allan Deviation (ADEV), derived from an Allan Variance (AVAR). This two-sample variance reflects the stability of frequency [99,100], often implemented in oscillator and amplifier studies. It estimates stability in instrumentation that originates primarily in noise processes, allowing one to understand the relationship between averaging time and measurement stability. A low AWDEV indicates that, for the averaging time corresponding to it, the measurement is more stable. As we can see in the aforementioned figure, our downwind path shows stability in both systems that closely resemble one another, with the DCS exhibiting a lower instability than the CRDS. The upwind path, however, shows a plummeting AWDEV value for the CRDS versus the DCS for lower averaging times. This gives the CRDS system a precision higher by an order of magnitude in comparison to the Agrocombs system.

It is important to consider the difference in sensing between the systems while interpreting the AWDEV plot. The upwind path shows higher precision for the CRDS, but does not account for uncertainty in sampling, as AWDEV is focused primarily on instability from noise. The uncertainty in sampling derives from the point-sensor ensemble of the CRDS system, where each path must have an uptime less than 50% for the CRDS instrument to accept samples before swapping to the opposite path within a single 5-minute measurement [86]. So, while the

CRDS system is more precise in the background measurement, it cannot escape variability in the methane plume that the continuous line sensor of the Agrocombs system is not affected by. If we look at the difference between the DCS and CRDS for the downwind path, the precision in the CRDS system can vary from 20 to 40 ppb in a methane detection measurement, whereas the DCS system has a precision in the background detection of 25 ppb [86].

3.3.2 A Model for Flux and its Results

With methane concentration measurements compared, it is time to incorporate our wind data more precisely and look towards flux as a more appropriate comparison of systems. While raw concentrations give us the enhancement in an area of methane over its measured background, it does not necessarily enlighten us to the source of said emissions, which is important in a system that contains a complex set of moving sources (cattle). In a feedlot, the cattle have less room to roam, and the source area is more confined, but this will not be the same for systems that allow free roaming, such as pastures. For the sake of continuity and for accurate quantification of gas emission variability, we combine our concentration measurements with our three-dimensional wind data to obtain flux.

To compensate for moving sources in an area, and to infer a backwards path of the gas between the two paths, a footprint model would be appropriate for these conditions [94,101], specifically the use of an inverse dispersion model [94,102–104]. These models simulate and narrow down statistically possible paths for the gas to flow through the two measured paths. A stochastic backwards Lagrangian model, or inverse dispersion model (IDM), would allow for compensation in the case of both the CRDS (point sensor) system and the DCS (line sensor)

system. Previous studies have applied IDMs for feedlot measurements [105–109], further solidifying the choice for modeling flux.

3-D wind data and corresponding concentration measurements from both systems were fed into the program WindTrax [110], a free software that allows for calculation of emission rate as the user places sensors, sources, anemometers, and relevant structure onto a map to simulate the experiment's area of interest. The program does assume horizontal homogeneity for the ground surface but does take inputs of known heights for sensors. From WindTrax, we are able to inversely relate our concentrations to the source area, which in this case would be the pens of the feedlot. Previous studies [94–97] have stressed the importance of a minimum averaging time of 15-minutes in concentration data in order to be taken as valid for flux calculations, thus leading to our 5-minute average concentration data being averaged to 15-minute concentrations.

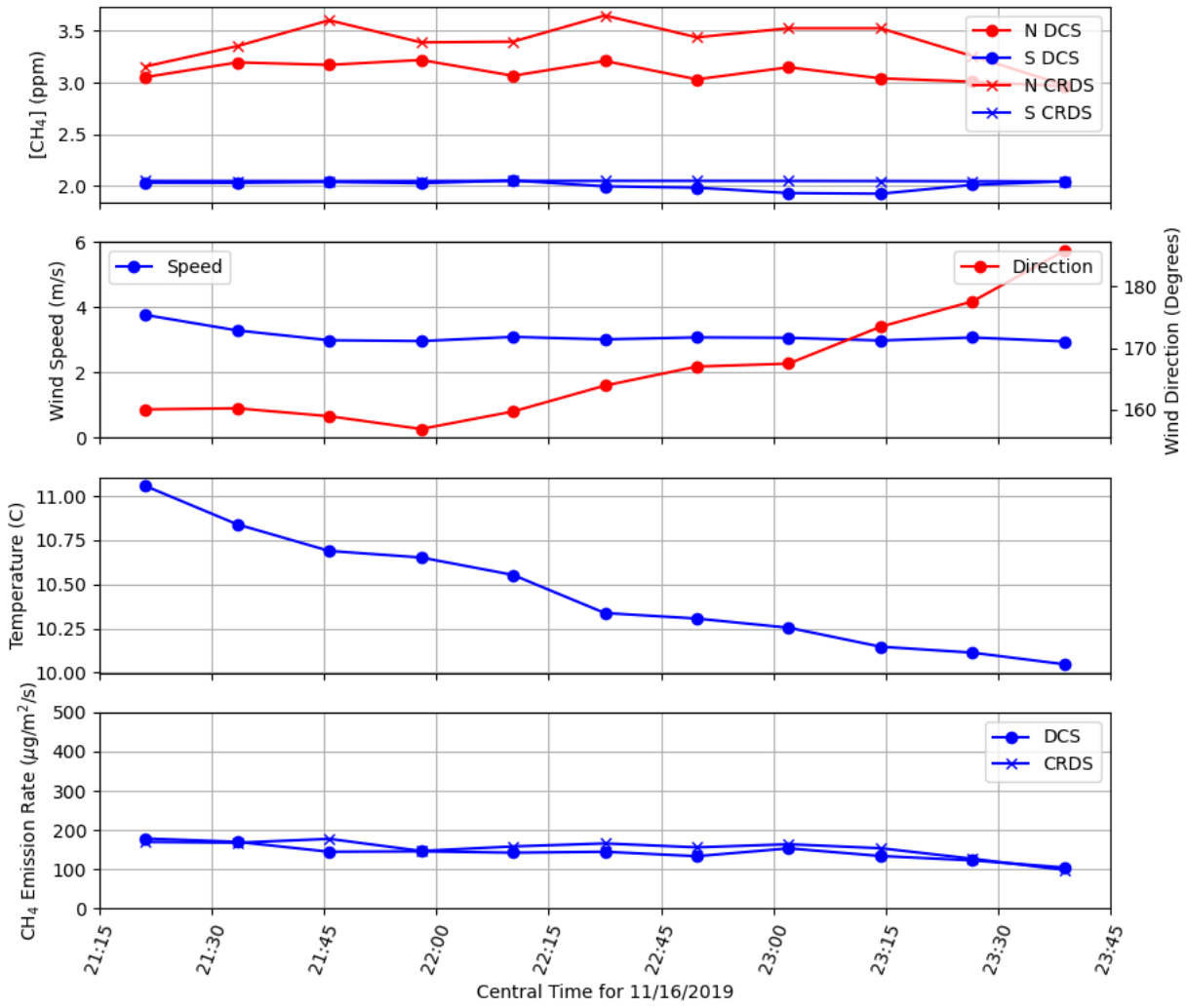

Figure 3.7 From top to bottom: 1) Methane concentration over the evening of November 16th, 2019, defined for both paths and both systems. 2) Wind speed over time, with corresponding direction. 3) Temperature measured, showing the drop over time as the cold set in for the night. 4) Emission rate of methane (flux) for both systems over time, showing their close agreement.

Figure 3.7 details flux over a night in November of 2019, allowing us to observe the relationship between our weather data, the methane flux derived from the systems' measured concentrations, and a comparison of the systems. If we look at the concentrations measured for this time period, the systems still closely follow each other in behavior. Wind speed mostly above 2 m/s in primarily a northern direction matches our ideal wind conditions for

measurement, allowing for appropriate enhancement detection over the background. If we look at the emission rate of methane in Figure 3.7, we can see both the DCS and CRDS systems present and see the close agreement between the two. The average flux for CH_4 detected from the Agrocombs system, keeping in mind to negate the manure contributions, was 137±86 $\mu g/m^2/s$. If we look to the Intergovernmental Panel on Climate Change (IPCC), in their 2006 report [10], the guideline for a feedlot of the size measured in Kansas dictates a normalized emission rate of approximately 135 $\mu g/m^2/s$. This leads us to conclude that our average methane flux per head of cattle agrees with the expected value. Methane fluxes for the two systems agreed within 6% of one another [86], successfully exhibiting the efficacy of the Agrocombs system against a commercially accepted standard, the CRDS system.

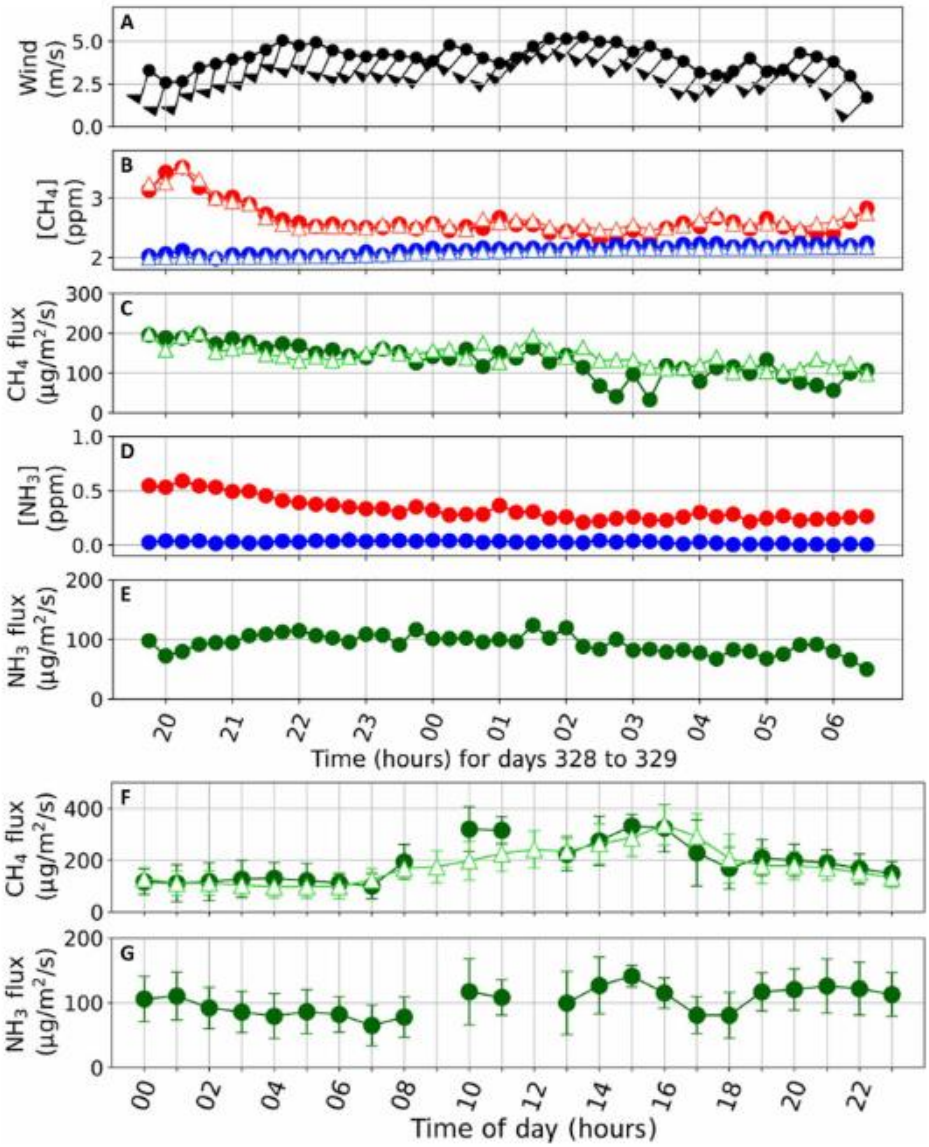

Figure 3.8 Long-term measurement showing the 24-hour span of methane and ammonia emissions. This exemplifies the diurnal cycle in a way that allows us to approximate the timing of components in the agricultural process. A) Wind data over twenty-four hours. B) Methane concentration and C) methane flux for both systems. D) Ammonia concentration and E) ammonia flux for the DCS system, simultaneously measured alongside methane. F) Methane flux comparison between systems. G) Ammonia flux determined from the DCS. DCS data is denoted as closed circles, open triangles for CRDS, with the north path (red) and south path (blue) compared. Image from Ref [86] and licensed under CC BY 4.0.

As we continue to measure longer and longer spans of significant gases, we begin to gain the ability to encompass an entire diurnal cycle. Observing the emissions from cattle in a feedlot

over an entire twenty-four hours can clue us in to specific components of the processes that occur on-site, primarily feeding times for the cattle. In Figure 3.8, parts B and C, we can see another example of methane concentration comparison between the systems, as well as the flux calculated from those concentrations, exhibiting once again their close agreement. It is worth repeating that the commercial CRDS is a closed-path system, implementing gas lines in its manifold system. Ammonia as a gas is "sticky", meaning it combines with other molecules at a high rate that makes it hard to discern from what it clings to, making its measurement difficult for closed-path systems that wish to keep their gas lines relatively clear. Because of the nature of NH_3 and the closed-path gas lines used in the CRDS setup, ammonia concentration was measured by the Agrocombs system as one of our other gases of interest in the feedlot but was not measured by the CRDS system. If we focus on the methane concentrations and their corresponding flux calculations, we can see the two systems corresponding in agreement. The stable wind conditions allow us to look at the flux as it changes without connecting those changes to weather, showing that flux is stable early in the day and upticks around the hour 8 mark. The flux increases and fluctuates back down to a stable condition around hour 18. This diurnal cycle shows a strong connection to observable feedings between 06:00-08:00 and 16:00-17:00 and could justify further studies of feeding times versus flux, as well as changes in feed and the effects on the diurnal results.

The measurement was concluded with data taken after the cattle had been moved onto the next step in their life cycle in mid-December, leaving the beef stocker site without livestock. By measuring emissions without cattle, we can further interrogate the lingering gas presence and stabilization of background without active sources. Both systems remained active until early

January of 2020, and the resulting data was used in conjunction with our data taken in the presence of cattle to assemble an array of fluxes for multiple runs.

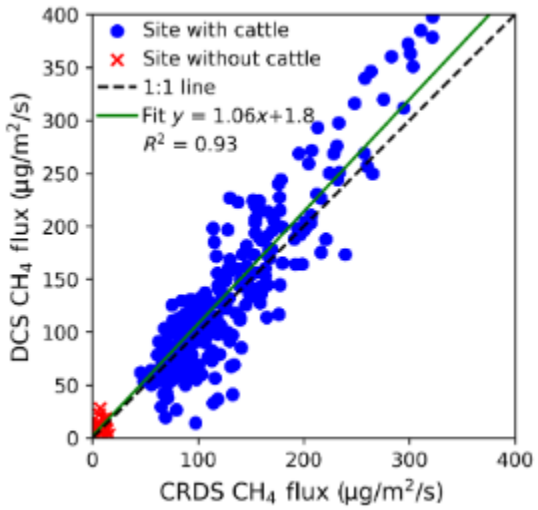

Figure 3.9 Methane flux data comparison of the two systems, both with and without cattle to compensate for background. Background offset was approximately 2 µg/m^2/s, which corresponds to about 2% of the flux in the presence of cattle. Image from Ref [86] and licensed under CC BY 4.0.

Figure 3.9 shows a direct and final comparison of the two systems, for cases of flux in and out of the presence of cattle. We can see that the resultant fit gives us a slope of 1.06, formally solidifying the 6% agreement between systems. Thus, this close agreement solidifies the Agrocombs in the use of agricultural sensing, proven through the first gas flux quantification in a beef cattle feedlot setting, performed by our group here at K-State [86].

Chapter 4 - From Feedlot to Pasture

The Agrocombs system proved its ability to compare with a widely accepted commercial closed-path system through our feedlot measurement in 2019 into early 2020. Our measurement was found to have a path-averaged precision for 15-minute averages of 1.25 ppm·m [86] in the case of 100 m roundtrip beam paths with a source of emissions containing approximately 300 heads of livestock. This experiment built a strong backbone for the Agrocombs project and laid the foundation for moving into bolder measurements, furthering the ability of precision agricultural sensing. This led to a rather natural progression of thought: If we could measure methane emissions in a more carefully controlled setting like a feedlot, could we perform a similar measurement in a more variable environment, such as a pasture?

When we measured emissions from cattle in a feedlot, there were preset expectations. We were comparing not only against the CRDS results for methane flux, but we were able to calculate the expected methane emissions per head of cattle in a feedlot of our site's size according to IPCC guidelines. As discussed in Chapter 3, the IPCC 2006 report [10] gives guidance on how to calculate gross energy intake, determined from several factors such as metabolic factors in cattle or types of feed. If we take the gross energy intake per cattle and multiply it by the number of animals, we find the expected emissions for the CEFM, used by the EPA to determine emission expectations from agricultural operations. The problem is that this is a model based almost entirely on just the cattle and does not consider sinks or sources in the operational system otherwise. In the feedlot, the system was primarily the cattle; there were no underlying agricultural operations at the beef stocker site aside from the cattle operation, and the cattle were confined in a controlled area. For a pasture, we know that the animals have far more room to roam, as well as less animals per area of interest. If we were able to estimate the

overwhelming emissions from approximately 300 animals, we now need to adjust to emissions over a much larger area for only about 25 head of cattle. By performing a measurement in a grazing system, we open the door to the possibility that emissions from a livestock operation are not as simple as the cattle themselves, where other factors may play a role in the net methane produced.

While one may ponder why to even consider pasture settings for a measurement when their emissions are lower than a feedlot system, grazing systems make up a majority of the livestock life cycle and present systems in the United States [111]. The emissions may be smaller for these more complicated pastures, but the sheer magnitude of systems that fall into this classification demands our attention in a remote sensing measurement if we are to truly understand the emissions related to particular agricultural processes, rather than linking emissions specifically to a number per head of cattle. Notable differences from the previous feedlot measurement to a pasture setting begin in the keeping of cattle, where the beef stocker site was designed to pen livestock into a smaller area to allow for less roaming, allowing the cattle to quickly gain weight as they became more sedentary. In a pasture setting, cattle will have the ability to roam, and the area of interest for gas emissions is several times larger than a feedlot's pens, often acres of land. There are also notably less cattle in a grazing environment, with a herd typically on the order of less than one hundred head of cattle, versus the 300 head we observed in a typical feedlot setting. Less cattle and a larger area of movement results in a direct reduction of the magnitude of emissions we would expect to see in a pasture. Past studies have already proven the efficacy of DCS in long-path open air measurements [34,35], making it an ideal candidate for measuring net methane emissions from a grazing setting.

The mobility and number of cattle are not the only complications to arise from these systems. In a feedlot, pens are not as well outfitted with foliage, and feed for the cattle is provided from site operators rather than grazed independently by the animals. Because of this, and the large area in which the animals are allowed to roam and choose their next meal, the native grasslands are relatively untouched. The soil in these systems is therefore less or often never fertilized, leading to significant differences in nitrogen fertilization specifically [112]. Studies have shown that microbial oxidation from bacteria in these less fertilized soils convert CH_4 to CO_2 at an estimated rate of 30±15 MMT/year [113,114]. This possible methane sink from microbial activity in soil means that the pasture setting could potentially involve less methane than expected from a specific number of cattle. The possibility of a sink from unfertilized soil means that models that estimate emissions from purely number of heads of cattle may miss a vital portion of a process's methane cycle.

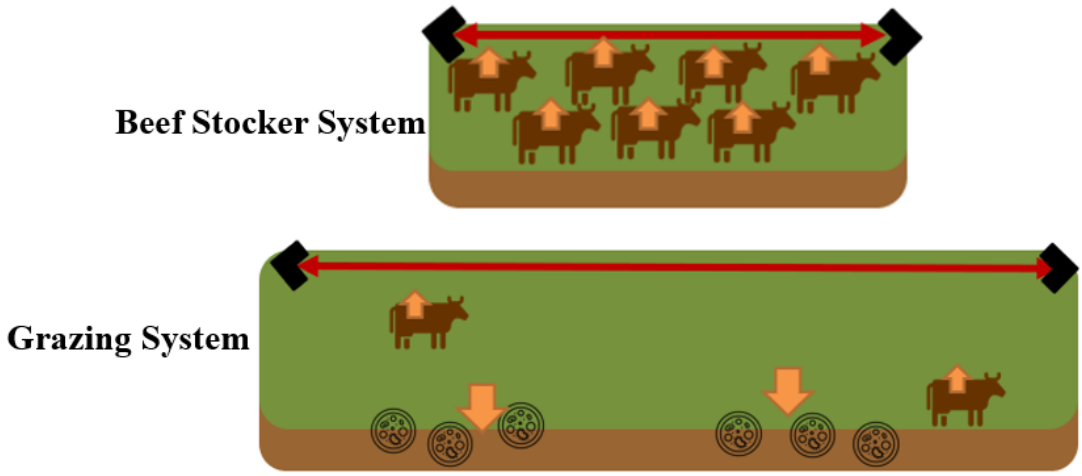

Figure 4.1 Above is a diagram to show the difference in measurement settings. The stocker site was more compacted and had more animals per area. The grazing system requires a larger area, less cattle, and a possible methane sink in soil microbial activity. The area difference alone leads to the need for a longer beam path to properly measure grazing emissions. The red indicates the beam paths from the DCS system that would be implemented in either measurement.

We can therefore narrow down our considerations to the changes of setting to three key factors: cattle mobility, smaller ratio of cattle to area, and microbial activity as a possible methane sink. These key differences mean that we need improvements to the system from our feedlot ensemble to properly measure emissions in a pasture. Larger areas of interest alone give way to the need for a longer beam path, and less animals means lower emissions, alongside the possible sink. The expected emissions are far lower than those measured in the feedlot, meaning our precision of the system must drastically improve. Adaptations to improve precision include manipulating the spectral window and will be discussed in Section 4.1 in greater detail. Furthermore, a newly packaged DCS system will be implemented in future measurements, creating the necessity to test this system and its corresponding optical transceivers. The largest visible update to the system is the move from our previous rack mount to a newly compacted system for better portability, including the control computer now being mounted into the new compact rack. Newly constructed optical transceivers make the move from our simplified transceivers in the feedlot experiment to packaging that includes better weather proofing, a detector within the transceiver box, and separate housing for a camera and LED system to use for nighttime alignment. On the software side, we have new data acquisition procedures and a more streamlined FPGA for real-time phase correction and hardware averaging of incoming interferograms. Between adapting the system's precision and testing new equipment, the Agrocombs project requires another proof of efficacy experiment.

Growing concerns over the differences in methane sources and sinks, as well as level of methane enhancements over background levels, have led to an intermediate experiment to take place before beginning live studies of pasture systems. This intermediate experiment is known as

a controlled release, allowing for the Agrocombs group to test the preliminary merit and precision of our DCS system against small enhancements above atmospheric background of methane in particular, as well as detection over large areas with fewer sources of CH_4. This experiment requires a known amount of methane to be released at a known flow rate comparable to the expected emissions of a small herd of approximately 20 cattle. This flow rate was determined by prior calculations and simulations performed by our agronomy colleagues, resulting in an estimate that, for low emissions, the rate would be approximately 100 g/day/head of methane, while a high emission scenario would produce 300 g/day/head. If our newly compacted Agrocombs system can detect the known emissions, measuring simultaneously once again against a CRDS closed-path system, we can assume that our precision is adequate for a pasture measurement involving actual cattle. This chapter relays the details of setting up and beginning this controlled release, including the difficulties of adapting to a pasture setting, considerations taken to improve our precision, and preliminary results.

4.1 Adaptation to the Pasture

As we began to consider the move to a pasture measurement, the opportunity to better the system also arose. In the feedlot measurement, a prototype of the Agrocombs system was implemented, contained in a large rack seen in Figure 2.4. This rack was not as portable as would be ideal and required the use of a forklift to transport. The rack also was not ideal for maintaining temperatures of the frequency combs, and the open structure led to concerns of damage from insects or rodents. While the mobile lab is secure enough to deter most rodents, insects can easily enter through port holes in the floor that allow us to run cables from the trailer to the transceivers, power, or CRDS inlets. This was a common problem with the original

Agrocombs system, where a mass of flies attracted to the cattle and manure easily found their way into the trailer, raising fears about their possible hazard to the rack's electronics and optics. These concerns are addressed in compacting the system with a rack that comes in at half the size of the prototype and can now be carried by two individuals by handles on the sides (as seen in Figure 2.4). This new system also has multiple fans to maintain temperature within, while also allowing us to close the front and back of the system from outside interference. Finally, a rack-mounted computer was included in the new version to narrow down machines connected outside of the rack and now functions as our primary DCS control computer.

Just as the primary rack system was improved, so were the optical transceivers. In the feedlot experiment, these devices were primarily a small optical bench mounted to a gimbal containing a servo motor [115]. The gimbals were wrapped in plastic to avoid water damage, while the optics were given wooden housing to keep rain off of them. This worked for our measurement but led to difficulties in alignment due to frost on cameras and slow gimbal responses. The new transceivers are instead packaged as a protective box around the optics, capable of heating and dehumidifying, while also containing a photodetector within the transceiver rather than the photodetector being in the trailer. This allows us to detect a voltage directly from returning light for use in a feedback system discussed later in this section. The new transceivers also include a box for newly improved cameras, allotting space for large lenses to improve our imaging, as well as protecting these cameras from the elements. Rather than our previous servo motor gimbals, we have moved on to a weather proofed stepper motor gimbal [116], allowing for fine control of our pan/tilt movements, and reacting quickly despite extreme weather conditions. Figure 4.2 shows the difference in transceivers from the previous measurement to the controlled release.

Figure 4.2 To the left, the transceiver used during the feedlot can be seen. While this was functional, it was not ideal, and left room for improvements in harsh weather conditions. To the right, the newly improved transceiver is pictured. These protective boxes shield optics and the camera from the elements. The accompanying boxes keep equipment off of the ground and protected from most rodents and insects. Photo credit courtesy of Brian Washburn.

In the feedlot, as we adapted to remote operations of the transceiver gimbals, we came across a problem with the gimbal furthest from the trailer; in order to improve responsiveness to commands, we needed a computer closer to the tripod, but kept safe from the elements. This led to an outdoor storage container modified to hold a small frame computer for the team to remotely access and control the far transceiver. In order to improve our control of the gimbals and create uniformity, we began to implement the ethernet connectivity of the new gimbal model to run to the trailer and connect to a single transceiver control computer. The new ensemble has been tested extensively with a newly developed gimbal alignment process, incorporating image

processing to recognize and align properly to the retroreflector. To support alignment, a voltage feedback system was implemented to read incoming voltage from returning light and relay that reading to a data logger to assist in correcting alignment on a finer level than image processing (see Figure 4.3). This is achieved by simply applying a bias T after the photodiode, allowing for the transmission signal to reach the DCS rack and the data logger without detracting from the RF signal sent through for data acquisition. The transceivers are able to automate a large portion of their alignment process through the use of spiral tracking, where the gimbal will take small steps in spiral motions and compare the DC voltage to determine in which direction to best move or when to stop based on the feedback voltage read on the data logger. Finally, a modified outdoor flashlight has been mounted atop the transceiver and can be remotely controlled to flash when the transceiver needs to align during the night, illuminating the path for the purpose of proper alignment. The final result is a system that can begin alignment, test movements through image processing and returning voltage, and move into alignment without an operator to instruct every step of the process.

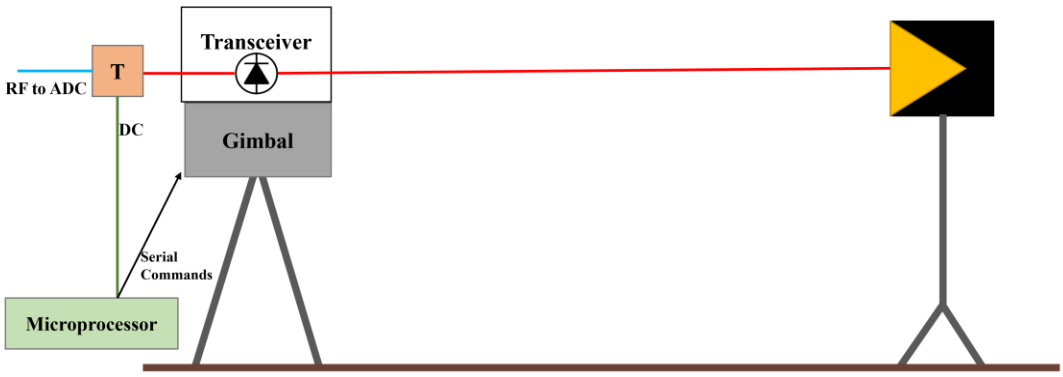

Figure 4.3 Schematic explaining the voltage feedback system implemented for the transceiver. The microprocessor (data logger) receives DC signals from the bias T, then communicates via ethernet to our alignment software to give us a visual representation of returning voltage as we align the transceivers, while also sending serial commands to the gimbal as we align.

We removed the rugged outdoor storage totes and replaced them with a sound alternative: latched equipment boxes on posts, removing the concern of water damage from sitting water, and minimizing exposure to the data logger, ethernet connections, and power strip for each transceiver station. These boxes, pictured in the right-hand side of Figure 4.2, are posted close to the tripods, and thus far have been proven to keep our accompanying electronics neatly organized while saving them from the elements and wildlife. Careful protection of cables is important, as our feedlot experiment revealed the appeal that some field rodents possess for chewing on cables. While we did run cables through conduits previously, this pasture setup has improved by adding flexible cable covers to some of the more fragile cables or the fiber entering conduits, providing another layer of protection from curious animals. These covers, the conduits, and a mixture of steel wool and dryer sheets stuffed into conduit ends have provided ample protection for the lines we must run from the trailer to the transceivers, as well as additional power lines.

With the equipment updated, we needed to solidify the precision adjustment for the detection of sub-ppb detection above background levels of methane. While several key parameters determine sensitivity in a DCS system, including the spectral bandwidth (Δn), acquisition time, and repetition frequency for the combs, we turned our eyes to another important attribute: the signal-to-noise ratio. As shown in Equation 3.11, the quality factor (QF) of a system is directly related to the SNR and spectral elements M, while inversely related to the acquisition time τ. This variable allows us to directly compare systems, which is important as we adapt our system to new processes to sense, allowing us to tune our precision and compare to past iterations. We know that $M = \Delta n / f_{rep}$, making clear the balancing act between spectral

bandwidth and SNR. Equation 3.11, in conjunction with Equation 2.4, gives us an understanding that if we were to narrow the spectral bandwidth, the SNR would increase. If we look at our feedlot experiment, we know that 5-minute averages were used with a SNR of 1000 over a 50-meter one-way beam path. The number of spectral elements required to cover the broad bandwidth in the feedlot measurement totaled 175000, allowing us to calculate a QF of approximately 10^7, as discussed in Chapter 3.

In reference [86], a path-averaged precision is discussed, determined through Allan-Werle analysis and the resulting methane concentration precision, dependent on acquisition time, and given as 1.5 ppm·m. If we were to expand to a longer path in the pasture, say to 500 meters, we would take this path-averaged precision and divide by the new path length, giving us the precision independent of the path for that particular setup. In comparative terms, we were able to detect 3 ppb in our feedlot study, but with the expected enhancements in a pasture to be a fraction of those detected in the feedlot, the estimated precision for a grazing system needs to be less than 1 ppb. We plan adjustments to the system through proposing that we narrow the spectral bandwidth and averaging over a longer acquisition time of 15 minutes (or 900 seconds). Our group determined that, for near-infrared methane absorption, the region of interest would cover approximately 4.5 THz, and with our repetition frequency still staying around 200 Hz, that gives us an M of 22500. If we wish to keep the same QF as our previous experiment, we will need to do some quick math to determine the needed precision.

$$\sqrt{\frac{300\ seconds}{900\ seconds}} * \frac{22500}{175000} * 3\ ppb = 0.2\ ppb \quad \textbf{4.1}$$

So, we see that, for the same QF from the feedlot experiment, we can adapt by narrowing the spectral window to focus specifically onto a window for near-IR methane absorption, as well as increase our acquisition time, and bring our precision below the necessary 1 ppb. While this may seem like a loss in terms of acquisition time, it is important to remember that in the feedlot our data recorded as 5-minute averages were averaged to 15-minute averages due to studies that cite this as the minimum time for these flux calculations with the IDM to be considered valid [94,96,97].

From the feedlot, we learned of numerous flaws in our setup procedure or equipment in terms of protecting the experimental setup from environmental dangers, including weather and wildlife. As detailed in this section, we have worked diligently to improve the system on several fronts. The rack has been compacted and ruggedized against insects and drastic temperature variations. We also have worked to implement our precision overhaul by adapting our spectral bandwidth in this new system, with the plan to take on a new acquisition time of 15 minutes, allowing us to reach the proposed precision necessary for the grazing system. The transceivers have been overhauled to be far more resistant to weather interference, as well as adding proper space for long-distance capable cameras to be utilized in image processing. In a combination of image processing, remotely illuminating the field, and interpreting voltage signals of received lights, the transceivers have become far more independent and capable of maintaining alignment as they work against drastic colds and strong winds. Finally, we have strengthened our protection of the cables, including the fibers, allowing for longer experimental runs as we deter wildlife and fight off the elements. With these improvements, we have taken the lessons learned from the feedlot in stride.

4.2 Controlled Release

With an improved system in tow, our group set out to plan a controlled release. A study of this magnitude requires a relatively large pasture at a reasonable distance from industrial agricultural processes so as to isolate emissions to as far of a degree as we can. We have been graciously given permission to operate at the Rannels Ranch, a research site operated by Kansas State University's Department of Agronomy and located outside of the primary area of the city of Manhattan, KS. This site contains several wedge-shaped pastures that contain grazing cattle during approximately May to late August or early September. For our controlled release experiment, in order to maximize our control of methane emissions, we needed cattle to be absent at the time of the measurement. Setup commenced during the summer of 2022 to test operations of the new comb system, as well as test the alignment procedure discussed in section 4.1.

4.2.1 Setup

We began by transporting our mobile lab to the Rannels Ranch, parking it near the fence line separating two pastures. Transportation was simple, as was the installation of a newly portable Agrocombs system. Two people were able to lift the rack into the trailer, and the wheels on the bottom of the rack allowed us to move it to an ideal position and adjust over time, as well as keep it in position with easy wheel locks. Adjustments were made by drilling a hole to the side of the rack to allow cables to pass through a small port hole for connections, as well as ports on top of the rack for the ADC connections and fiber. These adjustments to the rack allowed us to completely close the front and back of the system with covers, keeping out rodents and insects, as well as providing a more closed system for temperature control.

Figure 4.4 In the top left, our new beginning on the Rannels Ranch as we park the trailer in the pasture. In the bottom left, one can see the trailer in its current state, with the surrounding pasture recently having been through a controlled burn. To the right, the top of the DCS rack (seen in full in Figure 2.4). The red area shows the ports added for fiber and DAQ connections. In the light blue area, one can see the wall-mounted fiber and rf cables that allow us to strain relieve these connections, as well as easily access them.

As we did in the feedlot measurement, consideration of past wind conditions in this particular location was taken in order to plan the paths for the measurement. With this in mind, a wedge-shaped measurement was determined to be ideal, rather than the parallel path geometry used in the feedlot. This means that we still have two channels, now known as transceivers 0 and 1, or yet again a north and south path, that will measure methane emissions in a more triangular shaped area. In this area, the methane source is placed, allowing for gas to have a higher probability to pass through the paths of interest. Figure 4.5 shows the aerial visual of the Rannels Ranch experimental setup. In this configuration, beam paths are increased from the 200 m

roundtrip path to 400 m roundtrip paths, with space available for us to eventually push to longer beam paths for a pasture measurement.

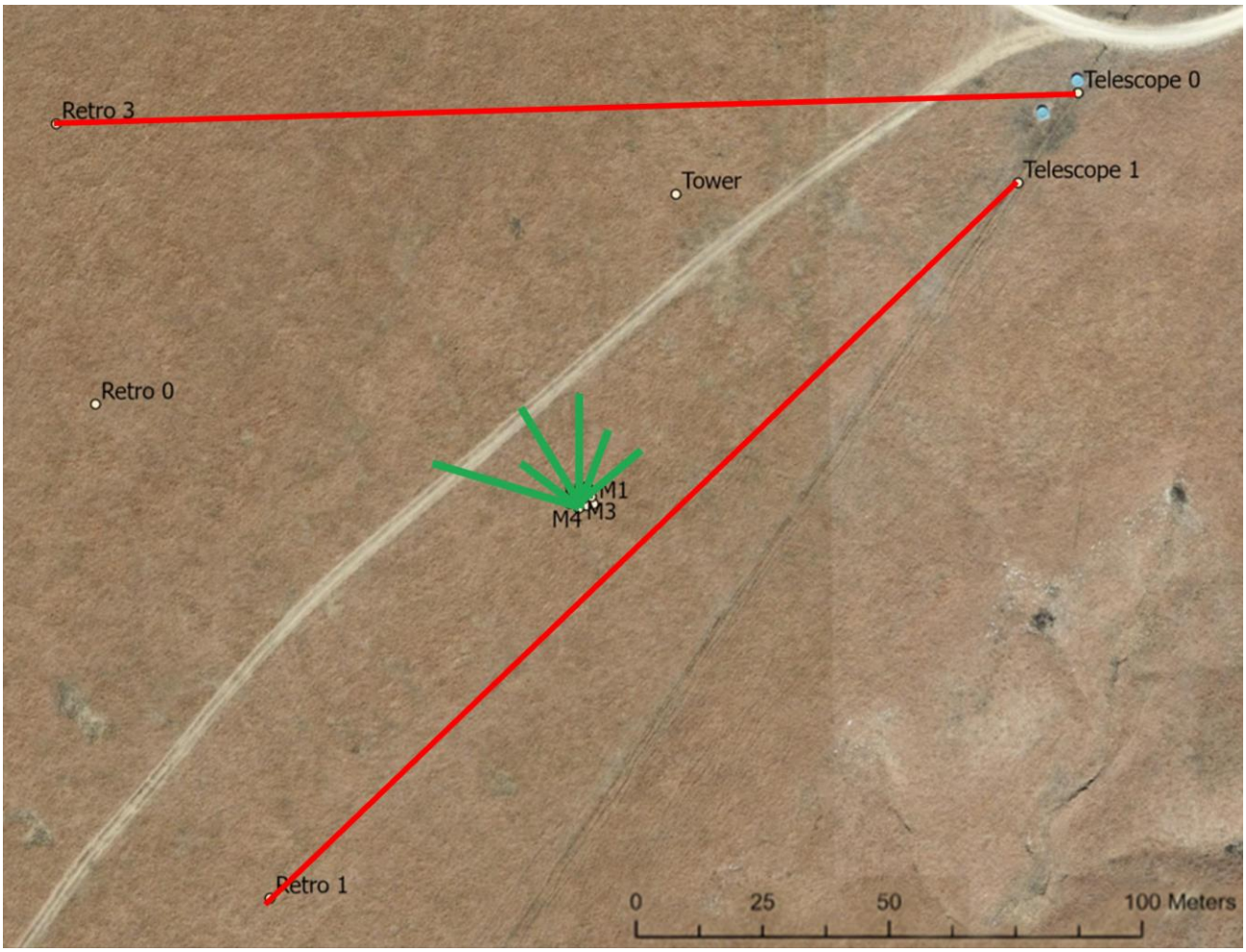

Figure 4.5 Aerial view of Rannels Ranch site for the controlled release. This view gives us locations for the transceivers (labeled as telescopes), with telescope 0 being our background detection, and variable choices for extra retroreflector setups for telescope 1 providing different enhancement measurements depending on the area of detection between the transceivers. Green is indicative of methane released from the controlled methane source at a known flow rate. Current paths are approximately 200 m in distance, but future paths will push to 400 km.

A third retroreflector was added as well, with the option to widen the wedge by transferring from one of the original retroreflectors. For the controlled release, additional

retroreflectors allow us to change our wedge area of detection and further test our sensing abilities of sub-part per billion enhancements in different geometries around the controlled methane source. The goal is to inevitably add further retroreflectors to aid in the detection of methane in conjunction with the mobility of cattle. While this is a feature that will be implemented more heavily once cattle are present, that does not stop us from setting up retroreflectors in the meantime, preparing for swapping what retros we are pointed towards with the beams. The complexity of changing retroreflectors has been taken into consideration in our analysis code as well, allowing us to change path lengths and combinations.

Figure 4.6 Left: North transceiver; note the box for electronics staked beside the tripod. Updated transceivers allocate protective housing for the camera, while having a modified flashlight mounted up top for flashing in nighttime alignments. Center: From North transceiver, an image of the South transceiver. Note the cattle pen gating used to protect transceivers from future animals, as well as conduit against the fence line. Right: Retro 1 on its stabilized tripod.

The methane source is designed to emit a known flow of methane under the group's control. This source begins with a gas canister of methane with a proportional valve attached to its output. This proportional valve allows for constant pressure in the manifold, also presumedly delivering equivalent flows of methane to our makeshift "cattle". For the cattle portion, ten outlet tubes are arranged equidistant from one another, each outlet representing two cows in a herd. This means in total, when these outlets release equivalent methane emissions, we will have a "herd" of 20 cattle to be the source for our measurement. We maintain a constant flow rate with the proportional valve, producing approximately 200 grams per head per day in our simulated cattle. At the beginning and end of each controlled release, we measure the weight of the gas canister to ensure that our flow properly resulted in the expected loss from our gas source.

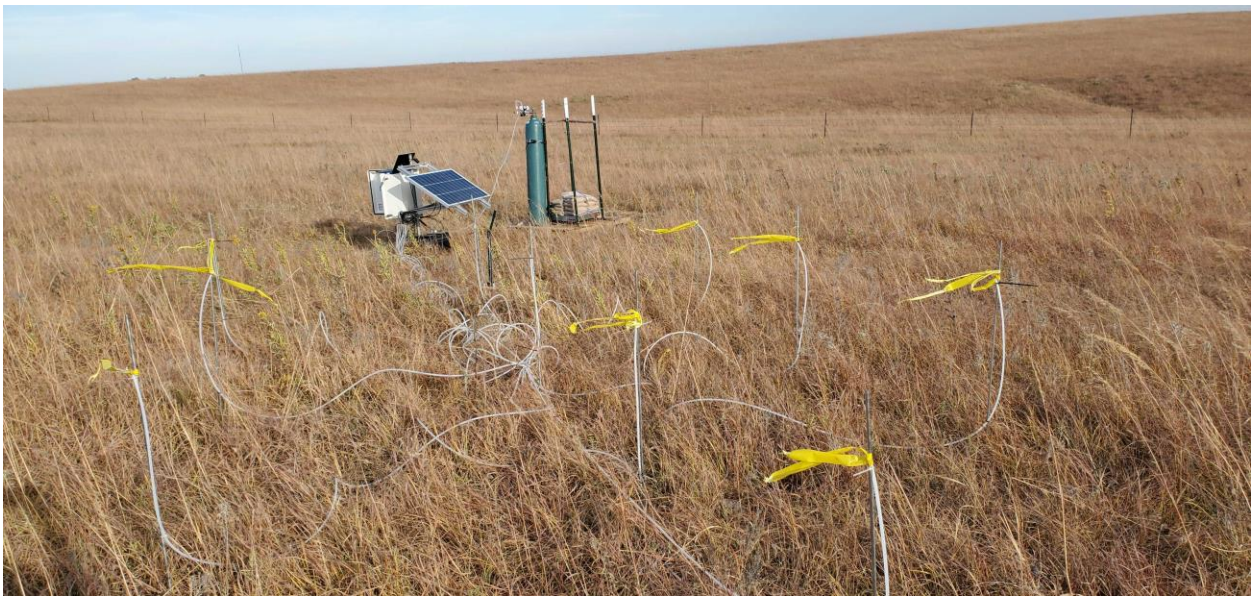

Figure 4.7 Manifold for the methane source. Note the gas canister in the background, mounted against a tall stake. Four stakes surround a digital scale (pictured with sand currently atop it for testing). The data logger in the enclosed box has a mounted solar panel as well to offset power consumption and is used for logging weights from the scale. Yellow flags tag the outlets that mimic our "herd". Photo credit Eduardo Santos.

In its totality, a controlled release at this stage of our project allows us to design an experiment in the same manner in which we would for the presence of cattle, but instead measure a methane source with a known flow such as our manifold to allow for simplicity in a measurement meant to ensure our proper precision for grazing systems. When cattle return to the pasture, the complexity of their mobility and scarcity per area will need to be addressed; the current idea would be to track animals in real-time to allow for released studies to take place when a herd comes into a viable area for the beam paths to capture emitting concentrations for measurements. This would take advantage of current technology to reduce our data collection to viable time periods for sensing, as well as allowing us to work towards adjustable beam paths that can change orientations and capture different areas of emissions for roaming cattle, who luckily tend to travel in a herd for an optimal source of emissions.

4.2.2 Addressing ADC Bias in two Channels

In a measurement of emissions so low as those expected in the pasture, we know that precision is of the upmost of importance. While our idea to narrow the spectral window does work towards gaining the resolution we desire of 0.2 ppb, there is still a problem with that precision if the equipment itself works against us. In a two-channel measurement, it is important to know that both channels will be able to give precise and replicable results. While DCS as a method is known for its measured spectrum being absent of distortions in the spectrum induced from the return of optical power on the detector [35], our setup still has the potential to create distortions as we record rf interferograms [117]. One of the most likely occurrences of distortions for a system like the Agrocombs project is bit-to-bit differential nonlinearity (DNL)

from analog-to-digital converters (ADC) commonly used in DCS systems for their operation in a desirable bandwidth region. These ADCs are used in data acquisition systems (DAQs) to digitize interferograms, meaning that any distortion from an ADC can result in distortions to the actual measured values on the DAQ.

Before we begin to address the problem of potential distortions, we must first discuss what exactly it means for DNL to cause these distortions. In the ideal ADC, the input and output are characteristically in a uniform staircase shape [118]. This means that, if we consider the input/output in terms of bits, each "step" is a transition from the previous least significant bit (LSB) to the next. So, if we were to look at a transfer curve of analog input to digital output for an ideal ADC, the steps should be equidistant from the transfer curve both below and above, as seen in Figure 4.8A.

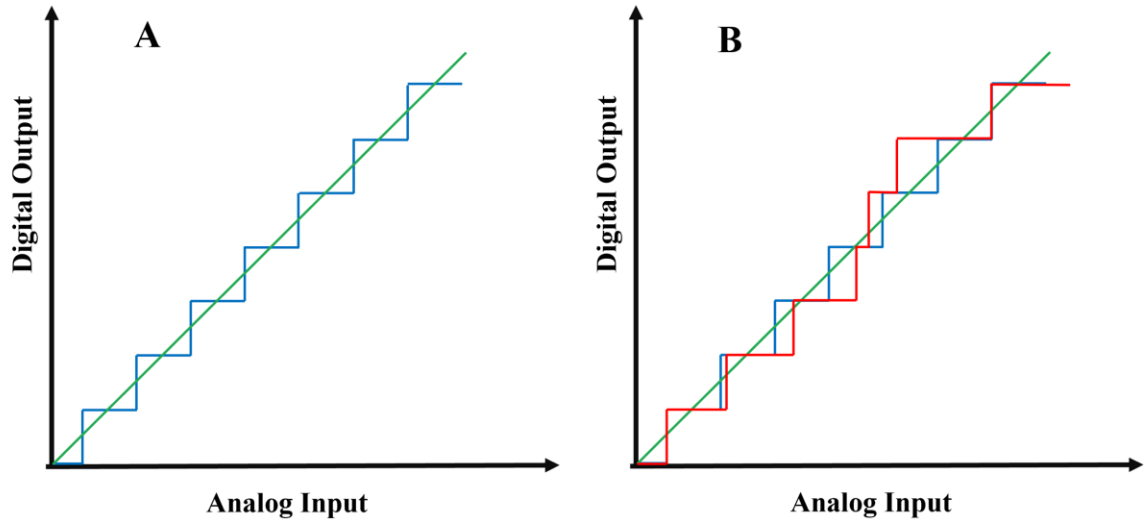

Figure 4.8 A) Green shows best fit line, with the blue being the ideal response from an ADC. Notice the equidistant differences below and above from the curve on the ideal response. B) Red now indicates the actual response from a real ADC, giving a visual representation of how distortions in signal can result. The deviation of the step width from the ideal step is what we call the DNL.

As seen in Figure 4.8B, an actual ADC does not perform with an ideal response. The step widths vary greatly, meaning that there is not a constant difference between the best fit and the steps in the response. Ideally, if we had adjacent digital codes, their analog input values would be separated by exactly 1 bit (or one step). The deviation from this ideal case is what defines DNL, and what causes problems in our experimentation. For a realistic measurement, our values will not follow a best fit line, which common falls at the center of the bit. RF inputs will not be quantized, and thus fall between bits at varying values (as an actual response).

In experimentation, there is a defined maximum deviation from the best-fit line known as the Integral Non-Linearity (INL) [119]. The INL is often expressed in binary and is measured from where the center of the ideal step is to the center of the actual response's step at that stage. This parameter cannot be calibrated out of the ADC. A visual aid to understand the difference between these nonlinearities is available in Figure 4.9. Between the DNL and INL, distortions need to be minimized in creative manners that do not necessarily involve calibration procedures.

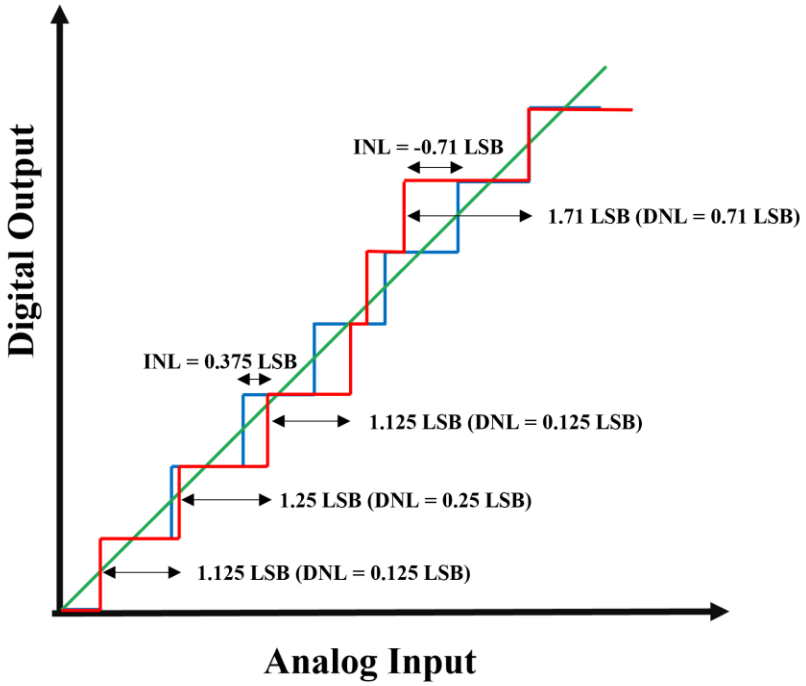

Figure 4.9 Visual representation of DNL vs INL. Notice that DNL is the difference from the ideal response (blue) step size (1 bit), showing how the actual response (red) differs from its expected step width. The INL is the difference between the actual and ideal responses, with positive INL indicating that the actual response is a higher analog input than the ideal response, and a negative INL indicating the reverse.

The distortions produced by an ADC can affect small signals, which is unfortunate in the case of absorption experiments. For our experiment's interferograms, the largest portion of the signal is a large center burst followed by small signals from the Free Induction Decay (FID) that can be affected by the ADC nonlinearity (see Figure 4.10). It has been shown that nonlinearity in the ADC is capable of distorting the absorbance shown in an interferogram by more than 1% [117], meaning that this is the predominant source of bias in the DCS. If we are to maintain high precision measurements and accurately represent the small FID signal, we need to ensure minimal distortions. Luckily for our experiment, the audio world has designed a unique way to minimize these distortions.

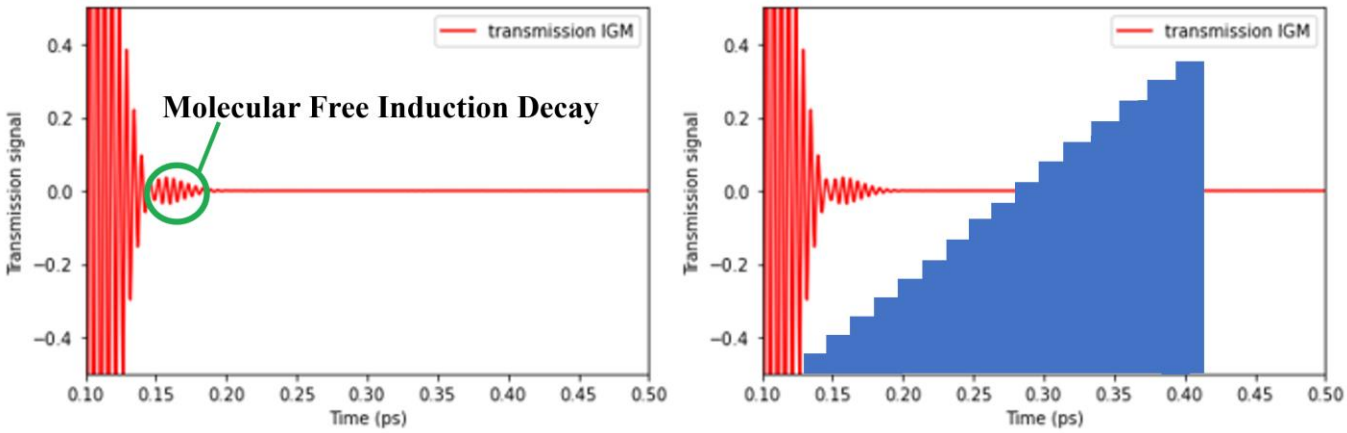

Figure 4.10 Left: Simulated interferogram zoomed in to see the tail end of the massive center burst (left hand side) versus the much smaller FID signal (oscillations after center burst). Right: Keeping in mind the sheer difference in magnitude between the center burst and FID, compare the 16-bit steps and observe the difference in magnitude. The center burst can typically cover 2000 bits, while the FID spans 4 bits [117].

In audio, a process has been developed to make quantization distortion less perceivable in the resultant signal [120]. Dithering as a whole is used primarily in audio and visual techniques, whether to minimize distortions through randomizing harmonics in audio or minimizing distortions in color tone. In the case of an RF signal, a dither means for us to add a sinusoidal signal onto our analog input for the ADC. This allows us to spread the incoming voltage from the FID across the ADC with the dither, thus making the FID span over larger portions of the bias in the ADC [117]. The result is a signal with less influence from the ADC's nonlinearity. As seen in Figure 4.11, if our signal is always changing which bit it is read on, we can eventually add errors from all interferograms to see that the errors balance closer and closer to zero, allowing us to hone into the small FID signal with greater ease without a loss of information due to the large difference between bit size and the signal magnitude.

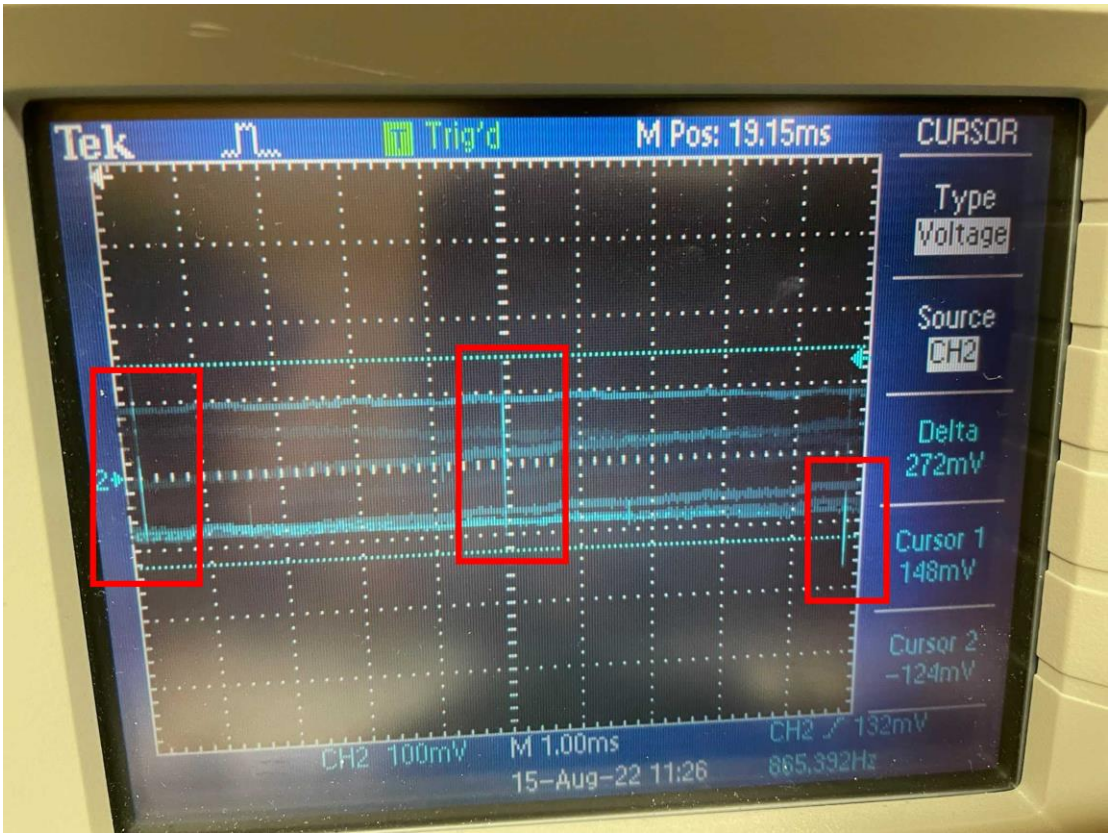

Figure 4.11 While it may be difficult to show, the oscilloscope in this image can see the overall dither frequency and the interferograms (outlined in red) on that signal. These interferograms show that the resultant signal we would usually receive can now be expanded over a larger signal to reduce bias from the ADC nonlinearity, by making the incoming RF signal span a larger portion of the ADC's bias function.

A previous study into the implementation [117] of a dither signal shows how successful a dither signal can be in one of these DCS systems. The study cited is particularly focused on one-channel DCS measurements, while the Agrocombs project has used two-channel measurements as a staple of capturing background and enhancement concentrations of agricultural gases. There are similarities to how we can test a dither signal with this two-channel measurement. For one, the most controlled manner in which we can ensure both channels measure the same concentration is to have our beam pass through a methane reference cell rather than perform an open-path measurement. In doing so, we take our light the DCS and couple it to a cell of known

length (5.45 cm) and pressure (10 kPa). The output from the cell is split after a photodetector to be input into both DAQ channels (one for each transceiver in regular experimentation). While we developed the circuit and installed it, we also tested filters existing around the connections to the ADC and verified their functionality or adjusted for proper signal processing.

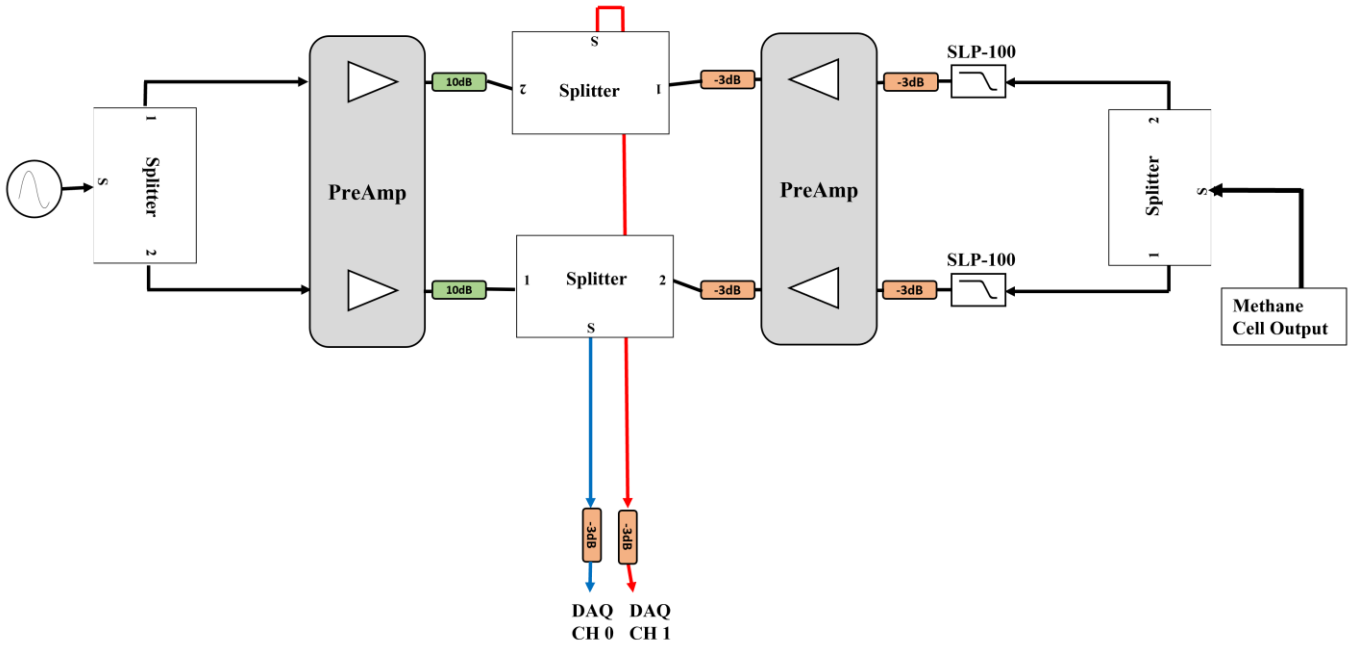

Figure 4.12 Above is a schematic of the dither circuit implemented for testing channel bias. Note, green components are 10 dB attenuations, orange are -3 dB attenuators. The circuit implements a single pre-amplifier and function generator, three splitters within the circuit itself, and low pass filters (100 MHz). The splitter to the far right of the schematic is used on the output from the cell in order to split the same signal to apply later to the two channels of the DAQ.

Once we set our system to measure a reference cell, we can begin to test dither signals. The sinusoidal signal used for the dither is generated with a Stanford Research Systems Model DS345 synthesized function generator capable of producing sine waves up to 30.2 MHz [121]. The configuration for an RF dither is compiled of RF components that are small enough to be mounted to a reasonably sized breadboard and mounted to the wall of the trailer. Testing the

dither means taking data with varying dither voltage to determine how, over time, the dither signal affects our measured concentration of methane. In the case of the cell measurement, we use the resultant concentration to calculate the corresponding cell length, and then evaluate those cell lengths from both DAQ channels.

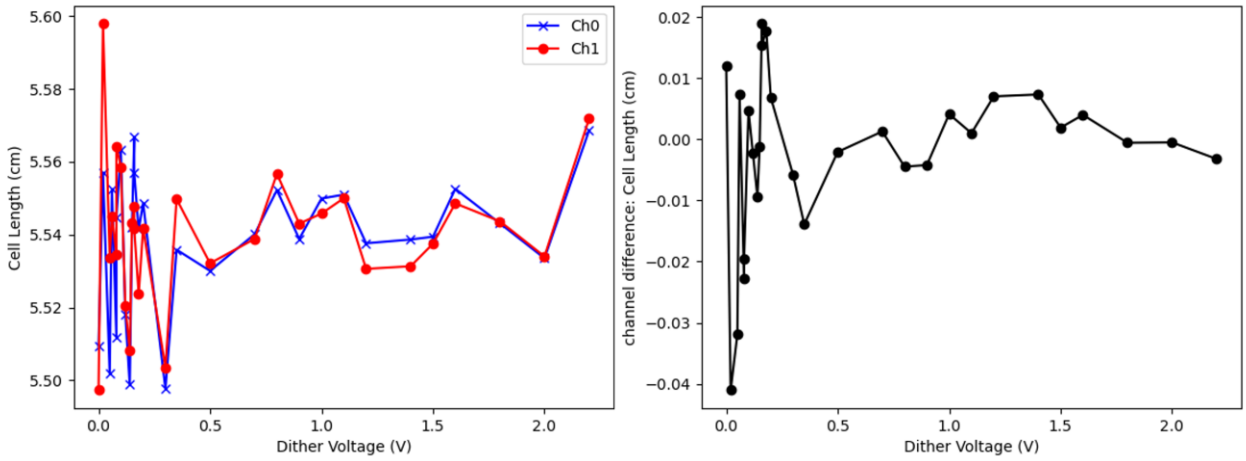

Figure 4.13 Data from methane cell measurement. Left: Both DAQ channels for comparison of corresponding cell length (in centimeters). Right: Difference cell length between two channels. Notice how at different dither voltages, we can see the narrow difference between channels.

In Figure 4.13, we can see the methane cell data from dither testing. Over varying dither voltages, we can compare what cell length can be calculated from measured concentrations on both DAQ channels. If we look at the two channels plotted at once, we can see there are differences, highlighted heavily around the 0.0 V point, or our baseline, no dither applied. As the dither is varied, we can see the two channels begin to track in similar fashion. If we now turn to analyzing the differences in cell length from the two channels, which is our Channel 1 data subtracted from the Channel 0 data, we can see that there is a large difference with no dither signal or low signal, but that it inevitably starts to balance out to a much smaller difference. If the

channels differ less, we are seeing less influence from the distortions coming from the ADC nonlinearities.

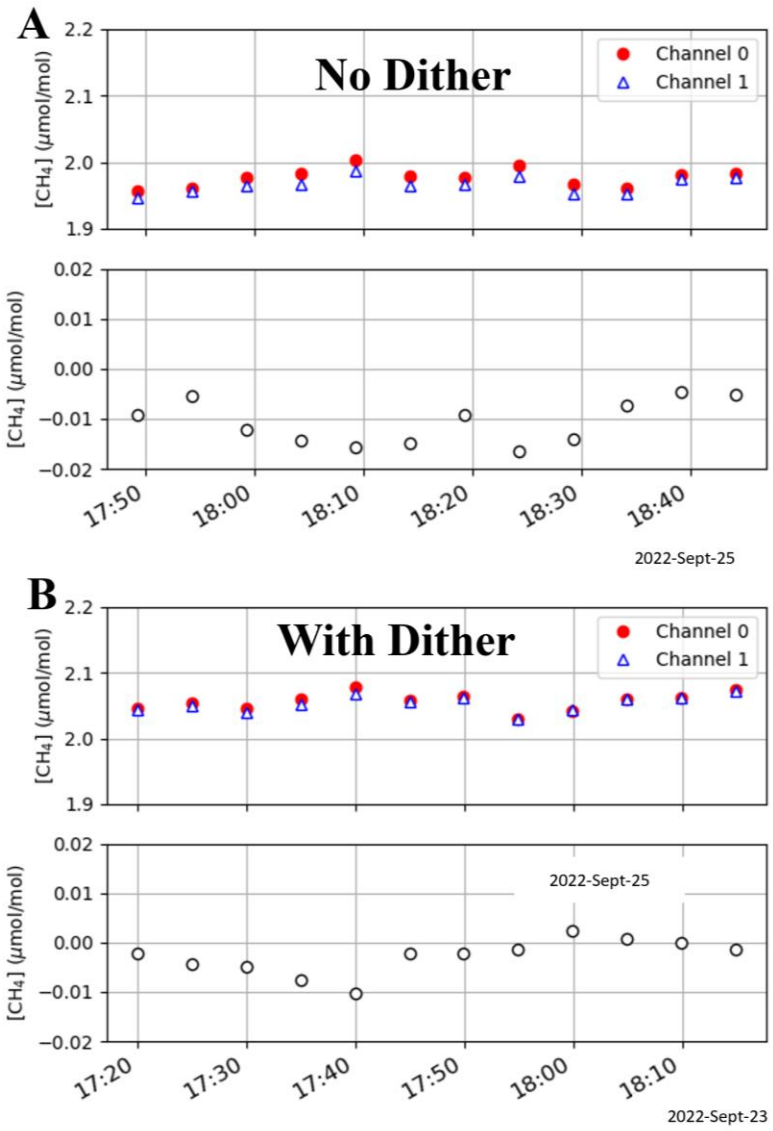

Figure 4.14 Single channel comparison with outdoor data. A) At the top, plot shows concentration measurements from both DAQ channels, fed one transceiver's signal. At the bottom, the difference between concentrations from the two channels is shown. B) Outdoor data showing both the two-channel DAQ concentration measurements, followed by difference in channel. Note the difference with the dither is finer than without the dither. Without the dither, the background concentrations are too low.

From the cell measurement, we moved to take outdoor data while testing the dither. Much like the single channel cell measurement, we once again feed a single signal into a splitter to be distributed into the dither circuit. In this case, instead of the output from the methane cell, we used the RF signal received from the North path transceiver (transceiver 0). Figure 4.14 lays out the story of our outdoor single channel dither testing, where part A of the figure represents our data with no dither, and part B represents that with the dither signal present. With no dither, there is a small difference in the mole fraction detected on each channel, but most notable is the difference between channels when one is subtracted from the other (Figure 4.14B). While that difference is on the order of one thousand times less than a μmol/mol, we never see that difference exactly reach something close to zero. If we turn our dither signal on, we see that the two channels now track even closer to one another, almost overlapping in concentration on the same scale as before. Now when we look at the difference in channels, we can see that the small difference is lessened to the extent of closing in on a zero difference. It is also important to note that without the dither signal, our background concentrations are too low for the expected atmospheric levels of methane. Realistically, there will most likely always be a difference between channels due to electronic signals, but the dither signal allows us to bridge a large portion of that gap, which minimizing distortions from the ADC nonlinearities, thus providing us a more appropriate measurement of such small signals such as the FID response.

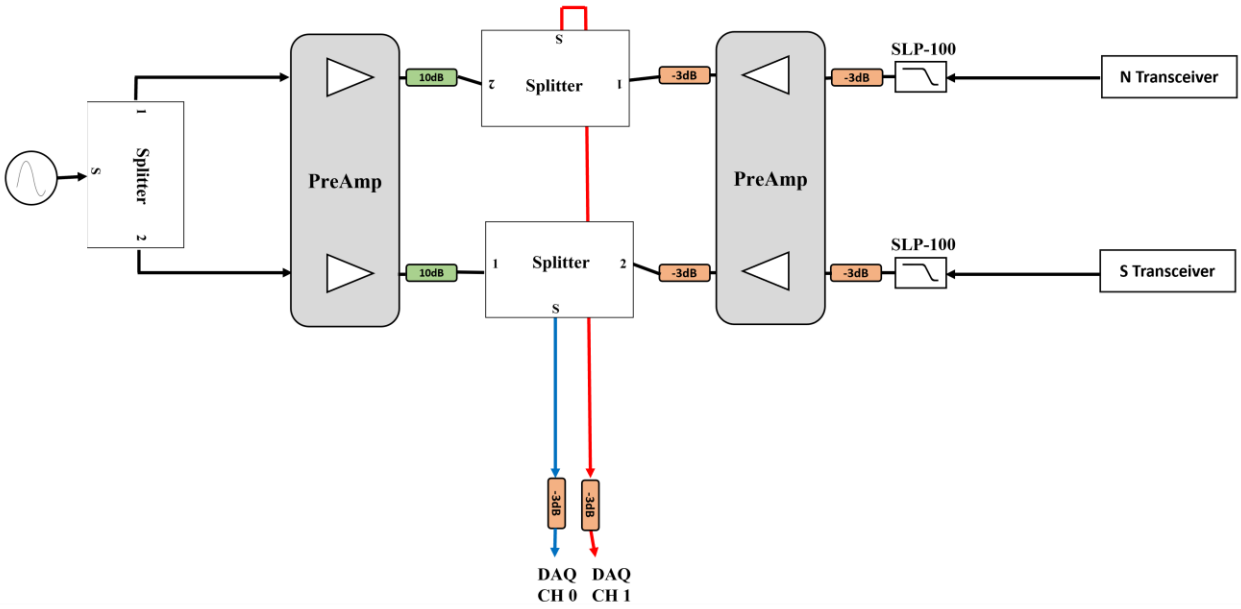

Figure 4.15 Dither circuit applied to outdoor, two channel measurement.

Now that we have tested our dither signal, we can see from Figure 4.14 that the signal does allow us to correct some of our channel bias in this two-channel DAQ setup. The methane cell provided us ample control data with its known path, allowing us to test both channels of the DAQ with varying dither voltages, as seen in Figure 4.13. From there, we can see in Figure 4.14, we moved to a single channel outdoor measurement, allowing us to see the dither signal over time on both channels and how the system functions with or without this dithering signal. While the difference may seem minimal in terms of mole fraction, there are two main points to draw from this. This is a precision measurement, made difficult by small emissions, meaning that any errors can propagate easily through our analysis. As well as the precision, we know from the beginning of this section that the small FID signal is where our absorption information is contained, meaning that we need to narrow the difference in digitized signals to be able to properly detect and analyze this tiny signal. Figure 4.15 shows our application of the dither circuit after testing, using both transceivers.

4.3 Preliminary Data

The controlled release study has begun as of the late winter of 2022 into the spring 2023 semester, allowing us to gather preliminary data as we improve the system. The methane manifold was installed in the fall/winter of 2022, near the end of the year, meaning that our current results are quite recent. Primary focus in the beginning of our time at the Rannels Ranch has been the channel bias, discussed heavily in Section 4.2.2. As we have become comfortable with our dither frequency and its role in the system, and the manifold came to fruition, we moved towards detection of methane in the hopes of pushing the Agrocombs system's boundaries in precision.

In the feedlot measurement, we can see from Figure 3.4 that the Agrocombs system operated with a broad spectral window that spanned from approximately 1.4 to 1.7 microns, or nearly 40 THz frequency range. We discussed the relationship between this spectral bandwidth and the SNR of the system in section 4.1, leading us to the conclusion that by narrowing this spectral window, we can improve the SNR of the system and thus forth improve the precision. With that in mind, the current goal is to capture methane concentration measurements in the pasture, meaning that our sole focus is on a band of strong methane absorption. This has led to the narrowing of our operational bandwidth to be now between 1.6 and 1.7 microns, approximately, a dramatic change from the previous experiment.

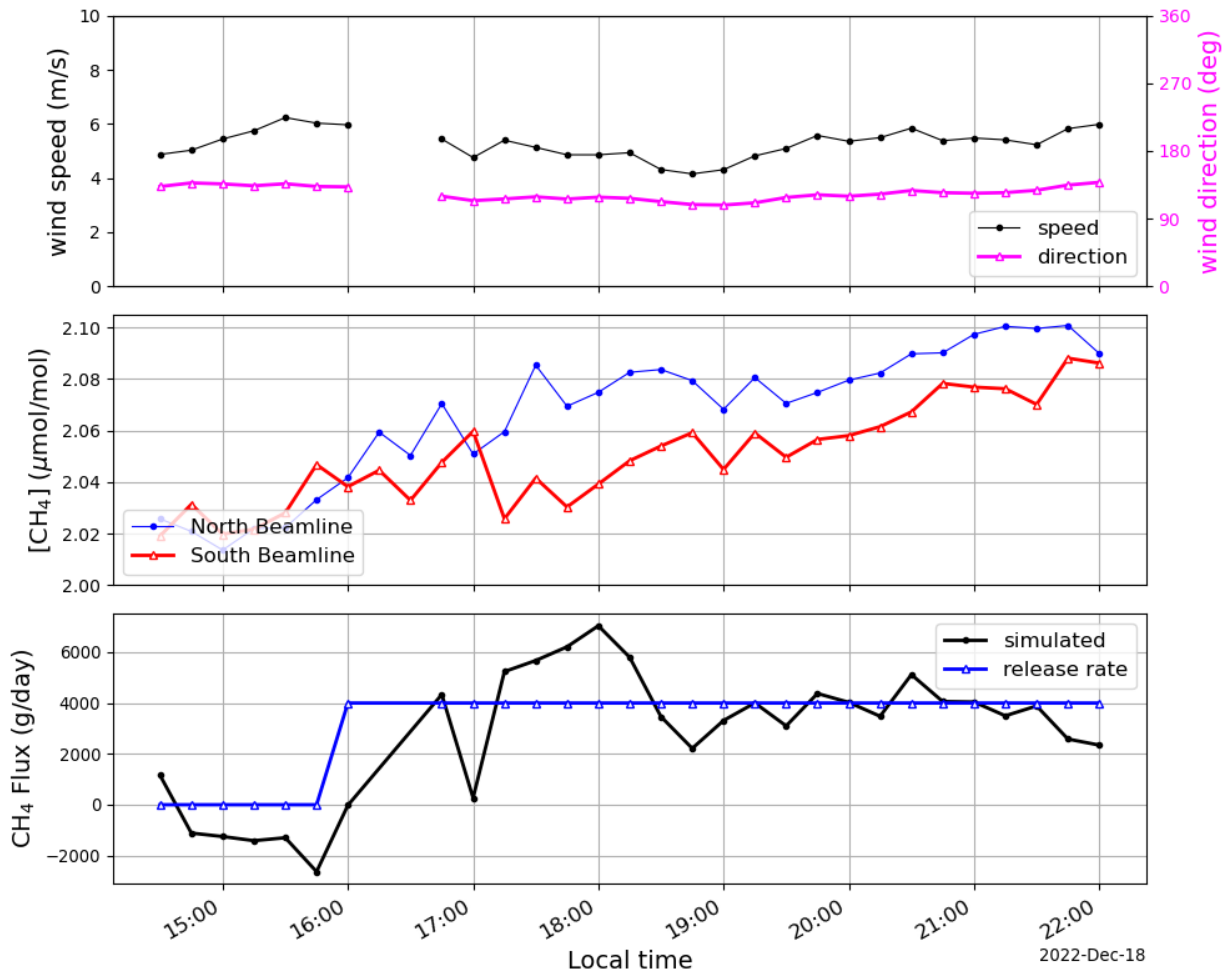

Figure 4.16 Data from a controlled release in December of 2022. Here we can see wind data in the first (top) plot, followed by a plot of the two beam path concentrations detected. Finally, we have the last plot, depicting the flux of methane and showing when the release began.

With our new spectral window in mind, and the controlled release formally in operation, we can view some of our preliminary data from a release in Figure 4.16. This release in particular took place with our 200-meter paths on retro 1 and 2 from Figure 4.5. The release began shortly before 16:00 on December 18th, 2022, for this particular data set, indicated on the flux plot of the results. The wind conditions are consistent, both with a speed above 4 m/s and a rather consistent direction to aid in the carry of the release within our beam path geometry. As

we can see, both paths are reactive, and the concentrations measured do increase with the release. Most importantly from this data, we prove our ability for the Agrocombs system to detect released methane at the expected emissions. For Figure 4.16, the flow rate is reflective of a 400 g/day emission rate. Simulations and calculated expected emission rates for grazing cattle more appropriately give us an expected emission rate of 200 g/day if we have the methane outlets representing 2 animals per outlet, resulting in a simulated herd of 20 cattle. Once again, much like the feedlot system, we use an IDM to determine flux from our measured concentrations and the locally gathered weather data.

4.4 Controlled Release Moving Forward

Our controlled release study is still ongoing. In its current state, the system is preparing for further releases at the 200-meter path length, while the emission rate from the manifold can potentially be lowered to further test our limitations. The addition of retroreflector 3 has prompted us to continue our addition of retroreflectors to the system, with plans currently allowing for two more, allowing us to adjust our beam paths and the area of source emissions we measure.

Further, as the release continues, the goal is to lengthen the beam paths, perhaps doubling to 400-meter paths. This greatly increases our area of measurement, allowing us to better detect emissions from cattle as they wander in these large pasture systems. The cattle are scheduled to return in the early summer of 2023, as is the natural timing of this portion of their life cycle, meaning that we need to develop means to measure emissions from livestock as they return to the site. One idea is to automate the controlled release to begin perhaps not at a time set by the operators, but instead determined by the proximity of animals. If we can track cattle and set up a

way to trigger a measurement based on a threshold of cattle either within our area of interest or in close proximity to it, we could perhaps save time and energy otherwise spent trying to catch the animals at odd hours of the day or night. With this idea, we can take advantage of the social nature of cattle, meaning that their penchant for moving as a herd rather than in scattered pairs or singular stragglers can work to our advantage to increase the emissions in the area. The tracking of these animals would also have a secondary necessity, in that we would be able to count the number of animals in the area at the time of a measurement, allowing us to better conduct our inverse dispersion simulation through Windtrax.

Chapter 5 - Conclusion

The purpose of this project was not to complete a singular goal. Throughout these chapters, it has been explained that for every step we take to further the development and ability of the Agrocombs, another goal comes forward in the natural progression of agricultural sensing. In the beginning, this project was intended to test the efficacy of dual-comb spectroscopy in field work for agricultural sensing, and from there, we have expanded our purview into a new system, with the hopes of continuing on in the foreseeable future to even more complex systems. The more complex of a system that we measure net emissions from, the more understanding can be gained about the totality of an agricultural process's contributions to greenhouse gas emissions.

5.1 Summary

As is detailed in this dissertation, the Agrocombs project began with the idea that current sensing methodology struggles to encompass a full picture of an agricultural system. In the current scientific climate, a strong push towards remote sensing of greenhouse gases has been made, but agriculture stands as a difficult setting to capture while staying non-invasive. Methane still stands as a greenhouse gas of interest for the EPA and international climate committees, and the largest producer of anthropogenic methane is enteric fermentation, directly tied to livestock operations. Select current methods can measure methane emissions in these systems but struggle to simultaneously measure several greenhouse gases of interest or may even give lower emission readings due to sampling practices. The open-path nature of dual-comb spectroscopy, its ability to exist in long-range, outdoor measurements, and its ability to simultaneously detect several gases makes it a prime candidate for these field measurements.

With DCS in mind, we set out to prove ourselves at a beef stocker site. This feedlot setting gave us approximately 300 head of cattle in relatively close quarters, allowing us to detect higher enhancements due to the high capacity of animals per area. This measurement required a comparative system, thus the parallel sensing experiment of the Agrocombs system and the closed-path CRDS system. With two 50-meter one-way paths, resulting in 100-meter roundtrip paths, our DCS system was able to measure methane emissions, among emissions of CO_2 and NH_3, and compare these measured concentrations to CH_4 and CO_2 concentrations measured by the CRDS system. Further, an inverse dispersion model used our measured concentrations and local weather and wind information to calculate methane flux about the site. With a background offset of approximately 2 $\mu g/m^2/s$, the flux calculated from measured concentrations agreed within 6% between the two systems. This was our indication that the Agrocombs project could continue with agricultural sensing, and that the system could appropriately measure emissions in a feedlot setting.

From the feedlot, we began to tackle the next step in complexity for livestock practices: grazing systems. Grazing cattle make up the majority of the livestock life cycle in the United States, meaning that despite the low animal density per large area, it is important to fully understand the entire scope of pasture emissions. In a feedlot, we were aware that cattle produced methane through enteric fermentation, and thus the production of methane primarily amounted to this process alone, with little consideration of methane sinks. Pastures present a complication in comparison; while the cattle may produce methane, microbial soil activity may provide a methane sink, shrinking already small enhancements of methane over background measurements. With this give and take in mind, and the precision of the Agrocombs system

sitting at approximately 3 ppb in the feedlot system, we knew that increased precision was necessary.

The goal has been to narrow the spectral window of the DCS system to increase precision, due to an inverse relationship between the number of spectral elements and the SNR. The appropriate precision for a grazing measurement has been determined to be approximately 0.2 ppb. Beyond the precision, we also have moved to a newly compacted DCS rack and improved transceivers. In order to test the proposed precision and prove that we can detect the expected small enhancements of methane above background, we have proposed a controlled release study to mimic the emissions of a herd of approximately 20 cattle. This study would utilize a known methane emission rate for us to detect with the newly improved Agrocombs system, allowing us to push the boundaries of our experimentation and adjust until we reach the desired precision.

We coordinated with the Department of Agronomy to conduct our research at the Rannels Ranch, a K-State operated site outside of the main city of Manhattan, elevated enough to isolate the pasture's methane cycle. While the cattle are present in the summer (from May through August, early September at latest), we worked to set up the equipment and test its basic alignment and operation conditions and held off on our controlled release until the animals were transported. Initial testing of automated transceiver alignment successfully allowed us to implement a voltage feedback system, as well as incorporate a flashing LED from a modified flashlight for nighttime alignment. Image processing was improved from the feedlot experiment, coming together with alignment procedures to better sustain the returning light from the retroreflectors to the transceivers. Furthermore, the newly compacted DCS rack proved rugged

enough to withstand extreme heat and later cold, as well as maintaining comb lock for long periods of time.

One aspect of the precision of the system that was heavily studied was our channel bias. It is a known problem with DCS systems that channel bias from distortions in ADC nonlinearities can be detrimental for higher precision measurements [117]. By adding a dither signal, we are able to minimize distortions for our two-channel measurement that derive from the ADCs that digitize signals before they are transferred to the DAQ. This RF circuit, composed of small RF components, a preamplifier, and a function generator, was tested thoroughly to find the correct frequency to allow our FID signal to span across the ADC.

With newly improved alignment procedures, a newly compacted rack, and a geometry that uses previous weather data to its advantage, the controlled release could finally take place. A methane source consisting of a gas canister, a scale, and a manifold system mimics 20 cattle (a small herd), releasing methane for the Agrocombs system to detect. Preliminary data has shown our ability to detect 400 g/day fluxes of methane for 200-meter paths. Further testing will take place, including doubling the path lengths to 400-meter beam paths, as well as changing the emission rate to see if lower emission rates are still within our window of detection. As the animals return, precautions to protect the equipment must be strengthened, as well as tracking methods for the cattle. If we can track cattle, we can count the number of heads in a measurement's source area at a given time, as well as possibly adapt our system to measure only when animals are within a viable proximity to that area of interest. Cattle return early this summer of 2023, meaning that the system will stay in its current pasture home and continue on with the hopes of completing a grazing measurement soon.

This thesis outlines the progression from the concept of remote sensing with DCS for agricultural purposes to the adaptation for a complex pasture system measurement. This progression has required the cooperation of two organizations, two departments within Kansas State University, and a team of minds with various backgrounds between physics and agronomy. My own personal contributions to this project come in several forms. In our feedlot measurement, I was tasked with maintenance of the system in lieu of robust remote access, as well as assistance with setup of the measurement and transceiver alignment. As we have moved the mobile lab for our controlled release, the measurement geometry and remote operation of the experiment have evolved with our knowledge from the feedlot and the nuances of the pasture setting. These evolutions include the carefully tested channel bias testing used to narrow in the difference between channels and their detected concentrations for methane. I was involved in the testing of dither signals and RF electronics for the channel bias measurements, as well as the fitting of concentrations and channel differences that followed. We also performed Allan-Werle deviations to thoroughly analyze these measurements and improve our precision over longer time scales. As we reach further into our controlled release, the system has become more independent, but still requires a group effort of periodic monitoring to maintain alignment for transceivers or to check the stability of our locks for the frequency combs.

5.1 Looking Towards the Future

In its current state, the Agrocombs system is set up to improve measurements in a pasture setting. As discussed in Chapter 4, our current experimental trajectory is to improve our controlled release detection before cattle return. The return of cattle to the pasture requires us to take precautions and consideration of the changes in the grazing system's details versus the

feedlot measurement we previously performed. As discussed in Section 4.4, low animal density per large area of emission means we're trying to detect emissions for approximately 25 cattle in a herd that can roam versus our previous feat of detecting emissions from nearly 400 cattle in a confined area, meaning the sheer magnitude of methane emissions are drastically different. Animal tracking must be established to allow us to detect our methane sources for the inverse dispersion model, as well as allowing for possible automation for beginning and stopping measurements according to population within an area of interest. We also want to add further retroreflectors to allow for multiple wedge-shaped detection areas, giving us a variety of detection to go with the high mobility of the animals. These adjustments need to be made before we properly measure emissions from the cattle.

Aside from the quickly approaching return of cattle, our system has a unique opportunity available due to its location. The Rannels Ranch, like many agricultural systems in Kansas, undergoes regular controlled burns. Reference [122] explains that Kansas implements these prescribed burns to reduce invasion of weeds and excess woody vegetation, while also promoting new growth in the grasslands without fertilizers or additional herbicides. The Rannels Ranch is not excluded from these burns, and thus we may have the opportunity, be it relatively soon or in the far future, to use the Agrocombs system for the detection of carbon monoxide from a controlled burn. The primary complication to this idea arises in the fact that we must ensure that our spectral window includes an absorption band for CO.

Thus far, the Agrocombs project has set its eye on livestock emissions, specifically those due to enteric fermentation. Its current stage in the pasture measurement still allows for improvements, including the change to a longer beam path for the potential of lower noise, thus improving the precision further. More precise movement in the gimbals may also help maintain

alignment in these longer paths, meaning we could possibly move to a different gimbal system than the one we use now. The comparison of average methane emission flux per head of cattle in a feedlot system versus a grazing system will be vital to understanding methane production in agriculture, as enteric fermentation still stands as one of the largest producers of anthropogenic methane in the sector. Possible future comparative measurements include sensing experiments centered around beef cattle versus dairy cattle, as the life cycle and feed quality or type differ between these two industries.

The future does not have to center itself around livestock. Dual-comb spectroscopy has the potential for detecting several greenhouse gases of interest, including nitrous oxide. In agriculture, nitrous oxide is heavily produced from crop systems, meaning that crop emission detection could be beneficial to understanding how different fertilizers and pesticides encourage or deter further nitrous oxide production. Mitigation studies would also benefit from having a real-time measurement of emissions [123]. In order to perform a proper crop emission measurement, our beams would most likely need to capture a vertical gradient, meaning that our long open-path measurement across a field of interest would instead be an open-path measurement above a source of nitrous oxide. The vertical gradient would require us to work with retroreflectors at different heights, suspended possibly by drones or outdoor balloons.

Aside from the complexity of the vertical paths, the primary difficulty with a crop system measurement is actually the nitrous oxide itself. More specifically, strong nitrous oxide absorption occurs in the region somewhere between 4 and 5 μm in the mid infrared region [124]. The modern state of mid-infrared DCS systems is still dependent upon a large free-space optical setup, rather than the near-IR system's predominantly fiber-based configuration. With free-space optics, field measurements are increasingly difficult, and maintaining operations for long periods

of time can be costly in terms of time and effort. Current infrared spectrometers utilize several methods of achieving a DCS system in this wavelength region [125–128], including advancements to implement fiber-based systems [129]. Unfortunately, until these spectrometers are composed of less free-space optical components, their robustness will be questionable in field operations. Their fragility could be a direct detriment to an outdoor measurement, especially in the case of a long-term measurement in harsh field and weather conditions.

The Agrocombs project has a large capacity for its implementation. Livestock systems alone grant us a myriad of different measurement potentials, be it comparing lifestyle sequences for the cattle, or beef versus dairy cattle. The detection of methane could potentially aid in mitigation studies, where the Agrocombs system can measure long-term changes in emissions as operations change (feed quality, change in cattle breed strains, etc.). Beyond livestock emissions, we hope to push into mid infrared regions in order to perform crop emission measurements, implementing the above-mentioned vertical gradient paths and perhaps aiding in emission mitigation due to fertilizer and pesticide choice and frequency in these crop operations. The agricultural sector will continue to grow as long as the population in need of food does the same, meaning that these precision measurements and mitigation studies are vital to sustainable farming in the future.

References

1. US EPA O. Inventory of U.S. Greenhouse Gas Emissions and Sinks: 1990-2018 [Internet]. 2020 [cited 2023 Jan 15]. Available from: https://www.epa.gov/ghgemissions/inventory-us-greenhouse-gas-emissions-and-sinks-1990-2018

2. Wyer KE, Kelleghan DB, Blanes-Vidal V, Schauberger G, Curran TP. Ammonia emissions from agriculture and their contribution to fine particulate matter: A review of implications for human health. Journal of Environmental Management [Internet]. 2022 Dec [cited 2023 Mar 30];323:116285. Available from: https://linkinghub.elsevier.com/retrieve/pii/S0301479722018588

3. Methane: A crucial opportunity in the climate fight [Internet]. Environmental Defense Fund. [cited 2023 Mar 31]. Available from: https://www.edf.org/climate/methane-crucial-opportunity-climate-fight

4. Martin C, Morgavi DP, Doreau M. Methane mitigation in ruminants: from microbe to the farm scale. Animal [Internet]. 2010 [cited 2023 Mar 31];4(3):351–65. Available from: https://linkinghub.elsevier.com/retrieve/pii/S1751731109990620

5. Smith P, Reay D, Smith J. Agricultural methane emissions and the potential formitigation. Phil Trans R Soc A [Internet]. 2021 Nov 15 [cited 2023 Mar 31];379(2210):20200451. Available from: https://royalsocietypublishing.org/doi/10.1098/rsta.2020.0451

6. US EPA O. Ammonia [Internet]. 2015 [cited 2023 Apr 13]. Available from: https://www.epa.gov/caddis-vol2/ammonia

7. Guthrie S, Giles S, Dunkerley F, Tabaqchali H. The impact of ammonia emissions from agriculture on biodiversity.

8. Klimczyk M, Siczek A, Schimmelpfennig L. Improving the efficiency of urea-based fertilization leading to reduction in ammonia emission. Science of The Total Environment [Internet]. 2021 Jun [cited 2023 Mar 31];771:145483. Available from: https://linkinghub.elsevier.com/retrieve/pii/S0048969721005519

9. AR4 Climate Change 2007: Synthesis Report — IPCC [Internet]. [cited 2023 Jan 25]. Available from: https://www.ipcc.ch/report/ar4/syr/

10. 2006 IPCC guidelines for national greenhouse gas inventories [Internet]. Institute for Global Environmental Strategies; Report No.: Vol. 4. Available from: www.ipcc-nggip.iges.or.jp/public/2006gl/index.html

11. Campbell GS, Norman JM. Introduction to environmental biophysics. 2nd ed. New York: Springer; 1998. 286 p.

12. Monteith JL, Unsworth MH. Principles of environmental physics. 3rd ed. Amsterdam ; Boston: Elsevier; 2008. 418 p.

13. Stull RB. An introduction to boundary layer meteorology. Dordrecht: Springer; 2009. 670 p. (Atmospheric and oceanographic sciences library).

14. Pan SY, He KH, Lin KT, Fan C, Chang CT. Addressing nitrogenous gases from croplands toward low-emission agriculture. npj Clim Atmos Sci [Internet]. 2022 Jun 2 [cited 2023 Mar 31];5(1):43. Available from: https://www.nature.com/articles/s41612-022-00265-3

15. Enteric fermentation [Internet]. Climate & Clean Air Coalition. [cited 2023 Mar 31]. Available from: https://www.ccacoalition.org/en/activity/enteric-fermentation

16. Castelán Ortega OA, Pedraza Beltrán PE, Hernández Pineda GS, Benaouda M, González Ronquillo M, T Molina L, et al. Construction and Operation of a Respiration Chamber of the Head-Box Type for Methane Measurement from Cattle. Animals [Internet]. 2020 Jan 31 [cited 2023 Mar 31];10(2):227. Available from: https://www.mdpi.com/2076-2615/10/2/227

17. Chagunda MGG. Opportunities and challenges in the use of the Laser Methane Detector to monitor enteric methane emissions from ruminants. Animal [Internet]. 2013 [cited 2023 Mar 31];7:394–400. Available from: https://linkinghub.elsevier.com/retrieve/pii/S1751731113000724

18. MethaneSAT [Internet]. MethaneSAT. [cited 2023 Mar 31]. Available from: https://www.methanesat.org/

19. Bai M, Loh Z, Griffith DWT, Turner D, Eckard R, Edis R, et al. Performance of open-path lasers and FTIR spectroscopic systems in agriculture emissions research [Internet]. Gases/In Situ Measurement/Instruments and Platforms; 2022 Jan [cited 2023 Mar 29]. Available from: https://amt.copernicus.org/preprints/amt-2021-347/amt-2021-347.pdf

20. Sypniewski M, Strabel T, Cieslak A, Szumacher-Strabel M, Pszczola M. Technical note: Interchangeability and comparison of methane measurements in dairy cows with 2 noninvasive infrared systems. Journal of Dairy Science [Internet]. 2019 Oct [cited 2023 Mar 29];102(10):9512–7. Available from: https://linkinghub.elsevier.com/retrieve/pii/S0022030219306393

21. Wang F, Jia S, Wang Y, Tang Z. Recent Developments in Modulation Spectroscopy for Methane Detection Based on Tunable Diode Laser. Applied Sciences [Internet]. 2019 Jul 15 [cited 2023 Mar 29];9(14):2816. Available from: https://www.mdpi.com/2076-3417/9/14/2816

22. Kormann R, Fischer H, Gurk C, Helleis F, Klüpfel T, Kowalski K, et al. Application of a multi-laser tunable diode laser absorption spectrometer for atmospheric trace gas measurements at sub-ppbv levels. Spectrochimica Acta Part A: Molecular and Biomolecular Spectroscopy [Internet]. 2002 Sep [cited 2023 Mar 29];58(11):2489–98. Available from: https://linkinghub.elsevier.com/retrieve/pii/S1386142502000665

23. Grossi G, Goglio P, Vitali A, Williams AG. Livestock and climate change: impact of livestock on climate and mitigation strategies. Animal Frontiers [Internet]. 2019 Jan 3 [cited

2023 Mar 29];9(1):69–76. Available from: https://academic.oup.com/af/article/9/1/69/5173494

24. Buckley S. Tunable Diode Lasers for Trace Gas Detection: Methods, Developments, and Future Outlook. Spectroscopy [Internet]. 2018 Sep 30 [cited 2023 Mar 29];33(10):26–9. Available from: https://www.spectroscopyonline.com/view/tunable-diode-lasers-trace-gas-detection-methods-developments-and-future-outlook

25. Gharavi M, Buckley SG. Single Diode Laser Sensor for Wide-Range H_2O Temperature Measurements. Appl Spectrosc [Internet]. 2004 Apr [cited 2023 Mar 29];58(4):468–73. Available from: http://journals.sagepub.com/doi/10.1366/000370204773580338

26. Schütze C, Lau S, Reiche N, Sauer U, Borsdorf H, Dietrich P. Ground-based Remote Sensing with Open-path Fourier- transform Infrared (OP-FTIR) Spectroscopy for Large-scale Monitoring of Greenhouse Gases. Energy Procedia [Internet]. 2013 [cited 2023 Mar 29];37:4276–82. Available from: https://linkinghub.elsevier.com/retrieve/pii/S1876610213005730

27. Chasse J. Coherent Anti-Stokes Raman Scattering Cell Imaging and Segmentation with Unsupervised Data Analysis. Spectroscopy [Internet]. 2023 Mar 1 [cited 2023 Mar 29];36(S9A):20-21,42. Available from: https://www.spectroscopyonline.com/view/common-problems-with-ft-ir-instruments-and-how-to-avoid-them

28. Bai M, Velazco JI, Coates TW, Phillips FA, Flesch TK, Hill J, et al. Beef cattle methane emissions measured with tracer-ratio and inverse dispersion modelling techniques. Atmos Meas Tech [Internet]. 2021 May 12 [cited 2023 Mar 29];14(5):3469–79. Available from: https://amt.copernicus.org/articles/14/3469/2021/

29. Schliesser A, Brehm M, Keilmann F, van der Weide DW. Frequency-comb infrared spectrometer for rapid, remote chemical sensing. Opt Express [Internet]. 2005 [cited 2023 Jan 25];13(22):9029. Available from: https://opg.optica.org/oe/abstract.cfm?uri=oe-13-22-9029

30. Hook LA, Christensen SW, Beaty TW. NARSTO Quality Systems Science Center 2004-2005 Annual Report.

31. Day M, Pouliot G, Hunt S, Baker KR, Beardsley M, Frost G, et al. Reflecting on progress since the 2005 NARSTO emissions inventory report. Journal of the Air & Waste Management Association [Internet]. 2019 Sep 2 [cited 2023 Mar 29];69(9):1023–48. Available from: https://www.tandfonline.com/doi/full/10.1080/10962247.2019.1629363

32. Coddington I, Swann WC, Newbury NR. Coherent Dual Comb Spectroscopy at High Signal to Noise.

33. Coddington I, Newbury N, Swann W. Dual-comb spectroscopy. Optica [Internet]. 2016 Apr 20 [cited 2023 Jan 13];3(4):414. Available from: https://opg.optica.org/abstract.cfm?URI=optica-3-4-414

34. Rieker GB, Giorgetta FR, Swann WC, Kofler J, Zolot AM, Sinclair LC, et al. Frequency-comb-based remote sensing of greenhouse gases over kilometer air paths. Optica [Internet]. 2014 Nov 20 [cited 2023 Jan 15];1(5):290. Available from: https://opg.optica.org/abstract.cfm?URI=optica-1-5-290

35. Waxman EM, Cossel KC, Truong GW, Giorgetta FR, Swann WC, Coburn S, et al. Intercomparison of open-path trace gas measurements with two dual-frequency-comb spectrometers. Atmos Meas Tech [Internet]. 2017 Sep 11 [cited 2023 Jan 15];10(9):3295–311. Available from: https://amt.copernicus.org/articles/10/3295/2017/

36. Cossel K, Waxman E, Herman D, Washburn B, Giorgetta F, Baumann E, et al. Field applications of dual frequency comb spectroscopy. In: Strojnik M, editor. Infrared Remote Sensing and Instrumentation XXVIII [Internet]. Online Only, United States: SPIE; 2020 [cited 2023 Jan 16]. p. 8. Available from: https://www.spiedigitallibrary.org/conference-proceedings-of-spie/11502/2568635/Field-applications-of-dual-frequency-comb-spectroscopy/10.1117/12.2568635.full

37. Hänsch TW. PASSION FOR PRECISION.

38. Picqué N, Hänsch TW. Frequency comb spectroscopy. Nature Photon [Internet]. 2019 Mar [cited 2023 Jan 23];13(3):146–57. Available from: http://www.nature.com/articles/s41566-018-0347-5

39. Ye J, Cundiff ST, editors. Femtosecond Optical Frequency Comb: Principle, Operation, and Applications [Internet]. Boston: Kluwer Academic Publishers; 2005 [cited 2023 Jan 23]. Available from: http://link.springer.com/10.1007/b102450

40. Udem T, Diddams SA, Vogel KR, Oates CW, Curtis EA, Lee WD, et al. Absolute Frequency Measurements of the Hg^+ and Ca Optical Clock Transitions with a Femtosecond Laser. Phys Rev Lett [Internet]. 2001 May 28 [cited 2023 Jan 23];86(22):4996–9. Available from: http://arxiv.org/abs/physics/0101029

41. Shelton RK, Ma LS, Kapteyn HC, Murnane MM, Hall JL, Ye J. Phase-Coherent Optical Pulse Synthesis from Separate Femtosecond Lasers. Science [Internet]. 2001 Aug 17 [cited 2023 Jan 23];293(5533):1286–9. Available from: https://www.science.org/doi/10.1126/science.1061754

42. Gordon IE, Rothman LS, Hill C, Kochanov RV, Tan Y, Bernath PF, et al. The HITRAN2016 molecular spectroscopic database. Journal of Quantitative Spectroscopy and Radiative Transfer [Internet]. 2017 Dec [cited 2023 Jan 28];203:3–69. Available from: https://linkinghub.elsevier.com/retrieve/pii/S0022407317301073

43. Coddington I, Swann WC, Newbury NR. Time-domain spectroscopy of molecular free-induction decay in the infrared. Opt Lett [Internet]. 2010 May 1 [cited 2023 Apr 13];35(9):1395. Available from: https://opg.optica.org/abstract.cfm?URI=ol-35-9-1395

44. Newbury NR, Coddington I, Swann W. Sensitivity of coherent dual-comb spectroscopy. Opt Express [Internet]. 2010 Apr 12 [cited 2023 Jan 28];18(8):7929. Available from: https://opg.optica.org/oe/abstract.cfm?uri=oe-18-8-7929

45. Blitz JP, Klarup DG. Information in the Instrumental Analysis Laboratory.

46. Roy J, Deschênes JD, Potvin S, Genest J. Continuous real-time correction and averaging for frequency comb interferometry. Opt Express [Internet]. 2012 Sep 24 [cited 2023 Apr 1];20(20):21932. Available from: https://opg.optica.org/oe/abstract.cfm?uri=oe-20-20-21932

47. Giorgetta FR, Rieker GB, Baumann E, Swann WC, Sinclair LC, Kofler J, et al. Broadband Phase Spectroscopy over Turbulent Air Paths. Phys Rev Lett [Internet]. 2015 Sep 1 [cited 2023 Jan 25];115(10):103901. Available from: https://link.aps.org/doi/10.1103/PhysRevLett.115.103901

48. US EPA O. Sources of Greenhouse Gas Emissions [Internet]. 2015 [cited 2023 Mar 20]. Available from: https://www.epa.gov/ghgemissions/sources-greenhouse-gas-emissions

49. Herman DI, Giorgetta FR, Cossel KC, Malarich NA, Hutcherson LC, Weerasekara C, et al. Broadband dual-comb spectroscopy for open-path field measurement of H216O and H218O. In: OSA Optical Sensors and Sensing Congress 2021 (AIS, FTS, HISE, SENSORS, ES) [Internet]. Washington, DC: Optica Publishing Group; 2021 [cited 2023 Apr 1]. p. JTu6E.5. Available from: https://opg.optica.org/abstract.cfm?URI=AIS-2021-JTu6E.5

50. Galewsky J, Steen-Larsen HC, Field RD, Worden J, Risi C, Schneider M. Stable isotopes in atmospheric water vapor and applications to the hydrologic cycle: ISOTOPES IN THE ATMOSPHERIC WATER CYCLE. Rev Geophys [Internet]. 2016 Dec [cited 2023 Apr 1];54(4):809–65. Available from: http://doi.wiley.com/10.1002/2015RG000512

51. Werner C, Schnyder H, Cuntz M, Keitel C, Zeeman MJ, Dawson TE, et al. Progress and challenges in using stable isotopes to trace plant carbon and water relations across scales. Biogeosciences [Internet]. 2012 Aug 13 [cited 2023 Jan 30];9(8):3083–111. Available from: https://bg.copernicus.org/articles/9/3083/2012/

52. Gloge D. Weakly Guiding Fibers. Appl Opt [Internet]. 1971 Oct 1 [cited 2023 Jan 28];10(10):2252. Available from: https://opg.optica.org/abstract.cfm?URI=ao-10-10-2252

53. Kao KC. Dielectric-fibre surface waveguides for optical frequencies. 1966;113(7).

54. Marcatili EAJ. Bends in Optical Dielectric Guides. Bell System Technical Journal [Internet]. 1969 Sep [cited 2023 Jan 31];48(7):2103–32. Available from: https://ieeexplore.ieee.org/document/6769759

55. Niizeki N. Recent Progress in Glass Fibers for Optical Communication. Jpn J Appl Phys [Internet]. 1981 Aug 1 [cited 2023 Jan 31];20(8):1347. Available from: https://iopscience.iop.org/article/10.1143/JJAP.20.1347

56. Kieu K, Mansuripur M. All-fiber bidirectional passively mode-locked ring laser. Opt Lett [Internet]. 2008 Jan 1 [cited 2023 Jan 27];33(1):64. Available from: https://opg.optica.org/abstract.cfm?URI=ol-33-1-64

57. Mehravar S, Norwood RA, Peyghambarian N, Kieu K. Real-time dual-comb spectroscopy with a free-running bidirectionally mode-locked fiber laser. Appl Phys Lett [Internet]. 2016 Jun 6 [cited 2023 Jan 27];108(23):231104. Available from: http://aip.scitation.org/doi/10.1063/1.4953400

58. Sinclair LC, Coddington I, Swann WC, Rieker GB, Hati A, Iwakuni K, et al. Operation of an optically coherent frequency comb outside the metrology lab. Opt Express [Internet]. 2014 Mar 24 [cited 2023 Feb 1];22(6):6996. Available from: https://opg.optica.org/abstract.cfm?URI=oe-22-6-6996

59. Truong GW, Waxman EM, Cossel KC, Baumann E, Klose A, Giorgetta FR, et al. Accurate frequency referencing for fieldable dual-comb spectroscopy. Opt Express [Internet]. 2016 Dec 26 [cited 2023 Feb 1];24(26):30495. Available from: https://opg.optica.org/abstract.cfm?URI=oe-24-26-30495

60. Garmire E, Yariv A. Laser mode-locking with saturable absorbers. IEEE J Quantum Electron [Internet]. 1967 Jun [cited 2023 Feb 14];3(6):222–6. Available from: http://ieeexplore.ieee.org/document/1074489/

61. Zhang L, Zhou J, Wang Z, Gu X, Feng Y. SESAM Mode-Locked, Environmentally Stable, and Compact Dissipative Soliton Fiber Laser. IEEE Photon Technol Lett [Internet]. 2014 Jul [cited 2023 Feb 13];26(13):1314–6. Available from: https://ieeexplore.ieee.org/document/6808485/

62. Adler F, Moutzouris K, Leitenstorfer A, Schnatz H, Lipphardt B, Grosche G, et al. Phase-locked two-branch erbium-doped fiber laser system for long-term precision measurements of optical frequencies. Opt Express [Internet]. 2004 [cited 2023 Jan 31];12(24):5872. Available from: https://opg.optica.org/oe/abstract.cfm?uri=oe-12-24-5872

63. Li B, Xing J, Kwon D, Xie Y, Prakash N, Kim J, et al. Bidirectional mode-locked all-normal dispersion fiber laser. Optica [Internet]. 2020 Aug 20 [cited 2023 Feb 14];7(8):961. Available from: https://opg.optica.org/abstract.cfm?URI=optica-7-8-961

64. Byun H, Sander MY, Motamedi A, Shen H, Petrich GS, Kolodziejski LA, et al. Compact, stable 1 GHz femtosecond Er-doped fiber lasers. Appl Opt [Internet]. 2010 Oct 10 [cited 2023 Feb 2];49(29):5577. Available from: https://opg.optica.org/abstract.cfm?URI=ao-49-29-5577

65. Paschotta DR. Semiconductor Saturable Absorber Mirrors [Internet]. [cited 2023 Feb 20]. Available from: https://www.rp-photonics.com/semiconductor_saturable_absorber_mirrors.html

66. Giechaskiel B, Clairotte M. Fourier Transform Infrared (FTIR) Spectroscopy for Measurements of Vehicle Exhaust Emissions: A Review. Applied Sciences [Internet]. 2021

Aug 12 [cited 2023 Feb 1];11(16):7416. Available from: https://www.mdpi.com/2076-3417/11/16/7416

67. Hosseini-Zavareh S. Acetylene-filled pressure broadened short photonic microcells.

68. Hosseini-Zavareh S, Luder R, Thirugnanasambandam M, Kushan Weerasinghe HW, Washburn BR, Corwin KL. Fabrication and characterization of short acetylene-filled photonic microcells. Appl Opt [Internet]. 2019 Apr 10 [cited 2023 Feb 14];58(11):2809. Available from: https://opg.optica.org/abstract.cfm?URI=ao-58-11-2809

69. Luder RJ, Hosseini-Zavareh S, Wang C, Thirugnanasambandam M, Washburn BR, Corwin KL. Short Acetylene-Filled Photonic Bandgap Fiber Cells Toward Practical Industry Standards. In: Conference on Lasers and Electro-Optics [Internet]. San Jose, California: OSA; 2016 [cited 2023 Feb 14]. p. SM2H.6. Available from: https://opg.optica.org/abstract.cfm?URI=CLEO_SI-2016-SM2H.6

70. Hosseini-Zavareh S, Thirugnanasambandam MP, Kushan Weerasinghe HW, Washburn BR, Corwin KL. Improved Acetylene-Filled Photonic Bandgap Fiber Cells Fabricated using a Tapering Method. In: Frontiers in Optics / Laser Science [Internet]. Washington, DC: OSA; 2018 [cited 2023 Feb 14]. p. JW4A.95. Available from: https://opg.optica.org/abstract.cfm?URI=FiO-2018-JW4A.95

71. Swann WC, McFerran JJ, Coddington I, Newbury NR, Hartl I, Fermann ME, et al. Fiber-laser frequency combs with subhertz relative linewidths. Opt Lett [Internet]. 2006 Oct 15 [cited 2023 Feb 2];31(20):3046. Available from: https://opg.optica.org/abstract.cfm?URI=ol-31-20-3046

72. 63.5mm Clear Aperture, 5 Arcsec, Gold Retroreflector [Internet]. [cited 2023 Jan 31]. Available from: https://www.edmundoptics.com/p/635mm-clear-aperture-5-arcsec-gold-retroreflector/6668/

73. Alden CB, Coburn SC, Wright RJ, Baumann E, Cossel K, Perez E, et al. Single-Blind Quantification of Natural Gas Leaks from 1 km Distance Using Frequency Combs. Environ Sci Technol [Internet]. 2019 Mar 5 [cited 2023 Feb 8];53(5):2908–17. Available from: https://pubs.acs.org/doi/10.1021/acs.est.8b06259

74. Mangino J. US EPA Cattle Enteric Fermentation Model (CEFM).

75. Open Path Gas Detection | Boreal Laser [Internet]. [cited 2023 Feb 8]. Available from: https://boreal-laser.com/

76. G2401 Gas Concentration Analyzer | Picarro [Internet]. [cited 2023 Feb 9]. Available from: https://www.picarro.com/products/g2401_gas_concentration_analyzer

77. Grinfelde I, Valujeva K, Zaharane K, Berzina L. Automated cavity ring down spectroscopy usage for nitrous oxide emission measurements from soil using recirculation system. In 2017 [cited 2023 Feb 9]. Available from: http://www.tf.llu.lv/conference/proceedings2017/Papers/N235.pdf

78. Maasikmets M, Teinemaa E, Kaasik A, Kimmel V. Measurement and analysis of ammonia, hydrogen sulphide and odour emissions from the cattle farming in Estonia. Biosystems Engineering [Internet]. 2015 Nov [cited 2023 Feb 9];139:48–59. Available from: https://linkinghub.elsevier.com/retrieve/pii/S1537511015001294

79. Kamp JN, Chowdhury A, Adamsen APS, Feilberg A. Negligible influence of livestock contaminants and sampling system on ammonia measurements with cavity ring-down spectroscopy. Atmos Meas Tech [Internet]. 2019 May 17 [cited 2023 Jan 16];12(5):2837–50. Available from: https://amt.copernicus.org/articles/12/2837/2019/

80. McHale LE, Hecobian A, Yalin AP. Open-path cavity ring-down spectroscopy for trace gas measurements in ambient air. Opt Express [Internet]. 2016 Mar 7 [cited 2023 Feb 9];24(5):5523. Available from: https://opg.optica.org/abstract.cfm?URI=oe-24-5-5523

81. Shadman S, Rose C, Yalin AP. Open-path cavity ring-down spectroscopy sensor for atmospheric ammonia. Appl Phys B [Internet]. 2016 Jul [cited 2023 Feb 9];122(7):194. Available from: http://link.springer.com/10.1007/s00340-016-6461-5

82. Lan X, Talbot R, Laine P, Torres A. Characterizing Fugitive Methane Emissions in the Barnett Shale Area Using a Mobile Laboratory. Environ Sci Technol [Internet]. 2015 Jul 7 [cited 2023 Feb 9];49(13):8139–46. Available from: https://pubs.acs.org/doi/10.1021/es5063055

83. Howarth RW, Santoro R, Ingraffea A. Methane and the greenhouse-gas footprint of natural gas from shale formations: A letter. Climatic Change [Internet]. 2011 Jun [cited 2023 Feb 9];106(4):679–90. Available from: http://link.springer.com/10.1007/s10584-011-0061-5

84. Yacovitch TI, Herndon SC, Pétron G, Kofler J, Lyon D, Zahniser MS, et al. Mobile Laboratory Observations of Methane Emissions in the Barnett Shale Region. Environ Sci Technol [Internet]. 2015 Jul 7 [cited 2023 Feb 9];49(13):7889–95. Available from: https://pubs.acs.org/doi/10.1021/es506352j

85. Gamage LP, Gichuhi WK. Efficacy of a Wavelength-Scanned Cavity Ring-Down Spectroscopic Technique in Estimating Enteric Methane Emissions in Ruminants. ACS Earth Space Chem [Internet]. 2018 Jul 19 [cited 2023 Feb 9];2(7):673–82. Available from: https://pubs.acs.org/doi/10.1021/acsearthspacechem.8b00023

86. Herman DI, Weerasekara C, Hutcherson LC, Giorgetta FR, Cossel KC, Waxman EM, et al. Precise multispecies agricultural gas flux determined using broadband open-path dual-comb spectroscopy. Sci Adv [Internet]. 2021 Apr 2 [cited 2023 Jan 13];7(14):eabe9765. Available from: https://www.science.org/doi/10.1126/sciadv.abe9765

87. CSAT3B - 3-D Sonic Anemometer with Integrated Electronics [Internet]. [cited 2023 Feb 17]. Available from: https://www.campbellsci.com/csat3b

88. Burns SP, Horst TW, Jacobsen L, Blanken PD, Monson RK. Using sonic anemometer temperature to measure sensible heat flux in strong winds. Atmos Meas Tech [Internet].

2012 Sep 3 [cited 2023 Feb 7];5(9):2095–111. Available from: https://amt.copernicus.org/articles/5/2095/2012/

89. Flesch TK, Baron VS, Wilson JD, Griffith DWT, Basarab JA, Carlson PJ. Agricultural gas emissions during the spring thaw: Applying a new measurement technique. Agricultural and Forest Meteorology [Internet]. 2016 May [cited 2023 Feb 17];221:111–21. Available from: https://linkinghub.elsevier.com/retrieve/pii/S0168192316301654

90. CR3000 - Measurement and Control Datalogger [Internet]. [cited 2023 Feb 17]. Available from: https://www.campbellsci.com/cr3000

91. Patrignani A, Knapp M, Redmond C, Santos E. Technical Overview of the Kansas Mesonet. Journal of Atmospheric and Oceanic Technology [Internet]. 2020 Dec [cited 2023 Jan 16];37(12):2167–83. Available from: https://journals.ametsoc.org/view/journals/atot/37/12/jtech-d-19-0214.1.xml

92. Rothman LS, Gordon IE, Barbe A, Benner DC, Bernath PF, Birk M, et al. The HITRAN 2008 molecular spectroscopic database. Journal of Quantitative Spectroscopy and Radiative Transfer [Internet]. 2009 Jun [cited 2023 Jan 27];110(9–10):533–72. Available from: https://linkinghub.elsevier.com/retrieve/pii/S0022407309000727

93. Cole RK, Makowiecki AS, Hoghooghi N, Rieker GB. Baseline-free quantitative absorption spectroscopy based on cepstral analysis. Opt Express [Internet]. 2019 Dec 23 [cited 2023 Feb 20];27(26):37920. Available from: https://opg.optica.org/abstract.cfm?URI=oe-27-26-37920

94. Flesch T, Wilson J, Harper L, Crenna B. Estimating gas emissions from a farm with an inverse-dispersion technique. Atmospheric Environment [Internet]. 2005 Sep [cited 2023 Feb 20];39(27):4863–74. Available from: https://linkinghub.elsevier.com/retrieve/pii/S1352231005004176

95. Baldé H, VanderZaag A, Smith W, Desjardins RL. Ammonia Emissions Measured Using Two Different GasFinder Open-Path Lasers. Atmosphere [Internet]. 2019 May 10 [cited 2023 Feb 20];10(5):261. Available from: https://www.mdpi.com/2073-4433/10/5/261

96. Bonifacio HF, Maghirang RG, Razote EB, Trabue SL, Prueger JH. Comparison of AERMOD and WindTrax dispersion models in determining PM $_{10}$ emission rates from a beef cattle feedlot. Journal of the Air & Waste Management Association [Internet]. 2013 May [cited 2023 Jan 16];63(5):545–56. Available from: https://www.tandfonline.com/doi/full/10.1080/10962247.2013.768311

97. Flesch TK, Wilson JD, Harper LA, Crenna BP, Sharpe RR. Deducing Ground-to-Air Emissions from Observed Trace Gas Concentrations: A Field Trial. J Appl Meteor [Internet]. 2004 Apr [cited 2023 Apr 13];43(3):487–502. Available from: http://journals.ametsoc.org/doi/10.1175/1520-0450(2004)043<0487:DGEFOT>2.0.CO;2

98. Werle P, M&#xfffd;cke R, Slemr F. The limits of signal averaging in atmospheric trace-gas monitoring by tunable diode-laser absorption spectroscopy (TDLAS). Appl Phys B

[Internet]. 1993 Aug [cited 2023 Feb 20];57(2):131–9. Available from: http://link.springer.com/10.1007/BF00425997

99. Allan DW. Statistics of atomic frequency standards. Proc IEEE [Internet]. 1966 [cited 2023 Feb 20];54(2):221–30. Available from: http://ieeexplore.ieee.org/document/1446564/

100. Cutler LS, Searle CL. Some aspects of the theory and measurement of frequency fluctuations in frequency standards. Proc IEEE [Internet]. 1966 [cited 2023 Feb 20];54(2):136–54. Available from: http://ieeexplore.ieee.org/document/1446557/

101. Kormann R, Meixner FX. An Analytical Footprint Model For Non-Neutral Stratification. Boundary-Layer Meteorology [Internet]. 2001 May [cited 2023 Feb 20];99(2):207–24. Available from: http://link.springer.com/10.1023/A:1018991015119

102. T. K. Flesch, L. A. Harper, J. M. Powell, J. D. Wilson. Inverse-Dispersion Calculation of Ammonia Emissions from Wisconsin Dairy Farms. Transactions of the ASABE [Internet]. 2009 [cited 2023 Mar 31];52(1):253–65. Available from: http://elibrary.asabe.org/abstract.asp??JID=3&AID=25946&CID=t2009&v=52&i=1&T=1

103. Flesch TK, Wilson JD. Estimating Tracer Emissions with a Backward Lagrangian Stochastic Technique. In: Hatfield JL, Baker JM, editors. Agronomy Monographs [Internet]. Madison, WI, USA: American Society of Agronomy, Crop Science Society of America, and Soil Science Society of America; 2015 [cited 2023 Mar 31]. p. 513–31. Available from: http://doi.wiley.com/10.2134/agronmonogr47.c22

104. Flesch TK, Vergé XPC, Desjardins RL, Worth D. Methane emissions from a swine manure tank in western Canada. Can J Anim Sci [Internet]. 2013 Mar [cited 2023 Mar 31];93(1):159–69. Available from: http://www.nrcresearchpress.com/doi/10.4141/cjas2012-072

105. Sun K, Tao L, Miller DJ, Zondlo MA, Shonkwiler KB, Nash C, et al. Open-path eddy covariance measurements of ammonia fluxes from a beef cattle feedlot. Agricultural and Forest Meteorology [Internet]. 2015 Nov [cited 2023 Feb 20];213:193–202. Available from: https://linkinghub.elsevier.com/retrieve/pii/S0168192315001860

106. Felber R, Münger A, Neftel A, Ammann C. Eddy covariance methane flux measurements over a grazed pasture: effect of cows as moving point sources. Biogeosciences [Internet]. 2015 Jun 29 [cited 2023 Feb 20];12(12):3925–40. Available from: https://bg.copernicus.org/articles/12/3925/2015/

107. Baum KA, Ham JM, Brunsell NA, Coyne PI. Surface boundary layer of cattle feedlots: Implications for air emissions measurement. Agricultural and Forest Meteorology [Internet]. 2008 Oct [cited 2023 Feb 20];148(11):1882–93. Available from: https://linkinghub.elsevier.com/retrieve/pii/S0168192308001974

108. McGinn SM, Turner D, Tomkins N, Charmley E, Bishop-Hurley G, Chen D. Methane Emissions from Grazing Cattle Using Point-Source Dispersion. J Environ Qual [Internet].

2011 Jan [cited 2023 Feb 20];40(1):22–7. Available from: http://doi.wiley.com/10.2134/jeq2010.0239

109. Prajapati P, Santos EA. Measurements of methane emissions from a beef cattle feedlot using the eddy covariance technique. Agricultural and Forest Meteorology [Internet]. 2017 Jan [cited 2023 Feb 8];232:349–58. Available from: https://linkinghub.elsevier.com/retrieve/pii/S016819231630380X

110. Thunder Beach Scientific [Internet]. [cited 2023 Feb 20]. Available from: http://www.thunderbeachscientific.com/windtrax.html

111. Greenwood PL. Review: An overview of beef production from pasture and feedlot globally, as demand for beef and the need for sustainable practices increase. Animal [Internet]. 2021 Dec [cited 2023 Mar 2];15:100295. Available from: https://linkinghub.elsevier.com/retrieve/pii/S1751731121001385

112. Mosier A, Schimel D, Valentine D, Bronson K, Parton W. Methane and nitrous oxide fluxes in native, fertilized and cultivated grasslands. Nature [Internet]. 1991 Mar [cited 2023 Jan 16];350(6316):330–2. Available from: http://www.nature.com/articles/350330a0

113. IPCC, WMO, editors. Climate change: the 1990 and 1992 IPCC assessments, IPCC first assessment report overview and policymaker summaries and 1992 IPPC supplement. Geneve: IPCC; 1992. 168 p.

114. Smith KA, Robertson GP, Melillo JM. Exchange of Trace Gases between the Terrestrial Biosphere and the Atmosphere in the Midlatitudes. In: Prinn RG, editor. Global Atmospheric-Biospheric Chemistry [Internet]. Boston, MA: Springer US; 1994 [cited 2023 Mar 5]. p. 179–203. Available from: http://link.springer.com/10.1007/978-1-4615-2524-0_11

115. CGEM II EQ Mount and Tripod | Celestron [Internet]. [cited 2023 Mar 5]. Available from: https://www.celestron.com/products/cgem-ii-eq-mount-and-tripod

116. FLIR PTU-D100E Pan/Tilt Unit for side-mounted payloads up to 25 lbs | Teledyne FLIR [Internet]. [cited 2023 Mar 5]. Available from: https://www.flir.com/products/ptu-d100e?vertical=mcs&segment=oem

117. Malarich NA, Cossel K, Giorgetta F, Baumann E, Mead G, Herman DI, et al. Countering nonlinearity in digitization for precise dual-frequency comb spectroscopy. In: Optical Sensors and Sensing Congress 2022 (AIS, LACSEA, Sensors, ES) [Internet]. Vancouver, British Columbia: Optica Publishing Group; 2022 [cited 2023 Mar 12]. p. EM3D.2. Available from: https://opg.optica.org/abstract.cfm?URI=ES-2022-EM3D.2

118. Understanding ADC Integral Nonlinearity (INL) Error - Technical Articles [Internet]. [cited 2023 Mar 14]. Available from: https://www.allaboutcircuits.com/technical-articles/understanding-analog-to-digital-converter-integral-nonlinearity-inl-error/

119. An ADC and DAC Integral Non-Linearity (INL) – Mastering Electronics Design [Internet]. [cited 2023 Mar 14]. Available from: https://masteringelectronicsdesign.com/an-adc-and-dac-integral-non-linearity-inl/

120. What is Dithering? — Sage Audio [Internet]. [cited 2023 Mar 14]. Available from: https://www.sageaudio.com/blog/mastering/what-is-dithering.php

121. Function Generator - DS345 [Internet]. [cited 2023 Apr 13]. Available from: https://www.thinksrs.com/products/ds345.html

122. - Kansas Environmental Public Health Tracking [Internet]. [cited 2023 Mar 20]. Available from: https://keap.kdhe.ks.gov/Ephtm/PortalPages/ContentData?CID=123

123. Decock C. Mitigating Nitrous Oxide Emissions from Corn Cropping Systems in the Midwestern U.S.: Potential and Data Gaps. Environ Sci Technol [Internet]. 2014 Apr 15 [cited 2023 Mar 21];48(8):4247–56. Available from: https://pubs.acs.org/doi/10.1021/es4055324

124. Bailey DM, Zhao G, Fleisher AJ. Precision Spectroscopy of Nitrous Oxide Isotopocules with a Cross-Dispersed Spectrometer and a Mid-Infrared Frequency Comb. Anal Chem [Internet]. 2020 Oct 20 [cited 2023 Mar 21];92(20):13759–66. Available from: https://pubs.acs.org/doi/10.1021/acs.analchem.0c01868

125. Ycas G, Giorgetta FR, Baumann E, Coddington I, Herman D, Diddams SA, et al. High-coherence mid-infrared dual-comb spectroscopy spanning 2.6 to 5.2 μm. Nature Photon [Internet]. 2018 Apr [cited 2023 Jan 28];12(4):202–8. Available from: http://www.nature.com/articles/s41566-018-0114-7

126. Sterczewski LA, Westberg J, Bagheri M, Frez C, Vurgaftman I, Canedy CL, et al. Mid-infrared dual-comb spectroscopy with interband cascade lasers. Opt Lett [Internet]. 2019 Apr 15 [cited 2023 Mar 20];44(8):2113. Available from: https://opg.optica.org/abstract.cfm?URI=ol-44-8-2113

127. Yan M, Luo PL, Iwakuni K, Millot G, Hänsch TW, Picqué N. Mid-infrared dual-comb spectroscopy with electro-optic modulators. Light Sci Appl [Internet]. 2017 May 3 [cited 2023 Mar 20];6(10):e17076–e17076. Available from: https://www.nature.com/articles/lsa201776

128. Herman DI, Mead G, Giorgetta FR, Baumann E, Malarich N, Washburn BR, et al. Open-path measurement of stable water isotopologues using mid-infrared dual-comb spectroscopy [Internet]. Gases/Remote Sensing/Instruments and Platforms; 2023 Jan [cited 2023 Mar 31]. Available from: https://egusphere.copernicus.org/preprints/2023/egusphere-2022-1263/

129. Makowiecki AS, Herman DI, Hoghooghi N, Strong EF, Cole RK, Ycas G, et al. Mid-infrared dual frequency comb spectroscopy for combustion analysis from 2.8 to 5 μm. Proceedings of the Combustion Institute [Internet]. 2021 [cited 2023 Mar 20];38(1):1627–35. Available from: https://linkinghub.elsevier.com/retrieve/pii/S1540748920302868

Appendix A - Abbreviations

ADC	**Analog-to-Digital Converter**
ADEV	**Allan Deviation**
AVAR	**Allan Variance**
AWDEV	**Allan-Werle Deviation**
CEFM	**Cattle Enteric Fermentation Model**
CRDS	**Cavity Ring-Down Spectroscopy**
CW	**Continuous Wave**
DCS	**Dual-Comb Spectroscopy**
DNL	**Differential Non-Linearity**
EDF	**Erbium-Doped Fiber**
EPA	**Environmental Protection Agency**
FID	**Free Induction Decay**
FPGA	**Field Programmable Gate Array**
FTIR	**Fourier-Transform InfraRed**
GPS	**Global Positioning System**
GUI	**Graphical User Interface**
IDM	**Inverse Dispersion Model**
INL	**Integral Non-Linearity**
IPCC	**Intergovernmental Panel on Climate Change**
LSB	**Least Significant Bit**
LMD	**Laser Methane Detector**
MMT	**Million Metric Tons**
NARSTO	**North American Research Strategy for Tropospheric Ozone**
PM	**Polarization Maintaining**
ppb	**part per billion**
ppm	**part per million**
QF	**Quality Factor**
RF	**Radio Frequency**

SESAM	**Semiconductor-Saturable Absorber Mirror**
SMF	**Single-Mode Fiber**
SNR	**Signal-to-Noise Ratio**
TLAS	**Tunable Laser Absorption Spectroscopy**
UPS	**Uninterruptible Power Supply**
VCO	**Voltage-Controlled Oscillator**

Appendix B - Copyright Permissions

B.1 Licensed by CC BY 4.0

The following images are licensed under Creative Commons BY 4.0, also known as Creative Commons Attribution 4.0 International.

Figure 2.2 from “Intercomparison of open-path trace gas measurements with two dual-frequency-comb spectrometers” by Waxman EM, Cossel KC, Truong GW, Giorgetta FR, Swann WC, Coburn S, et al.

Figures 3.2, 3.5-3.7, 3.9-3.10 from “Precise multispecies agricultural gas flux determined using broadband open-path dual-comb spectroscopy” by Herman DI, Weerasekara C, Hutcherson LC, Giorgetta FR, Cossel KC, Waxman EM, et al.

The license deed can be found at:

https://creativecommons.org/licenses/by/4.0/

B.2 Optica Publishing (Figure 2.1)

Dear Lindsay Morris,

Thank you for contacting Optica Publishing Group.

For the use of figure 2 from Ian Coddington, Nathan Newbury, and William Swann, "Dual-comb spectroscopy," Optica 3, 414-426 (2016):

Optica Publishing Group considers your requested use of its copyrighted material to be Fair Use under United States Copyright Law. We request that a complete citation of the original material be included in any publication.

While your publisher should be able to provide additional guidance, we prefer the below citation formats:

For citations in figure captions:

[Reprinted/Adapted] with permission from [ref #]. (Please include the full citation in your reference list)

For images without captions:

Journal Vol. #, first page (year published) An example: Biomed. Opt. Express 6, 793 (2015)

Please let me know if you have any questions.

Kind Regards,
Hannah Greenwood

Hannah Greenwood
April 7, 2023
Authorized Agent, Optica Publishing Group